Ben Boudinar, Mourad (1991) *Performance prediction and optimisation of spiral wound modules.*

PhD thesis

http://theses.gla.ac.uk/3235/

Copyright and moral rights for this thesis are retained by the author

A copy can be downloaded for personal non-commercial research or study, without prior permission or charge

This thesis cannot be reproduced or quoted extensively from without first obtaining permission in writing from the Author

The content must not be changed in any way or sold commercially in any format or medium without the formal permission of the Author

When referring to this work, full bibliographic details including the author, title, awarding institution and date of the thesis must be given

Glasgow Theses Service
http://theses.gla.ac.uk/
theses@gla.ac.uk

PERFORMANCE PREDICTION AND OPTIMISATION OF SPIRAL WOUND MODULES.

MOURAD BEN BOUDINAR

THESIS SUBMITTED TO THE FACULTY OF ENGINEERING FOR THE DEGREE OF DOCTOR OF PHILOSOPHY (Ph.D)

DEPARTMENT OF MECHANICAL ENGINEERING

UNIVERSITY OF GLASGOW

DECEMBER 1991

© M. BEN BOUDINAR, 1991.

بِسْمِ اللهِ الرَّحْمٰنِ الرَّحِيمِ

وَجَعَلْنَا مِنَ الْمَاءِ كُلَّ شَيْءٍ حَيٍّ

To my wife, parents, brothers and sisters, this thesis is affectionately dedicated.

SUMMARY

The work deals with the modelling and optimisation of reverse osmosis (RO) spiral wound elements. It is aimed at improving areas of uncertainty and possible limitations which remain with current published predictive schemes. These were compromised mainly by the lack of adequate experimental data representative of actual operating conditions.

Two different mathematical models, termed the "Slit" and the "Spiral" model, were developed. These models differ on the geometrical idealisation of a spiral wound element as indicated by their names. The Solution Diffusion model is used to describe water and salt transport across the membrane. The differential equations governing the process were solved numerically using a finite difference method. The resulting computer programs enable concentrations, pressures and flow rates in the brine and permeate channels to be obtained at any point in the module.

The investigation covered a wide range of feed conditions by using experimental data provided from two different types of commercial spiral wound modules. These were the ROGA-4160HR [29] and the Filmtec FT30SW2540 [28] modules. The former type dealt with data typical of brackish water desalination whereas the second type provided data typically encountered in sea-water desalination.

The required intrinsic membrane characteristics were determined experimentally using small samples of membrane in a test cell in a closed loop system.

For both models, the predictions agree very well with the experimental data over the entire range of operating conditions:- with the exception of some few cases, typical deviations were of the order of ±6% for the module productivity and of about ±10% for the permeate quality. In addition, parametric studies were performed to establish the programs consistency and the results were in accordance with the theory.

A comparison of the predictive accuracy of both models did not reveal any significant differences thereby suggesting that the effect of the spiral geometry is not as critical as one might think.

As an illustrative example of the application of such model the effects of some geometrical variables, on the performance of a spiral wound element supplied with a membrane and spacers characteristics similar to those of the FT30 module, were investigated with a view to its optimisation.

ACKNOWLEDGEMENTS.

I wish to express my sincere appreciation to my supervisor, Dr. W.T. Hanbury, for his valuable guidance, advice and encouragement throughout the project.

I am greatly indebted to my wife, Yvette, for her patience, understanding and support.

Many thanks are also due to Mr A. Ritchie for his technical assistance with the experiments and my friend, Dr. S. Avlonitis, for his constant collaboration.

Finally, I would like to thank the Algerian Government who, through the Ministry of High Education, provided me with the financial support necessary to complete this research project.

CONTENTS

LIST OF FIGURES.

LIST OF TABLES.

LIST OF SYMBOLS.

A_M : Total membrane area (m^2)
b : Osmotic coefficient (bar)
C : Concentration (ppm)
d_h : Hydraulic diametre (cm)
Ds : Diffusion coefficient (cm^2/s)
E : Friction parameter ($1/cm^2$)
h : Height (cm)
J_1 : Water flux (cm/s)
J_2 : Salt flux (cm/s)
KB : Brine spacer mixing efficiency (see eq.(3-1))
k_1 : Water permeability coefficient (cm/s.bar)
k_2 : Salt permeability coefficient (cm/s)
k : Mass transfer coefficient (cm/s)
L : Membrane axial length (cm)
M : Number of grid points along axial membrane length.
MB : Brine spacer characteristic length (see eq.(3-1)) (cm)
N : Number of grid points along spiral membrane length.
NLE : Number of membrane leaves
P : Pressure (bar)
Pe : Peclet number ($=v\ d_h/Ds$)
P_D : Packing density (m^2/m^3)
Q : Flow (cm^3/s)
R : Salt Rejection (%).
Re : Reynolds number ($=\rho\ v\ d_h/\mu$)
Sc : Schmidt number ($=\mu/\rho\ Ds$)
Sh : Sherwood number ($=k\ d_h/Ds$)
T : Temperature (°C)
TSH : Term defined in eq.(4-19).
V_{MOD}: Module volume (cm^3)
v,V : Velocity (cm/s)
W : Membrane spiral length (cm)
W_{BS} : Brine spacer spiral lengths (cm)
Wg : Membrane leaf glue line width (cm)

Greek letters.

δ : Boundary layer thickness (cm)
μ : Viscosity (g/cm.s)
ζ : Volume specific productivity ($cm^3\ s^{-1}/cm^3.bar$)
Π : Osmotic pressure (bar)
ρ : Density (g/cm^3)
θ : Incremental angle

Subscripts.

B : Brine
BW : Brine wall
M : Membrane
P : Permeate
PW : Permeate wall

Abbreviations.

RO : Reverse Osmosis
SP : Spiral
SL : Slit
SPW : Spiral Wound
SW : Sea water
HF : Hollow Fibre
CP : Concentration polarisation

CHAPTER ONE

GENERAL INTRODUCTION

I-1- Water Supply : is there a need for Desalination?

Water is a primary and indispensable natural resource which is required by all countries for their development. Currently, two different types of water related problems can be identified, depending on whether arid or humid countries are considered, as follows :

- In arid or desert countries where water may be scarce, brackish or even non-existent, this resource is a matter of major concern particularly for the domestic supplies and also for industrial development.

- In the more humid countries, the problem of water supply and water treatment has, recently, been brought sharply into focus not so much for domestic consumption but for the increasing environmental problems due to water pollution by industrial wastes which need treating.

With regard to the different problems encountered in both the arid and humid countries a paradox is clearly depicted as follows : in the arid case, the lack of water is one of the prime constraints on economic development whereas, in the humid case, the preservation of adequate standards of purity is not easily compatible with industrial and economic growth.

Therefore, one can conclude that the steepness of the demand curves is bound to increase for the foreseeable future. Already, one can notice that, over the past few years and depending on geographical and hydrological parameters, trends of conventional water supply costs have been steadily increasing. Recognition of the growing demand for fresh and clean water has, in the past decades, stimulated great interest and intensified research in salt water purification. At that time, it was anticipated that salt water conversion could represent a potential market especially in situations in which a new or additional water supply is needed As a result of this research activity, various separation and purification methods, such as distillation, ion-exchange and membrane processes have been developed. Among these different methods, membrane processes have, in recent years, gained popularity. These processes are attractive chiefly because of the many advantages

that they offer, namely :

-a- The processing equipment is usually relatively simple resulting in low equipment cost

-b- The 'Leadtime' for treatment plants using membrane processes, i-e the period of time required from the moment the order for the plant is placed to its actual startup, is significantly shorter than the one required for any distillation plant for example.

-c- Low energy consumption since no change of phase is involved.

-d- The operation is essentially at ambient temperature which minimises scale and corrosion problems and is very important in applications where temperature-sensitive substances are involved.

Currently, the most important membrane processes include :

- Reverse Osmosis.
- Ultrafiltration.
- Electrodialysis.
- Microfiltration.
- Nanofiltration.

Since here we are mainly concerned with the application of the membrane processes to water desalination, for the rest of this work the discussion will be restricted to the reverse osmosis (RO) process. This process has had significant development in the last three decades and has proved its reliability and economics to such extent that it has become, recently, a major method for water desalination, competing successfully with the more traditional methods such as distillation . In fact, the success of RO is also due to its versatility as a separation process. Indeed, RO has also found important other applications in diverse areas, notably in :

- Pollution control by processing industrial waste streams.
- Participating as a unit process in ultra-pure water production systems for the electronics and pharmaceutical industries.
- The food industry with for e.g. the concentration of whey and skimmed milk.

In the following sections of this introductory chapter, several features of the RO process will be described.

I-2- Reverse Osmosis.

I-2-1-Fundamental Process of Reverse Osmosis.

As shown in Fig.1a, natural osmosis can be defined as the spontaneous passage of pure water from a dilute solution to a more concentrated solution across a semi-permeable membrane (i-e a barrier which allows the passage of the solvent (water) but not of the solutes (dissolved solids)).

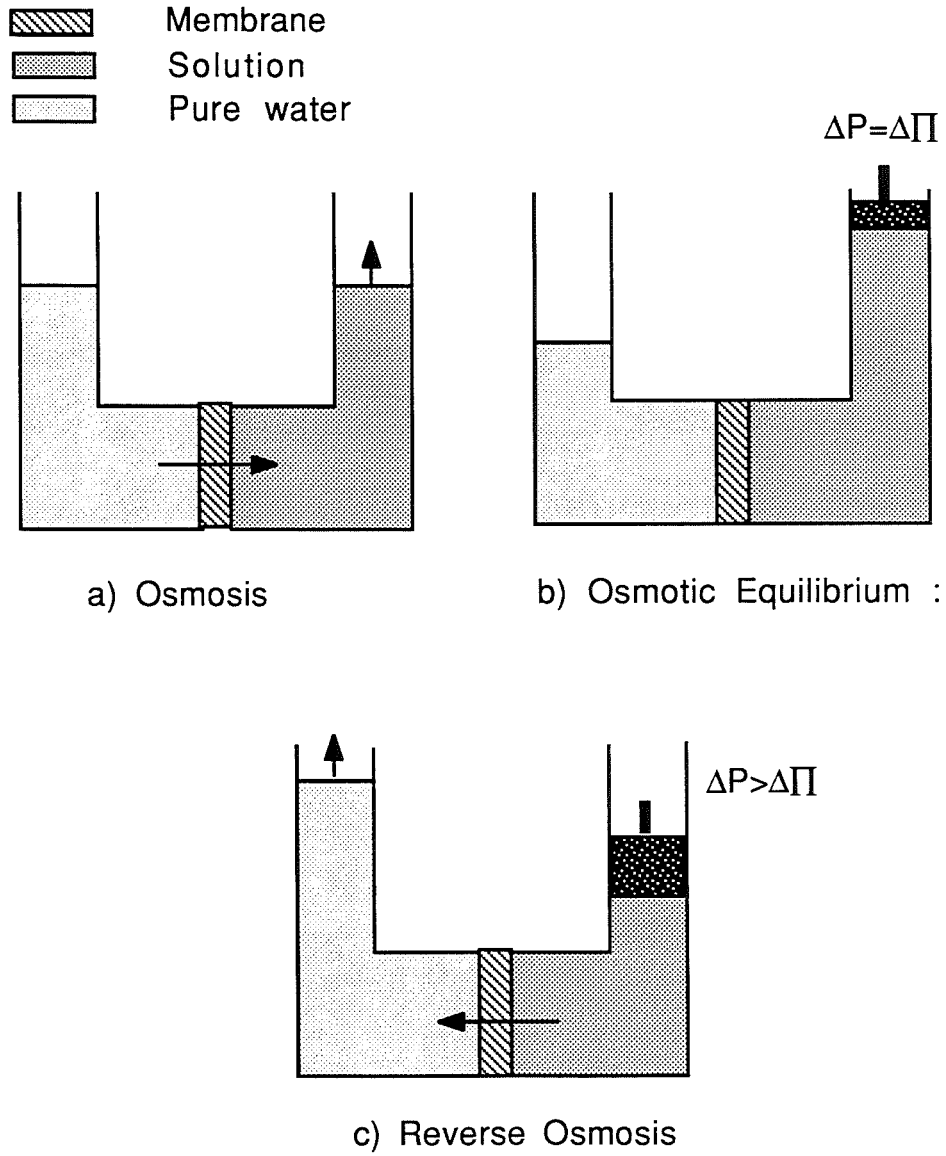

FIG.1: Osmosis and Reverse Osmosis Principles.

If a pressure (ΔP), just equal to the osmotic pressure difference between the two solution ($\Delta \Pi$), is applied to the concentrated solution, water flow ceases and we have osmotic equilibrium. This state is shown in Fig.1b. The osmotic pressure of a solution is defined to be the pressure necessary to halt the osmotic flow through a semi-permeable membrane separating it from the pure solvent. This osmotic pressure depends upon the types of solutes in the solution and their concentration : the higher the concentration, the greater the osmotic pressure. If a higher pressure ($\Delta P > \Delta \Pi$) is applied, water will flow out of the concentrated solution through the membrane. This is the phenomenon of reverse osmosis and is depicted in Fig.1c. Theoretically, in the ideal plant, the only energy required is that to pump the feed water to the osmotic pressure. In practice, higher pressures must be used in order to obtain a reasonable flux of water passing through the membrane. An important consequence of the action of a salt-rejecting membrane in promoting selective transport of water from a solution is the concentration of the rejected salt in a layer next to the membrane surface. This salt build-up at the membrane interface is called concentration polarisation (CP).

This phenomenon, which will be treated in detail in a later section, has a number of undesirable effects. It is sufficient at this stage to mention that it reduces the product quality on two counts :

1- Salt build up at the interface increases the osmotic pressure of the solution at the interface, which in turn decreases the effective pressure in driving the water through the membrane.
2- The concentration of salt in the product increases with the concentration at the feed-membrane interface.

Further, excessive concentration polarisation may cause precipitation of dissolved components, possibly destroying sensitive membrane surfaces and causing failure of the equipment.

I-2-2-Historical Background.

I-2-2-1- Introduction.

The phenomenon of Osmosis, across natural semi-permeable membranes, had been discovered in the mid 1700's by Abbe Nollet who used a semi-permeable animal bladder (i.e. a membrane) to separate wine and water. Since then, many efforts had been devoted to understand the transport phenomena involved. As a result of this, the concept of reverting the natural process, by means of an applied pressure, termed Reverse Osmosis was theoretically conceived. However, its practical value as a separation media was, as

described below, not possible until the late 1950's when an era of rapid advance in membrane and module technology was initiated. This in turn made it possible to achieve the economic goal of desalting brackish and sea water by RO

I-2-2-2- Reverse Osmosis membranes.

The practical feasibility of the RO process was first demonstrated in 1959 by Reid and Breton [1] with the finding that the passage of saline water over a supported dense film of cellulose acetate (CA) at elevated pressure resulted in the permeation of water with a salt rejection of 95% or greater. At this point, it was realised that producing potable water from sea-water, could be possible with these membranes. However, the fluxes resulting from these membranes were far too low for the process to be an economical desalting technique. The problem was how to produce membranes with both high rejection and high water fluxes.

The major technological breakthrough that established RO as a versatile and economically attractive process came in 1960 when Loeb and Sourirajan [2] invented the first asymmetric CA membrane which enabled comparable salt rejection with an improvement in the flux by about two orders of magnitude at comparable pressures. This event resulted in the commercialisation of RO technology with several industrial companies developing different designs for housing these asymmetric CA membranes into modules (see section I-2-2-3). CA membranes dominated the market throughout the 1960s. During this period, practical experience revealed that these membranes have some properties that limit their applicability as follows :

- CA membranes are subject to hydrolytic attack at extreme pH and relatively high temperatures. This resulted in manufacturers recommending the use of the membrane between the pH limits of 4.0 and 6.0 and temperatures below 30 ^{o}C.
- CA membranes are susceptible to compaction which results in a gradual loss of membrane flux.

The search for alternatives to CA, led to the development of synthetic membranes with better properties. After several years, improved membranes did emerge : in 1970, aromatic polyamid (PA) membranes were introduced in the market [3]. The hydrolytic stability of these membranes was superior to that of CA membranes which enabled an extended pH operational range between 4.0 and 11.0. However, the PA membranes are considerably more sensitive to oxidising species such as chlorine. The ability of a

membrane to withstand exposure to chlorine is an important membrane property since chlorine is used extensively, as a disinfectant and bactericide where large amounts of water are processed, primarily because of its low cost and effectiveness.

In the mid 1970s, polymer chemists were successful in developing thin film composite (TFC) forms of polyamid membranes [4]. Compared with the CA and the PA membranes, the TFC membranes appear to exhibit superior performance on most counts : they could be operated over a much wider pH (3-11) and at higher temperatures (up to 50 ^{o}C). The membrane was also capable of operating at the high pressures (55 bar) required to overcome the osmotic pressure of sea water. Compaction resistance was also improved. However, like virtually all polyamid membranes, the early TFC were found to be extremely sensitive to the presence of free chlorine in solution. Since then, a number of other composite membranes, with a slightly enhanced chlorine resistance, have been introduced commercially. Among these, one of the most successful product appears to be the FT30 membrane, that is manufactured by FilmTec [5]. It is the characteristics and performance of this membrane that will be assessed in this study.

At the present time, although the TFC membranes have gained an appreciable market share, the technology of composite membranes is still developing rapidly and further advances in properties can be expected in the next few years. Currently a number of manufacturers are investigating ways of developing membranes that are chlorine resistant but still have the excellent properties of the non-cellulosic membranes, namely, high flux, excellent rejection, and wide range of operating pH and temperature capability. In this context, a variety of potential materials are being investigated including the development of novel, non-polymeric membranes such as ceramics [6].

As a final note, it should be recognised that although the importance of membranes to the RO process is obvious, membranes alone cannot be expected to function as an operational desalination equipment unless a means of housing it, in a properly designed module, are provided. The next section will introduce the basic requirements for such modules and details of those modules considered relevant to this work.

I-2-2-3- Reverse Osmosis Modules.

I-2-2-3-a- Introduction.

There are many problems and technical aspects to be considered in the development of R.O. devices. The main requirements and objectives of module design should include

the following :

1- Support the membrane against the high differential pressures (14 to 80 bar), and provide effective sealing between the feed and the permeate streams.

2- Good hydrodynamics, to minimise concentration polarisation effects.

3- Compactness, i-e high membrane packing density in order to maximise productivity per unit volume.

4- Low fouling tendencies and ease of cleaning.

Depending on the particular separation problem, one or other of the above aspects is of prime importance and consequently a number of different module configurations are available. However, for the desalination of brackish water and sea-water, which is more relevant to this work, two types of module have come to dominate the market. These are the hollow fiber (HF) and spiral wound (SPW) modules. Their success is associated with the fact that both modules are very compact, i.e. they have the largest membrane area for a given module volume. This characteristic is very important for large scale desalination applications where reduced module volume tends to lower costs and floor area requirements.

In this section, the basic design feature of these modules are described starting with the SPW modules.

I-2-2-3-b- Spiral Wound Modules.

Spiral Wound modules have been available since 1966 when the concept was developed by General Atomic Co. [7], now the Roga Division of Universal Oil Products Co (UOP). The basic design of module has changed little and now a number of American, Japanese and European manufacturers market essentially similar products.

Spiral wound modules, like the one illustrated in Fig.(2), are constructed from flat sheets of membranes. It consists of a sealed envelope of two membranes containing a porous material separating the two membranes, and of a feed brine spacer placed between successive envelopes. The envelope is sealed on three edges with the fourth edge sealed around a central perforated tube. The product water emerges through this tube and the envelope or leaf is rolled spirally around it.

The resultant spiral-wrap unit is fitted into a tubular pressure vessel. The pressurised feed solution flows axially through the brine spacer along the surface of the membranes. The product, which permeates through the membranes, flows into the porous material (or permeate spacer), flows spirally towards the permeate collector tube and out of the module.

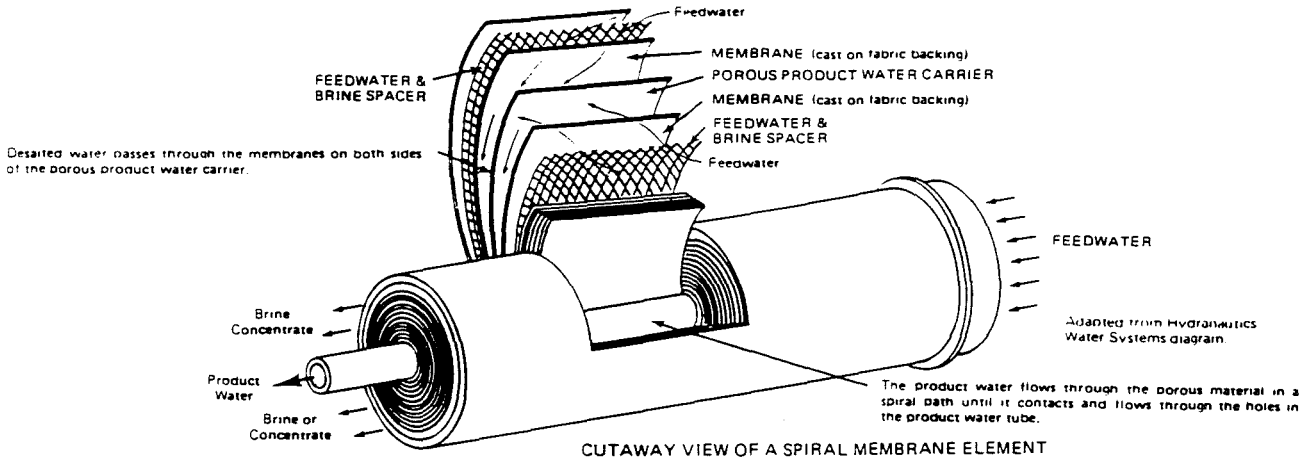

FIG.2: Spiral Wound Module Element (from Ref.34).

Many types of membrane material have been used in the spiral wound configuration-cellulose acetate, polyamid, composite etc. Spiral modules have membrane packing densities of the order of P_D=600 m^2/m^3 with fluxes range of about $7x10^{-4}$ cm/s. Also, the narrowness of the channels and the presence of the mesh result in the SPW module's being sensitive to the presence of large feed particles.

As a final word, it is considered that Spiral Wound systems account for about half the world's capacity in reverse osmosis. Broadly speaking the other half consists of hollow fibre systems which main characteristics will be introduced next.

I-2-2-3-c- Hollow Fibres Modules.

HF design was started in the early 1960's at Dow by using cellulose triacetate (CTA) fibres [8] and subsequent development followed with notably the introduction by DuPont of a series of non-cellulosic membranes including PA membranes [9].

In this design, several million hollow fibre membranes, almost as fine as human hair, are bundled together. Each fibre is a microscopic high pressure tube with an outside

diametre of 80-200 microns. Because the ratio of outside to inside diametre is, usually, of the order of 2 to 1, these fibres have the strength to resist the high pressures involved without the need for an additional support. Figure 3 illustrates the principle of a HF module. Its construction resembles that of a shell and tube heat exchanger. Millions of fibres are formed into a cylindrical bundle laid in parallel around a central feedwater distribution pipe and fixed in epoxy resin tube sheets at both ends. One of these blocks is then shaved off, exposing the open ends of the fibres through which the product water can then emerge. The central distribution pipe is sealed at one end and has a series of holes along its length to distribute the feed uniformly within the fibre bundle.

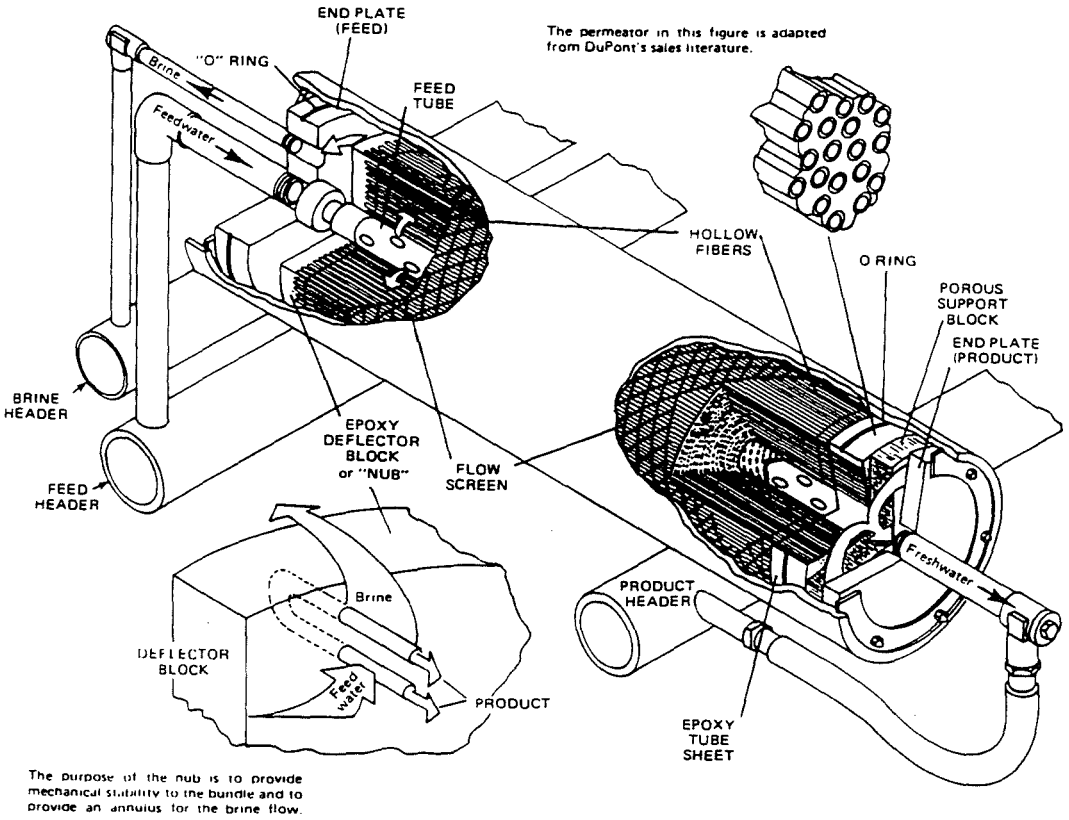

FIG.3: Hollow Fibre Module Element (from Ref.34).

Feed water under pressure enters one end of the module through the central distribution pipe , then flows radially outward across the fibres in the bundle. Part of it permeates through the fibre walls, under the high operating pressure, into the fibre bores and flows along the bores and out through the permeate discharge port of the module. The concentrated brine, emerging from the outer surface of the bundle, exits at the brine outlet.

The HF module is characterised by the highest membrane area per unit volume so far

developed. Indeed, membrane packing densities of the order of P_D=30,000 m^2/m^3 are obtained. However, HF membranes exhibit a relatively low flux at around $7x10^{-6}$ cm/s. Further, because of the high packing density of the fibres, the HF modules are very susceptible to particulate 'plugging' and hence flux decline ; consequently, to reduce the 'plugging', the feed water for HF modules requires an extensive pretreatment to remove the suspended and particulate matter prior to RO treatment.

I-2-2-3-d- Closure.

As a final note, it has been shown that both type of modules have similar characteristics. It was particularly seen that, although HF modules have the greatest packing density, their productivity per unit volume is not too far different from that of SPW modules. However, at the moment, there seems to be a trend towards the use of SPW modules because of the better performance that they offer in terms of fouling resistance, ease of maintenance and a broader range of industrial applicability. Further, the membrane fabrication technique is less difficult and thus less expensive.

I-3- Reverse Osmosis Theory.

I-3-1- Generalities.

After demonstration of the performance of the CA type membrane, a number of models were suggested to explain its high selectivity combined with a quite high water permeability. Unfortunately, despite the considerable amount of work on the subject, scientific understanding of the mechanism by which RO membranes separate solute from solvent is still incomplete : this is reflected, in the published literature, by the development of various membrane transport models, based on different possible mechanisms, which do not reveal a great deal of compatibility between them.

To date, two different categories of models, derived from two different approaches, are available. These are:

1- Models based on irreversible thermodynamics (I.T.), where no information on the mechanism of transport is needed.

2- Models based on some mechanism of transport.

In the I.T. models, the membrane is taken as a " black box" in which relatively slow processes occur near equilibrium. This method is particularly useful when flow coupling

exists between various species which are transported through the membrane. Indeed, the models evolving from I.T. are three parameter models characterising the membrane by water permeability, osmotic permeability and a third parameter which takes into account the coupling of the solute and solvent fluxes that takes place in the more open membranes. Of these I.T. models, one can mention the Kedem-Katchalsky [10] and the Spiegler-Kedem [11] models. An in depth description and discussion of the theory related to these models is found in reference [12].

In the following, the discussion will be restricted to the second type of models which are more pertinent to this work.

I-3-2- Review of Membrane Transport Models.

These models, being based on different membrane separation mechanisms, are therefore conceptually different and each of them provides its own specific set of insights into membrane function and the interactions between solute, solvent, and membrane. Among these models, the most important ones include:

- The solution-diffusion (SD) model.
- The solution-diffusion imperfection (SDI) model.
- The preferential sorption capillary flow (PSCF) model.
- The surface force pore flow (SFPF) model.

A brief description of each of these models is given below, starting with the SD model :

The Solution Diffusion Model

To date, for RO membranes, the most commonly used model is the SD model [13]. The model assumes that water and salt dissolve in the membrane and diffuse through the membrane in an uncoupled manner. Further, it assumes the membrane to be non-porous so that pore flow does not exist. In this context, Banks and Sharples [14] have shown that the contribution of pore flow to both salt and water transport is negligible. This model gives the following relationships for the solvent and solute fluxes respectively :

$$J_1 = k_1(\Delta P - \Delta\Pi) \qquad (1\text{-}1)$$

$$J_2 = k_2 (C_{BW} - C_{PW}) \qquad (1\text{-}2)$$

The value of k_1 in eq.(1-1) is dependent on : membrane material, operating temperature, feed composition and membrane thickness. It may also be thought of as the hydraulic resistance of the membrane. In the absence of membrane compaction k_1 remains constant at constant temperature. The salt transport coefficient, k_2, in eq(1-2) may be thought of as a measure of salt leakage through the membrane. This model has proved to be reasonable when one deals with very dense membranes and solutes which are almost totally rejected.

The Solution Diffusion Imperfection Model.

The SDI model is similar to the SD model, with the inclusion of terms to account for pore flow of solute and solvent [15]. Mathematically, this is represented by:

$$J_1 = k_1(\Delta P - \Delta\Pi) + k_3 \Delta P \qquad (1\text{-}3)$$

$$J_2 = k_2(C_{BW} - C_{PW}) + k_3 C_{BW} \Delta P \qquad (1\text{-}4)$$

The constants k_1 and k_3 are generally a function of concentration and pressure. The model is expected to describe the performance of imperfect membranes.

The Preferential Sorption Capillary Flow Model.

The PSCF model was put forward by Sourirajan [16]. This model assumes that one species (usually the solvent) is preferentially adsorbed at the membrane-solution interface. The solution which passes through the membrane derives from this interfacial layer. The equations for solvent and solute flow are identical to those of the SD model. Briefly, in this model, viscous flow for water transport and pore diffusion for solute transport are involved. However, water is preferentially adsorbed onto the pore walls and salt is rejected at the surface for physicochemical reasons.

The Surface Force Pore Flow Model.

The SFPF model was proposed by Matsuura et al [17]. It clarifies the major role of the interactions between solute, solvent and the membrane pore wall in the separation process. It includes the average pore size and the pore size distribution and predicts the effect of the interaction forces and the pore size distribution on RO performance. Indeed, it involves the balance of forces inside the membrane pores to get the fluid velocity profile, which is dependent on pore radius and solute concentration.

All of the above mentioned membrane transport models need to be coupled with a

concentration polarisation model. This latter should describe the mass transport within the concentrated boundary layer in the vicinity of the membrane surface. One such model, which has been widely used in the literature, is the film-theory model. The following section outlines the basis of this theory.

I-3-3- The thin-film theory.

As mentioned briefly in section I-2-1, concentration polarisation (CP) is inevitable in RO because selective transport through the membrane causes accumulation of solutes at the solution-membrane interface. This accumulation increases until the back-diffusion, caused by the concentration difference, balances the convective flow of salt to the membrane and that which permeates through the membrane. It is well known that CP affects membrane performance in terms of the separation efficiency, limiting flux and encouraging fouling. To describe CP, relationships, between the concentrations C_B (in the bulk) and C_{BW} (at the membrane surface), the flux and the parameters of fluid flow in the channel near the membrane, are needed. A useful approach to this problem is the application of the relatively simple film theory for the concentration boundary. Fig.4 is a schematic of the boundary layer formation.

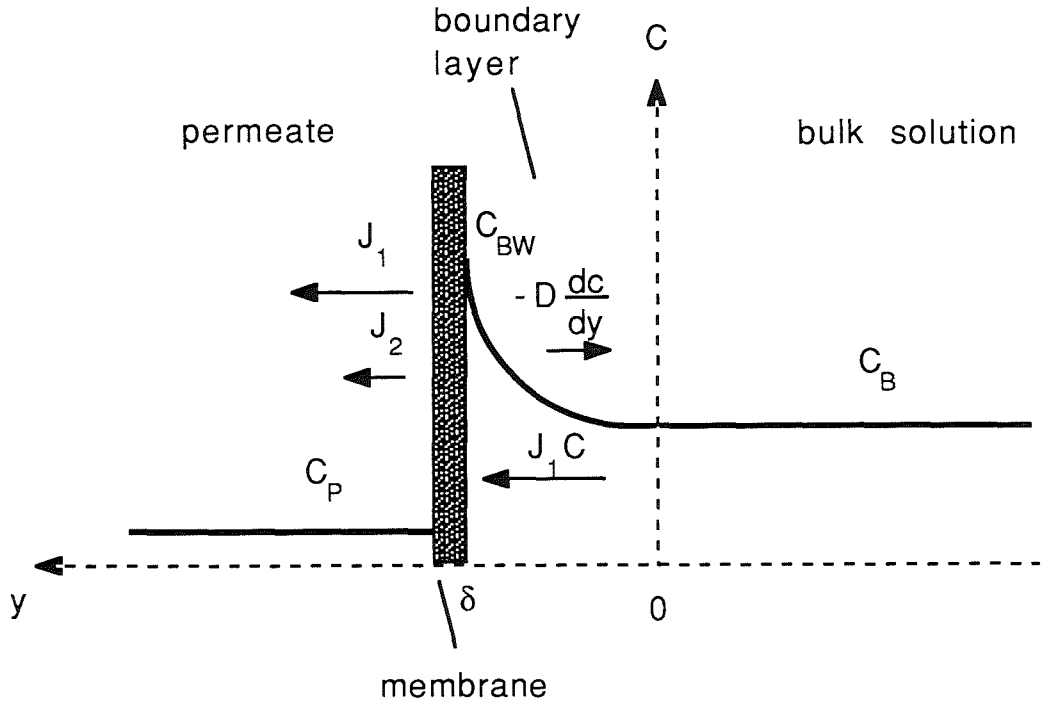

FIG.4: Concentration profile near the membrane surface and schematic of the film-theory model.

The basic assumptions of this theory are as follows:

1- The boundary layer is considered to be a stagnant thin liquid film which separates the membrane surface from the bulk flow.

2- The bulk flow is assumed to be so turbulent that concentration gradients are absent.

3- Longitudinal (parallel to the membrane) mass transport within the film is assumed negligible. Therefore, mass transport within the film may be considered to be one-dimensional.

With a steady state established, the salt flux is determined by the following differential equation :

$$J_2 = J_1 C_P = J_1 C - Ds\frac{dC}{dy} \qquad (1\text{-}5)$$

The boundary conditions applicable in this case are :

$$\text{(i) } C = C_B \quad \text{at } y = 0$$
$$\text{(ii) } C = C_{BW} \text{ at } y = \delta \qquad (1\text{-}6)$$

where δ is the boundary layer thickness.
Solving the simple differential eq.(1-5) with the above boundary conditions yields :

$$\frac{C_{BW} - C_P}{C_B - C_P} = \exp\left(\frac{J_1}{k}\right) \qquad (1\text{-}7)$$

where the mass transfer coefficient, k, is defined as follows:

$$k = \frac{Ds}{\delta} \qquad (1\text{-}8)$$

Note : In the above theory, a number of simplifying assumptions known to be incorrect, were included. However, the effect of these assumptions upon the film-theory

predictions are often found to be small. For example, the assumption, that longitudinal mass transport within the boundary layer is negligible, is not rigorously true since the magnitude of the transfer between the wall and the bulk varies somewhat with the manner in which the flux varies with the longitudinal position.
But on the whole such effects are quite small in turbulent flow, and for mass transfer at high Schmidt numbers, such as those of aqueous salt solutions, the concentration boundary layer is generally so thin relative to the dimensions of the bulk fluid that the effect of longitudinal mass transport within the boundary layer is indeed quite small.

I-4- Closure.

In this chapter, a general overview on different aspects of the RO process was given. The next chapter will deal with a critical review of the research work published so far in the literature and will underline the major objectives of the present work which was instituted to remedy the deficiencies of the previous investigations.

CHAPTER TWO

LITERATURE SURVEY AND SCOPE OF RESEARCH.

II-1- Literature Review.

II-1-1- Introduction.

The interest in RO is reflected by the extensive literature on the subject which has appeared over the past two decades. Much of this work was aimed at developing mathematical models for the prediction of module performance which, in turn, may be used to improve the hydrodynamic and optimal module arrangements. This is illustrated through both approximate and rigorous approaches. Approximate analyses have, generally, been formulated from analytical solutions where simplifications are often adopted to make the problem mathematically tractable. The more rigorous treatments, are usually in the form of more complex models which dictate numerical solutions, but tend to be more accurate. Here, consideration will be restricted to the case of SPW modules. A brief review of the most important investigations to date is presented below, starting with the analytical studies.

II-1-2- Review of Analytical Investigations.

In RO, because of the presence of concentration polarisation, the expressions for the solute and the solvent fluxes are not of the explicit type. Indeed, the solvent flux expression is a function of the brine wall solute concentration which in turn is a function of, among others, the solvent flux itself. Under such conditions, any attempt to find an analytical solution without resorting to simplifications and suitable assumptions would seem hopeless. In this context, several analytical studies have been performed all of which are limited, to some extent, by the nature of the assumptions on which they are based. Although these studies may result in solutions that have restricted practical value, they do, however, provide a basis for first approximations which may be used to speed up, more precise, numerical solutions.

Sirkar et al [18] developed analytical design equations for SPW modules. They derived explicit equations for calculating the membrane length and permeate solute concentration of SPW modules equipped with almost perfect rejecting membranes under both turbulent and laminar flow conditions. This was achieved after introduction of a numerical approximation for the concentration polarisation relationship. Indeed, by

applying the stagnant film model to a high rejecting membrane (i-e negligible permeate concentration), the following expression was obtained :

$$C_{BW} = C_B \, e^{(J_1/k)} \qquad (2\text{-}1)$$

By expanding the exponential term and truncating the resulting expression after the second term, they obtained the following approximation:

$$C_{BW} = C_B[1 + \frac{J_1}{k} + \left(\frac{J_1}{k}\right)^2 \frac{1}{2!}] \qquad (2\text{-}2)$$

They stated that this procedure does not cause a significant error in the wall concentration, C_{BW}, under normal operating conditions.

Prasad and Sirkar [19] have developed a similar procedure for multi-solute feeds under the same conditions and assumptions with the exception that they assumed the mass transfer coefficient as constant owing to the relatively low recoveries that, according to them, are pertinent to SPW module applications.

At this stage, it should be noted that in all of the above treatments [18,19] the effect of frictional pressure loss along the channels is neglected. However, in high brackish water applications where low pressure operation is practiced to conserve energy, such frictional pressure loss may become important.

Evangelista [20], using the SD model, developed an analytical design procedure for high rejecting membranes which took into account the two-dimensional nature of the process. His method predicts the permeate flow rate and concentration as well as the pressure drops in both the brine and permeate channels. In his analysis, he dealt with the concentration polarisation effects by assuming a constant reduction of the permeate flux which was derived from an earlier investigation [21]. The resulting approximate expression for the net driving force took the following form :

$$\Delta P_{eff}(x,y) = \frac{[P_B(x,y) - P_P(x,y) - \Pi_F]}{1 + (k_1 \Pi_F / k)} \qquad (2\text{-}3)$$

It was stressed that this assumption becomes less valid if the module length increases, the feed concentration increases and the applied pressure decreases. He compared his results with Taniguchi's [29] experimental data and found that the agreement was very satisfactory for all operating conditions. However, at this point it should be noted that the reported data refer to low pressures and concentrations.

Evangelista and Jonsson [22] extended the applicability of the above analysis to looser (less rejecting) membranes by incorporating a three parameter transport model instead of the solution diffusion model. In addition, they derived explicit equations for the design of SPW modules with constant and tapered permeate channels. From their analysis, explicit relationships for the evaluation of optimum brine and permeate channel thickness were proposed.

In summary, it can be seen that while some analytical methods [18,19] may result in solutions that have limited practical value, others [20,22] do provide some basis for fast estimation of the process efficiency or for preliminary optimisation purposes. However, for module refinement and optimisation more exact design procedures are required. In this context, numerical schemes are more appropriate.

II-1-3- Review of Numerical Investigations.

In recent years, a number of numerical modelling approaches have appeared. Some of these will be presented in this section.

Chiolle et al. [23] discuss a calculation procedure for a SPW module with a turbulence promoting net. In their model, the problem was made one dimensional by neglecting, notably, the permeate side pressure drop. For the mass transfer coefficient, they use a correlation established by Winograd et al.[24]. Another limitation of their model was the assumption of a constant rejection coefficient, R. A constant value of the rejection implies that the solute transport parameter k_2, as defined in the Solution-diffusion transport model, is decreasing with the increase in brine wall concentration C_{BW}, which is highly unrealistic. Therefore, it is seen that this assumption is likely to introduce a significant error in the evaluation of the permeate concentration especially at high recoveries.

Rautenbach and Dahm [25] developed a mathematical model in which a particularly doubtful assumption was made in that concentration polarisation (CP) was neglected. This does not correspond with real situations. In fact, it is well known that one of the

limiting factors in the performance of RO is concentration polarisation. Despite this, the authors tested the accuracy of their mathematical model with the experimental data of Taniguchi [29] and an excellent agreement with their prediction was found. The mean relative error was about 2.5% for the recovery and about 6.5% for the salt passage. One plausible explanation for this relative success could be associated with both the dilute feed solutions (less than 2,000 ppm) and low feed pressures (less than 36 bar) that were used in Taniguchi's experiments.

Recently, Evangelista and Jonsson [26] developed an improved numerical model with fewer and less controversial assumptions. Indeed, they do consider concentration polarisation effects by incorporating the thin film theory combined with a published mass transfer coefficient correlation [24]. However, they did not attempt to validate their model with experimental data. Instead, they chose to perform parametric studies in order to investigate optimum module geometrical characteristics for given operating conditions.

An interesting study can be found in the work of Shock and Miquel [27] who presented some experimental data for pressure drop and mass transfer characteristics of several commercially available SPW modules. The friction coefficient for the different channels were correlated in terms of the Reynolds number. For the brine channel, they found that, despite the differences in thickness and mesh types experimented, its friction coefficient can be described by one single expression, i-e :

$$\lambda_B = 6.23\ Re_B^{-0.3} \qquad (2\text{-}4)$$

For the permeate channel, they pointed out the difficulty in collecting reliable data on actual SPW modules. This resulted in experiments being performed with different permeate spacers in flat channels. Unlike the brine case, they found that the permeate friction coefficient was, to some extent, specific to the type of permeate spacer tested. They proposed the following relationship :

$$\lambda_P = a\ Re_P^{-0.8} \qquad (2\text{-}5)$$

where the constant "a" differed according to the type of spacer used.

Their mass transfer measurements were done in spacer filled channels owing to the difficulty in realising them in real SPW modules. Despite that they did not examine all the factors affecting the mass transfer coefficient, their preliminary experimental results

suggested that the mass transfer coefficient could be independent of both the membrane and the brine spacer type. Additionally, they performed a simulation and optimisation analysis using a computer program of which details were not revealed. As a conclusion of their work, they claimed that the efficiency of available SPW modules can be significantly enhanced by modifying the spacer materials.

A common feature of these studies was that they considered the SPW module as unwound, i-e the module was assumed to consist of two flat spacer filled channels. This model has generally been termed as the "Slit" (SL) model. Possible weaknesses of this model are identified below and a different approach is adopted in this work.

II-2- Aim of Present Work.

A review of the published literature indicates that the problem of SPW module performance prediction has been given considerable attention and that many attempts at an accurate mathematical solution have been presented [23,25,26]. However, one of the major difficulties in validating the models proved to be the lack of comprehensive operating and experimental data. In the event, all comparisons that have been made have used Taniguchi's experimental work on the Roga type module [29]. This data was limited to those pressures and feed concentrations typically encountered in brackish water desalination. Indeed, it was taken from experiments where the maximum feed concentration and pressure were about 2000 [ppm] and 36 [bar] respectively. Although this data has, in practice, provided a useful comparison for brackish water situations, it is, however, not suitable for ascertaining the validity of correlations describing important phenomena such as concentration polarisation (CP). An element of evidence which would reinforce this observation could be found in Rautenbach's model [25]. The fact that Rautenbach obtained very satisfactory predictions, with a model which neglects concentration polarisation, suggests that, at such low feed concentrations and operating conditions, concentration polarisation does not have a very significant effect.

Further, the implications which result from the physical model adopted, i-e the SL model, may affect the predictions at the more severe feed conditions. In particular, as it will be shown in chapter III, the application of the Slit model results in a symmetry of the concentration profiles on either sides of the brine channel which does not occur in reality. From this, it can be speculated that the predictive accuracy of the Slit model would tend to decrease as the solvent recovery increases.

Therefore, a major question that remains is whether the models developed in the

earlier studies are valid at the elevated pressures and high feed concentrations specific to sea water desalination where concentration polarisation is significant.

In this work an attempt is made to address the above problem by developing improved models of SPW modules and assessing their validity against new experimental data covering a wide range of operating conditions including seawater feeds. Two different modelling approaches were used :

- The first one is a Slit model, but, unlike previous studies, it takes into account all of the following:-

(i)- Membrane and fluid properties variation with operating conditions.
(ii)- Pressure drops in both channels.
(iii)- Concentration polarisation.

- In the second, a more rigorous approach was adopted in which the spiral element is modelled in three dimensions. This model, has been named the "Spiral Model", denoted by SP. It overcomes the restriction of a symmetrical concentration profile implicit in the Slit model.

The differential equations involved in both models have to be solved numerically (using a finite difference (FD) technique) and are incorporated in two computer programs. Extensive experimental data is used to assess the validity of the models. This data originated from experiments performed on two different types of SPW modules. These were the Roga-4160HR [29] and the Filmtec FT-30SW2540 [28] which provide data typical of brackish and sea water desalination respectively.

Since we are concerned, in this work, with tight membranes, we have chosen to use the solution-diffusion model to represent the transport mechanism through the membrane.

Apart from the task of developing the two mathematical models, other objectives of this work were concerned with the following :

- Compare the results with experimental data in order to validate and/or determine the range of the models applicability.

- Assess the effects of the spiral geometry of the SPW element by analysing the

outputs from both programs.

- Examine the effect of operating variables on module performance.

- Evaluate the influence of various key geometrical parameters on module performance and to provide a means of module optimisation.

CHAPTER THREE

MATHEMATICAL MODELS.

III-1- Description of the problem.

The mathematical treatment of the fluid dynamics in a spiral wound module is very complicated because the velocities, pressures and concentrations profiles in the brine and permeate channels are three dimensional. In addition, the coupling between feed and permeate, by the flow through the membrane, results in a further complication: as a consequence of the permeate flux, the pressure as well as the mean velocity and concentration will vary along the membrane surface on the feed-side. Qualitatively the major events that take place, during the flow of the feed solution through SPW modules, are as follows :

a)- A decrease of the transmembrane pressure difference resulting from the frictional pressure drop in the brine channel which tends to decrease the permeate flux.

b)- An increase of the mean concentration of the feed solution which has the consequence of increasing the osmotic pressure and thus tending to decrease the permeate flux.

c)- A decrease of mean brine velocity thereby tending to increase concentration polarisation which tends to decrease the permeate flux and increase the salt flux.

With regard to the complexity of the phenomena involved, the need to simulate and predict the performance of a SPW element, realistically and accurately, is very great. In response, it was seen in Chapter II that the literature of the subject has grown rapidly and in a somewhat incomplete way. Therefore, it is hard for anyone to form a correct judgement as to :

- capabilities of current prediction procedures.
- the nature of the limitations of these capabilities and
- in what direction practical research can make a useful contribution.

This chapter deals with the development of the two models of spiral would element operation.

III-2- Modelling Approach.

III-2-1- Introduction.

The development of a mathematical model which has flexibility and is sophisticated enough to account for all the effects taking place during SPW modules operation is problematic. Therefore, the first problem is to implement a physical model which, with the aid of some approximations and assumptions, will render an analysis tractable without affecting seriously the accuracy of the calculations. Such physical model will form the basis for the formulation of the governing differential equations describing the water and salt transport throughout the membrane and element. The second problem is that of providing a suitable numerical technique and of programming the calculations on a computer to obtain a solution to the problem. These various aspects will be examined in details through this chapter.

III-2-2- Physical Models and Present Contribution.

In this work, two different physical models, which will consequently generate two mathematical models, were adopted. The first one, termed "Slit" (SL) model, is similar to that used by previous authors [25,26]. The uncertainties resulting from the simplicity and the many approximations made in previous analyses based on the SL model call for an improved analysis. One of the goals of this work is to produce a more precise analysis based on the Slit model. A further goal is to to develop a new model, the "Spiral" (SP) model, upon which a more realistic analysis may be based. As its name reveals, this latter model is represented by the SPW element itself.

Qualitatively, the usefulness of the proposed model can be determined in the following way : the Spiral model does relax one of the critical assumptions resulting from the adoption of the SL model. The situation is depicted in Fig.5 where a restricted portion of both models is sketched. It is clearly seen that a specific weakness of the SL model lies in the concentration variation along the brine channel which in turn affects the membrane permeability. Indeed, Fig.5a shows that the application of the SL model would imply that, at a given brine location, the values of the permeate pressure on either side of the brine channel are equal. This would result in a symmetry of the brine wall solute concentration which does not correspond to the real case (Fig.5b).

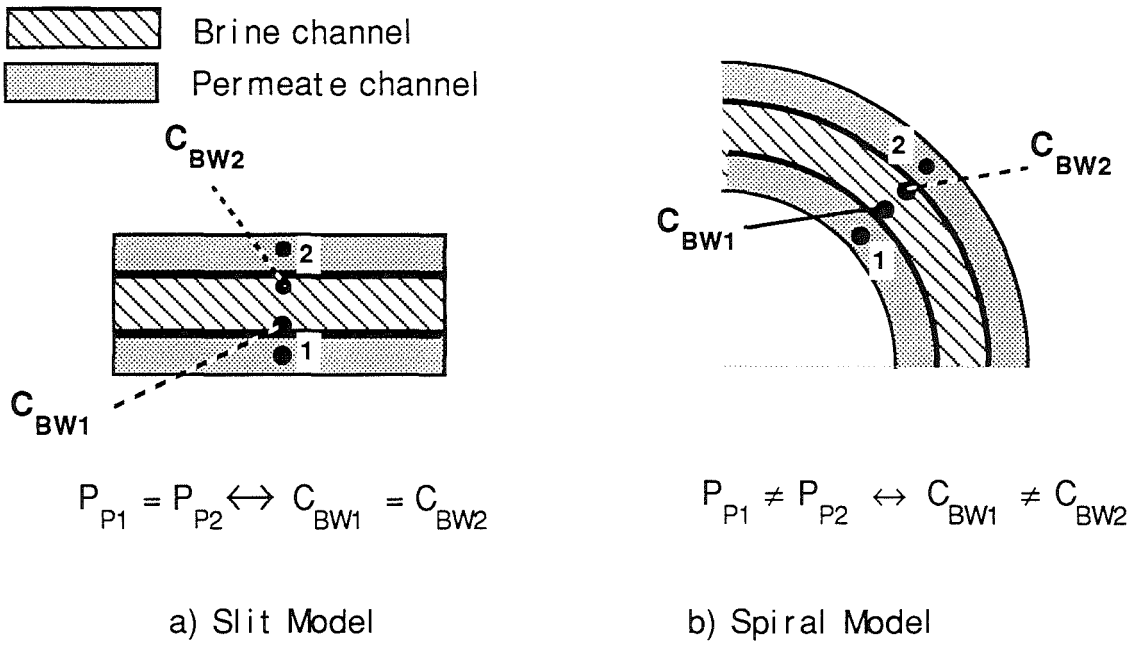

FIG.5: Comparative sketches of Slit and Spiral Models.

The improved prediction method would be one that accurately predicts concentrations and flow rates at any point in the module (Fig.5b). It is our opinion that the spiral model would account for pressure and concentration changes in the brine as well as in the permeate flow since in its physical concept the SP model does represent the spatial distribution as realistically as possible. To the best of our knowledge, to date, no one has ever attempted this approach.

However, it was felt that, the difficulties associated with making the SP model emphasise the need to establish confidence in a numerical procedure which could be best tested, at a preliminary stage, on a simpler model such as the SL model. This can be done by comparing the SL model predictions with brackish water published data as was customary in the published literature. In addition this would allow an investigation related to the extent of the SL model validity when applying sea water data which will be provided in this work. Finally, some form of comparative exercise for the merits of the two models would seem desirable.

Therefore, for all the above reasons, it was decided to develop both models. Their formulation will be introduced in the following section.

III-3- Mathematical Formulation of the Models :

A reasonable modelling of the SPW modules must be based on the momentum and material balances formulated, in differential form, for the feedside and for the permeate-side together with reasonable boundary conditions and assumptions. These different aspects of the modelling approach will be introduced.

III-3-1- Assumptions and Approximations.

Due to the complexity of the SPW process, alluded to in the previous sections, one must start with the formulation of reasonable approximations and assumptions which simplify the mathematical treatment of the problem.

The assumptions, on which the developement of both models were based include:

1- Negligible component of the brine and permeate flow velocities in the radial and axial directions respectively.

2- The volumetric flow through the membrane consists mainly of the solvent flux.

3- For the calculation of the mass-transfer coefficient in channels equipped with a spacer the following relationship, which is in agreement with experiments reported in [20,23], has been assumed:

$$k=0.753\left(\frac{KB}{2-KB}\right)^{1/2}\frac{D_s}{h_B}\,Sc^{-1/6}\left(\frac{Pe\,h_B}{MB}\right)^{1/2} \qquad (3\text{-}1)$$

where the constants KB and MB depend on the characteristics of the brine spacer and those reported in [23], i-e KB=0.5 and MB=0.6 (cm), have been kept in this study.

4- Validity of the Darcy's Law for the pressure drop in porous media.

5- The pressure drop along the central permeate collector tube is neglected (i-e pressure considered as atmospheric).

6- Validity of the Solution diffusion transport model.

The above assumptions are unlikely to be a major source of errors in the calculations for the following reasons :

Assumptions 1 and 5 are very reasonable and, therefore should not affect, crucially, the accuracy of the results.

Assumptions 2 and 6 are quite realistic since practical RO is usually carried out with membranes having a high solute rejection. In such cases the solution-diffusion model, a two parameter model, provides a suitable description of the mass transport through the membrane.

Assumption 4 was made to allow for the calculation of the pressure losses in both the brine and the permeate channels. In this regard, it must be said that the Darcy relation is more appropriate for the permeate channel which is in fact a porous spacer. The brine channel is not a porous spacer but a turbulence promoting net the main roles of which are to act as a spacer and to increase mass transfer.

In assumption 3, the choice of this particular equation for the mass transfer coefficient was due to the fact that it takes into account the fundamental characteristics of the mesh spacer in a fairly simple manner, i-e : mesh size MB, mixing coefficient KB, channel thickness h, as well as the usual fluid dynamics and physical properties of the solution (Pe and Sc). However, although eq.(3-1) seems to be accepted by a majority of workers in the field of SPW reverse osmosis, it should be emphasised that, to the best of our knowledge, its validity has never been tested against sea water data. Therefore, an examination of the extent of its applicability will be performed.

Note: Eventually, additional assumptions, pertinent to the particular model considered, will be presented as the analysis goes along.

III-3-2- Formulation for the Slit Model.

In this model, as shown in Fig.6, a SPW membrane is simply conceived of as two parallel flat channels. In other words, the curvature of the channels has been neglected. This assumption is justified because the ratio of the channel height to mean module diameter is small.

Using the previously listed assumptions, the differential solvent and solute material balances for both channels are as follows :

- Permeate Channel :

* Darcy's Law :

$$\frac{\delta P_P(x,y)}{\delta x} = -\mu\ E_P\ V_P(x,y) \qquad (3\text{-}2)$$

* Solvent material balance :

$$\frac{\delta V_P(x,y)}{\delta x} = 2\,\frac{J_1(x,y)}{h_P} \qquad (3\text{-}3)$$

* Solute material balance :

$$\frac{\delta C_P(x,y)}{\delta x} = \frac{2\left(J_2(x,y) - C_P(x,y)\ J_1(x,y)\right)}{V_P(x,y)\ h_P} \qquad (3\text{-}4)$$

Similar expressions for the brine channel are obtained as follows :

* Darcy's Law :

$$\frac{\delta P_B(x,y)}{\delta y} = -\mu\ E_B\ V_B(x,y) \qquad (3\text{-}5)$$

* Solvent material balance :

$$\frac{\delta V_B(x,y)}{\delta y} = -\,2\,\frac{J_1(x,y)}{h_B} \qquad (3\text{-}6)$$

* Solute material balance :

$$\frac{\delta C_B(x,y)}{\delta y} = 2\,\frac{J_1(x,y)}{V_B(x,y)\ h_B}\left(C_B(x,y) - C_P(x,y)\right) \qquad (3\text{-}7)$$

III-3-3- Formulation for the Spiral Model.

In addition to the assumptions mentioned in section III-3-1, a further assumption, which offers convenient mathematical simplification without compromising the essential nature of the problem, has been introduced : although the geometry is spiral, the

differential equations governing the phenomena have been taken in cartesian coordinates.

Here, equations (3-2) and (3-5) of the SL case are still applicable for the SP model, but the solvent and solute balances are modified to take account of the geometry as well as the non symmetry of the model. In this regard, subscript index notations are used whose meaning is described in Fig.5.

Starting with the permeate channel, we have :

* Solvent material balance :

$$\frac{\delta V_P(x,y)}{\delta x} = \frac{J_{11}(x,y) + J_{12}(x,y)}{h_P} \qquad (3\text{-}8)$$

* Solute material balance :

$$\frac{\delta C_P(x,y)}{\delta x} = \frac{1}{V_P(x,y)\ h_P} * \left[\left(J_{21}(x,y) + J_{22}(x,y)\right) + C_P(x,y)\left(J_{11}(x,y) + J_{12}(x,y)\right)\right] \qquad (3\text{-}9)$$

Likewise for the brine channel,

* Solvent material balance :

$$\frac{\delta V_B(x,y)}{\delta y} = -\frac{\left[J_{11}(x,y) + J_{12}(x,y)\right]}{h_B} \qquad (3\text{-}10)$$

* Solute material balances :

$$\frac{\delta C_B(x,y)}{\delta y} = \frac{1}{V_B(x,y)\ h_B} * \left[-\left(J_{21}(x,y) + J_{22}(x,y)\right) + C_B(x,y)\left(J_{11}(x,y) + J_{12}(x,y)\right)\right] \qquad (3\text{-}11)$$

III-3-4- Initial and Boundary Conditions.

The initial and boundary conditions, applicable for both models, are set as follows:

- Permeate Flow :

$$P_P(x,y) = P_{atm} \quad \text{for } x=W \text{ and } 0 \le y \le L \qquad (3\text{-}12)$$

$$V_P(x,y) = 0 \text{ for } x=0 \text{ and } 0 \le y \le L \qquad (3\text{-}13)$$

$$\frac{\delta P_P(x,y)}{\delta x} = 0 \text{ for } x=0 \text{ and } 0 \le y \le L \qquad (3\text{-}14)$$

$$\frac{\delta C_P(x,y)}{\delta x} = 0 \text{ for } x=0 \text{ and } 0 \le y \le L \qquad (3\text{-}15)$$

- Brine Flow:

$$V_B(x,y) = V_F \text{ for } y=0 \text{ and } 0 \le x \le W \qquad (3\text{-}16)$$

$$C_B(x,y) = C_F \text{ for } y=0 \text{ and } 0 \le x \le W \qquad (3\text{-}17)$$

$$P_B(x,y) = P_F \text{ for } y=0 \text{ and } 0 \le x \le W \qquad (3\text{-}18)$$

At this stage, it should be noted that, while the conditions related to the brine flow (i-e eqs.(3-16) to (3-18)) are straightforward to derive, the ones concerned with the permeate flow are less obvious and, perhaps, need some explanation. Conditions (3-12) to (3-15) are a sequence of logical facts as follows :

- Condition (3-12) results from assumption 5 (see section III-3-1) which states that the pressure drop in the permeate collector tube is neglected. Therefore, the permeate pressure, at the open end of the membrane, is equal to the atmospheric pressure.

- Condition (3-13) is rather obvious and indicates that the permeate velocity at the closed end of the membrane is nil.

- Condition (3-14) follows from condition (3-13) and eq.(3-2).

- Finally, condition (3-15) results from a combination of condition (3-14) and the fundamental equations of the transport model (i-e eqs(3-19), (3-20) and (3-21)) which will be presented next.

III-3-5- Auxiliary Equations.

In addition to the above equations, the analysis is based on the solution-diffusion model (assumption 6) which is widely used in R.O. literature. This model gives the following relationships, valid locally at any point in the system, for the solvent and solute fluxes respectively :

$$J_1 = k_1 \left[(P_B - P_P) - (\Pi_B - \Pi_P) \right] \qquad (3\text{-}19)$$

$$J_2 = k_2 (C_{BW} - C_P) \qquad (3\text{-}20)$$

Assuming a linear relation between osmotic pressure and concentration of the form

$$\Pi_i = b\, C_i \qquad (3\text{-}21)$$

where : $b=f(C_i,T_i)$ and obtained through a combination of a correlation giving the variation of the osmotic pressure with both concentration and temperature (see eqs.(A-3) and (A-4) in Appendix A).

Eq.(3-19) becomes :

$$J_1 = k_1 \left[(P_B - P_P) - b\, (C_{BW} - C_P) \right] \qquad (3\text{-}22)$$

Since the concentration of the permeate is determined by the relative amounts of J_1 and J_2 fluxes, C_P may be evaluated through the following formula :

$$C_P \approx \frac{J_2}{J_1} = \frac{k_2 (C_{BW} - C_P)}{J_1} \qquad (3\text{-}23)$$

For the concentration polarisation relationship, the stagnant film model proposed in Sourirajan [7] is adopted :

$$\frac{C_{BW} - C_P}{C_B - C_P} = \exp\left(\frac{J}{k}\right) \qquad (3\text{-}24)$$

III-3-6- Closure.

The above basic equations, i-e balances combined with the transport equations, represent a complete system. There are, however, no simple means of reducing it by elimination because of the complications that arise as many of the parameters involved cannot be expressed explicitly and are mutually interrelated. Therefore, one must solve these equations approximately using a numerical technique. In this work, a discrete finite difference (FD) approach is used.

III-4- Finite Difference Formulation.

The numerical method will be developed from basic principles keeping the procedure as simple as possible. In this work, the numerical technique of Finite Differences is adopted. Such techniques are described in numerous references; see, for example ref.[31].

The first step in any numerical treatment is to cover the physical models by a discrete number of node points. Figs.6 and 7 show the grid layout for the SL and the SP models respectively. The next steps consists in writing the governing equation in a discrete form in terms of values at node points and generating a numerical solution algorithm. This last aspect will be discussed in detail in the next section. In this section, we will focus our attention on the formulation of the differential equations in equivalent Finite Differences form. At this stage, it should be noted that, for the sake of simplicity of presentation, only those equations relevant to the SP model will be considered. This is because the basic numerical approach is similar for the two programs despite that, as seen in III-2-2, their different physical considerations do directly bear on the establishing of a proper mathematical hydrodynamic framework.

Before introducing the Finite Differences form of the governing equations, it is very instructive, at this point, to compare and to comment on the effect of the grid points layout involved in the discretisation of the two models. It is known that, in general, an accurate

solution can be achieved only when the grid points spacing is sufficiently fine. However, it should be recognised that, in order to realise substantial savings in computer time and storage, there is no need to employ a very fine grid in regions where the different process variables change rather slowly. Therefore, the grid points spacing should be directly linked to the way these variables change in the calculation domain by using, for instance, adaptative mesh refinement methods.

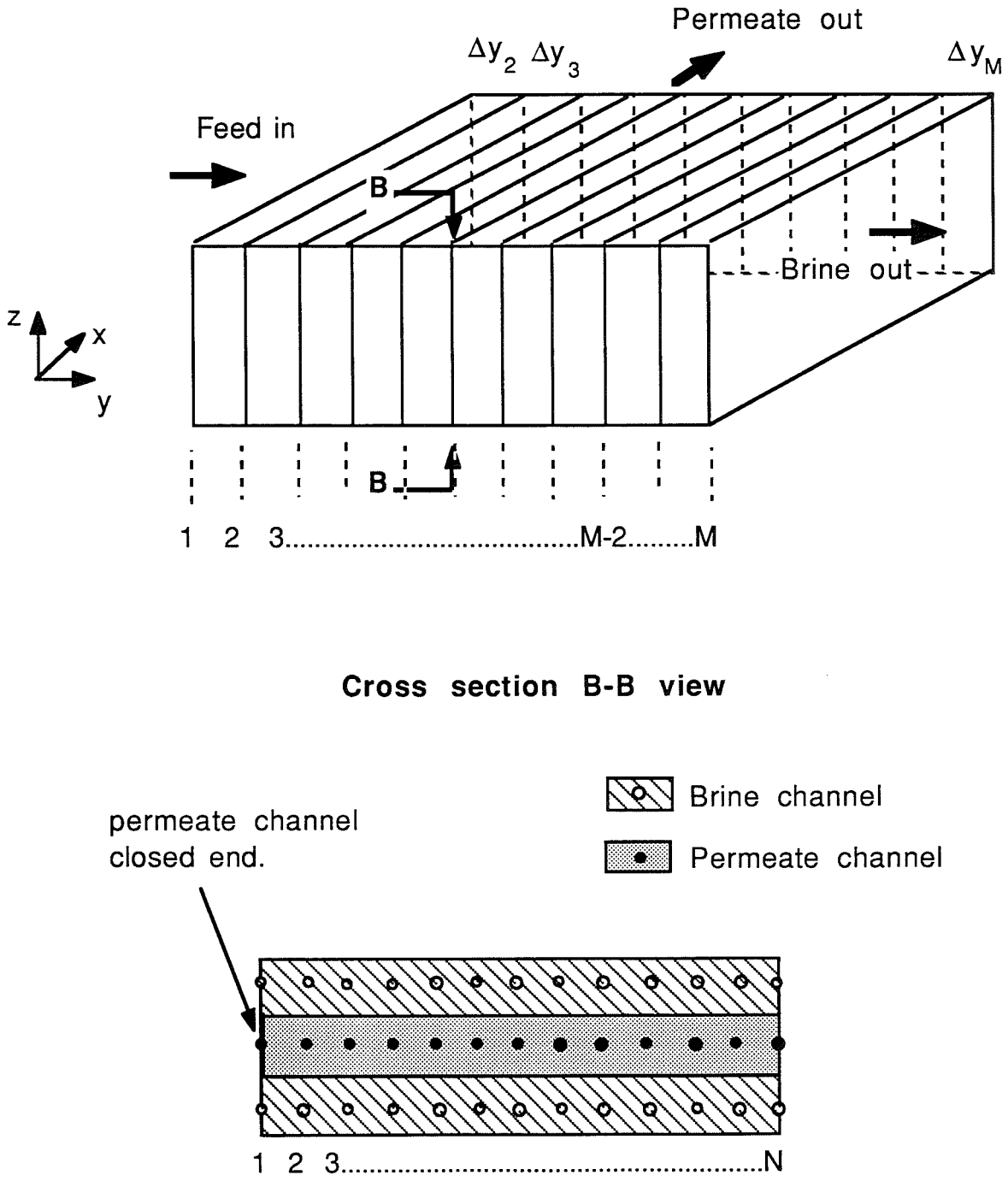

FIG.6 : Grid Layout for Slit Model.

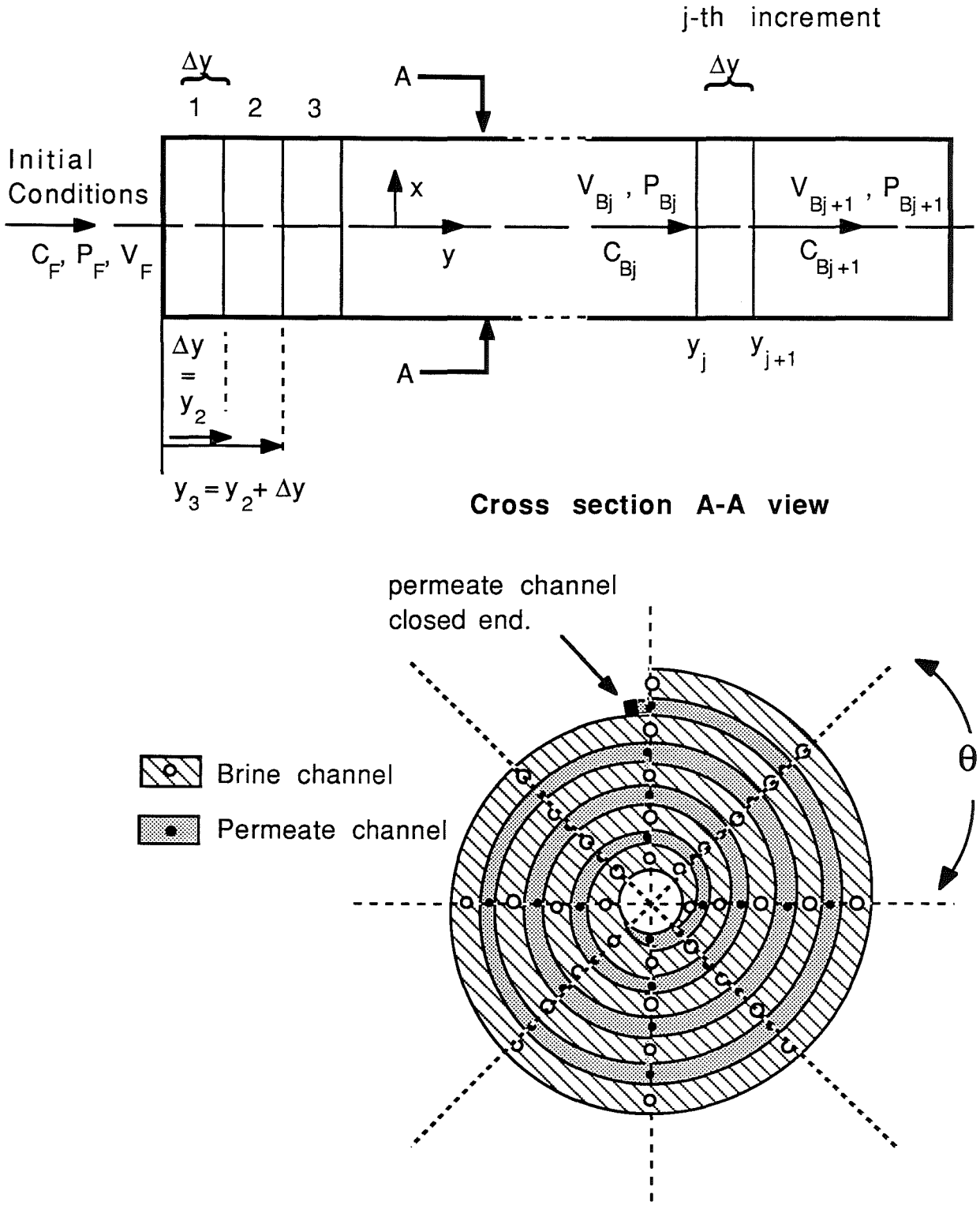

FIG.7 : Grid Layout for Spiral Model.

The SP model presented does not require such mesh refinement technique. Indeed, as shown in Fig.7, due to the incremental angle, a finer grid spacing is provided where it is needed most i-e as the membrane open end is approached where the variation of the

different process variables is expected to be steeper.

Having mentioned that, the question now arises as to which finite difference scheme to use on the partial derivatives. To this end, it should be noted that the choice of using either backward or forward progression is made such as to account for the special forms of the boundary conditions. On the brine side (i-e y direction) since we know the initial conditions, it would be natural to use a forward difference approximation (FDA) since this would allow us to start with initial data on y and use a step marching process. Therefore, eqs (3-5), (3-10) and (3-11) can be written in Finite Differences form as :

$$P_{B_{i,j+1}} - P_{B_{i,j}} = -\mu\, E_B\, \Delta y_j\, V_{B_{i,j}} \qquad (3\text{-}25)$$

$$V_{B_{i,j+1}} - V_{B_{i,j}} = -\Delta y_j \frac{\left[J_{11_{i,j}} + J_{12_{i,j}}\right]}{h_B} \qquad (3\text{-}26)$$

$$C_{B_{i,j+1}} - C_{B_{i,j}} = \frac{\Delta y_j\left[-(J_{21_{i,j}} + J_{22_{i,j}}) + C_{B_{i,j}}(J_{11_{i,j}} + J_{12_{i,j}})\right]}{V_{B_{i,j}}\, h_B} \qquad (3\text{-}27)$$

The local brine wall concentration is obtained from eq.(3-24) :

$$C_{BW1_{i,j}} = C_{P1_{i,j}} + (C_{B_{i,j}} - C_{P1_{i,j}})\exp\left(\frac{J_{11_{i,j}}}{k_{i,j}}\right) \qquad (3\text{-}28)$$

A similar expression is used for $C_{BW2_{i,j}}$.

On the other hand, since the boundary conditions for the permeate channel are not completely known at either end, the differential equations specific to the permeate side (x direction) should be written in Finite Differences form using forward and backward schemes depending on the parameter considered and where its value is known.

$$P_{P_{i,j}} - P_{P_{i-1,j}} = -\mu\, E_P\, \Delta x_i\, V_{P_{i,j}} \qquad (3\text{-}29)$$

$$V_{P_{i+1,j}} - V_{P_{i,j}} = \frac{\Delta x_i \left[J_{11_{i,j}} + J_{12_{i,j}} \right]}{h_P} \qquad (3\text{-}30)$$

For the local permeate concentration, the Finite Differences form of eq.(3-9) was not used in order to avoid further unnecessary complications. Instead, the use of the Finite Differences form of an equation derived from eq.(3-23) was judged more appropriate. Details of its derivation will be given in the next section. Here, it suffice to say that this equation took the following form :

$$C_{P1_{i,j}} = \frac{k_2\, C_{B_{i,j}}\, \exp\left(\frac{J_{11_{i,j}}}{k_{i,j}}\right)}{J_{11_{i,j}} + k_2\, \exp\left(\frac{J_{11_{i,j}}}{k_{i,j}}\right)} \qquad (3\text{-}31)$$

A similar expression is used for $C_{P2_{i,j}}$.

Note : The node numbers and position are specified in Figs 6 and 7.

III-5- Solution Procedure.

In this section, a solution method to obtain the required quantities in the flow domain will be presented. The problem is to find all the process variables described by the discretised equations, eqs. (3-25) to (3-31), at node points. A close inspection of these equations reveals that they are all flux dependent. Therefore, as expected, the flux is the governing variable which affects the variation of the remaining process parameters and hence needs particular attention. Recalling the basic equation for the flux, eq.(3-22), given by the Solution Diffusion transport model, we have :

$$J_1 = k_1 \left[(P_B - P_P) - b\, (C_{BW} - C_P) \right] \qquad (3\text{-}22)$$

It is seen that the flux is a function of the pressure difference across the membrane and of the wall concentrations which are, themselves, function of the flux. Therefore, it is clear that the flux expression is nonlinear and hence can be calculated only on an iterative numerical basis. To this end, before attempting to generate any proper problem solver, an expression of the flux depending only on the flux itself and other obtainable variables should be sought.

In this context, eq. (3-24) gives a relationship for the $(C_{BW}-C_P)$ term which when used in eq.(3-22) gives :

$$J_1 = k_1 \left[(P_B - P_P) - b\,(C_B - C_P)\ \exp\left(\frac{J_1}{k}\right) \right] \qquad (3\text{-}32)$$

In the above equation, C_P is still a function of J_1 as seen in section III-3-5 and therefore should be replaced by eq.(3-23).

Using eq.(3-23) and (3-24) gives the following equation :

$$C_P = \frac{k_2\,(C_B - C_P)\ \exp\left(\frac{J_1}{k}\right)}{J_1} \qquad (3\text{-}33)$$

Rearrangement of the above equation yields to eq.(3-34).

$$C_P = \frac{k_2\,C_B\,\exp\left(\frac{J_1}{k}\right)}{J_1 + k_2\,\exp\left(\frac{J_1}{k}\right)} \qquad (3\text{-}34)$$

This yields the following expression for J_1 :

$$J_1 = k_1 \left[(P_B - P_P) - b\,C_B \left(\frac{J_1\,\exp\left(\frac{J_1}{k}\right)}{J_1 + k_2\,\exp\left(\frac{J_1}{k}\right)} \right) \right] \qquad (3\text{-}35)$$

However, the above equation is not yet a complete expression of J_1 since P_P is a direct function of J_1. This is best illustrated by the governing discretised equations for the permeate flow where it is clearly seen that the permeate pressure expression (eq.(3-29)) is in terms of the permeate velocity which is expressed in terms of the fluxes via eq.(3-30). Therefore, the permeate pressure variation is related to the flux which is itself function of the permeate pressure as witnessed by eq.(3-35).

Therefore, to tackle the problem a suitable expression, linking the variation of the permeate pressure between two successive grid points, in terms of the fluxes only, would be required. The contribution of such expression is two fold :

- It will allow an iterative technique to be applied on the permeate pressure for which the exit condition is known to be the atmospheric pressure (eq.(3-12)).

- This, in turn, will form a practical scheme of computation in order to reduce the amount of computing time needed to perform the iteration.

The derivation of such relationship must be based on eqs.(3-29) and (3-30). To turn the latter equations into a practical scheme for manipulation, these are expressed in matrix form as follows :

Eq.(3-29) may be rewritten as:

$$\begin{bmatrix} -1 & 1 & \cdots & 0 \\ 0 & -1 & 1 & 0 \\ 0 & 0 & -1 & 1 \\ 0 & 0 & 0 & -1 \end{bmatrix} * \begin{bmatrix} P_{P_{1,j}} \\ P_{P_{2,j}} \\ \cdot \\ P_{P_{N,j}} \end{bmatrix} = -\mu E_P \begin{bmatrix} \Delta x_2 V_{P_{2,j}} \\ \Delta x_3 V_{P_{3,j}} \\ \cdot \\ \Delta x_N V_{P_{N,j}} \end{bmatrix} \qquad (3\text{-}36)$$

and eq.(3-30) equivalent to :

$$\begin{bmatrix} 1 & 0 & \cdots & 0 \\ -1 & 1 & \cdots & 0 \\ 0 & -1 & 1 \cdots & 0 \\ 0 & 0 & -1 \quad 1 & 0 \\ 0 & \cdots & \cdots & -1 \quad 1 \end{bmatrix} * \begin{bmatrix} V_{P_{2,j}} \\ V_{P_{3,j}} \\ \cdot \\ \cdot \\ V_{P_{N,j}} \end{bmatrix} = \frac{1}{h_P} \begin{bmatrix} \Delta x_2 (J_{11_{1,j}} + J_{12_{1,j}}) \\ \Delta x_3 (J_{11_{2,j}} + J_{12_{2,j}}) \\ \cdot \\ \cdot \\ \Delta x_N \ (J_{11_{N-1,j}} + J_{12_{N-1,j}}) \end{bmatrix}$$

(3-37)

At first sight, it should be noticed that an implicit solution exits as witnessed by the presence in both equations of the permeate velocity vector term. Therefore, by a suitable manipulation of both matrices, the velocity vector can be eliminated leading to the following explicit relationship:

$$\begin{bmatrix} -1 & 1 & \cdots & 0 \\ 0 & -1 & \cdots & 0 \\ 0 & 0 & -1 \quad 1 & 0 \\ 0 & 0 & 0 \quad -1 \quad 1 & 0 \\ 0 & \cdots & \cdots & -1 \quad 1 \end{bmatrix} * \begin{bmatrix} P_{P_{1,j}} \\ P_{P_{2,j}} \\ \cdot \\ \cdot \\ P_{P_{N,j}} \end{bmatrix} = \frac{\mu E_P}{h_P} * \begin{bmatrix} \Delta x_2^2 (J_{11_{1,j}} + J_{12_{1,j}}) \\ \Delta x_3 [\Delta x_2 (J_{11_{1,j}} + J_{12_{1,j}}) + \Delta x_3 (J_{11_{2,j}} + J_{12_{2,j}})] \\ \cdot \\ \cdot \\ \Delta x_N \ [\Delta x_2 (..) + \ldots + \Delta x_N \ (J_{11_{N-1,j}} + J_{12_{N-1,j}})] \end{bmatrix}$$

(3-38)

which is equivalent to the following recurrence expression :

$$P_{P_{i,j}} = P_{P_{i-1,j}} - C\,\Delta x_i \sum_{k=2}^{k=i} \Delta x_k \,(J_{11_{k-1,j}} + J_{12_{k-1,j}})$$

$$i = 2,N \; ; \; j = 1,M \qquad (3\text{-}39)$$

where

$$C = \frac{\mu E_P}{h_P} \qquad (3\text{-}40)$$

As it will be seen later, although the above expression cannot be incorporated directly in eq.(3-35), it does, however, greatly simplify the construction of the iterative technique.

For the time being, we turn our attention to eq.(3-35), which can be solved numerically in terms of J_1, assuming that all other parameters can be supplied. Various methods for solving such equations are available; among these, the Newton-Raphson method was chosen for its high reliability. Starting with an estimated value J_1^n eq.(3-35) can be solved iteratively. The algorithm is ended when the difference $J_1^{n+1} - J_1^n$ is below a chosen error limit. Briefly, noting that the index of iteration is n, the principle of this method is as follows :

$$J_1^{n+1} = J_1^n - \frac{f(J_1^n)}{f'(J_1^n)} \qquad (3\text{-}41)$$

where

$$f(J_1^n) = J_1^n - k_1\left[(P_B - P_P) - bC_B\left(\frac{J_1^n \exp(\frac{J_1^n}{k})}{J_1^n + k_2 \exp(\frac{J_1^n}{k})}\right)\right] \qquad (3\text{-}42)$$

and,

$$f'(J_1^n) = 1 + k_1 b\, C_B \left[\frac{(J_1^n)^2 \left(\frac{\exp(\frac{J_1^n}{k})}{k} \right) + k_2 \exp(\frac{2J_1^n}{k})}{\left(J_1^n + k_2 \exp(\frac{J_1^n}{k}) \right)^2} \right] \qquad (3\text{-}43)$$

At this stage, the construction of a general solution procedure will be implemented : in the above treatment, it is clear that in order to calculate the fluxes at a given grid location the local values of the brine pressure and concentration as well as the local permeate pressure are required. Considering the boundary conditions associated with these variables, i-e initial values for brine conditions and exit value for permeate pressure, the simpler solution technique that can be devised would be to use a numerical procedure similar to the well known "Pointwise heat exchanger rating method". This method consists in treating each axial increment of the module element as an individual module element. Therefore, the calculation procedure would take the following steps : starting with the first increment (i-e j=1) and using the initial conditions (eqs.(3-16),(3-17) and (3-18)), an initial guess for the permeate pressure at the closed end ($P_{P_{1,j}}$) is introduced which will allow to estimate J_1, at that particular grid point, using the iterative technique outlined previously. Then, using alternatively the recursive pressure expression (eq.(3-39)) and the iterative procedure on the corresponding flux, an explicit marching solution, grid point by grid point, in the streamwise direction is performed up to the open end where the value $P_{P_{N,j}}$ is obtained. This value is then compared to the atmospheric pressure (exit condition eq.(3-12)) : if different, then the initial guess is readjusted and the whole iterative procedure repeated. In this way, the correct value of the permeate pressure at the closed end is found by iteration until the required condition at the exit is met. At this point, velocities and concentrations are calculated at any grid point in the increment using their respective discretised equations. Then using eqs.(3-25) to (3-27) the information related to the brine feed conditions for the second axial increment are obtained and the procedure is repeated. In this fashion, the process variables at all grid points are calculated with an increment by increment calculation until the reject end of the module element is reached. A particular advantage of this method is that computationally only a one-dimensional problem needs to be handled at a time.

This method requires a good initial guess of P_P at the closed end since the number of iterations necessary, to satisfy the exit boundary condition, is very sensitive to this

guessed value. Therefore, to minimise the number of iterative steps, the first guess was performed using an analytical solution of which details are included in Appendix B.

The above solution technique has been subsequently used for developing a computer program whose main characteristics will be described next.

III-6- Program Features and Organisation.

This section will describe the general characteristics of the computer program which resulted from the application of the mathematical model detailed previously. Here, only those features with particular interest will be presented.

The computer program is organised by subroutines which successively generate the mesh by carrying all the indexing and geometric information about the grid points locations, then for each axial increment, compute the increment matrix, implement the boundary conditions, solve the resulting system of non-linear equations, calculate the process variables, locally, at each grid point and finally compute the initial feed conditions for the next axial increment.

Furthermore, owing to the fact that the solution properties (i-e density, viscosity, diffusitivity and osmotic pressure) are functions of the solution temperature and/or concentration which varies with the considered position in the membrane vicinity, all these properties have been considered as local and have been calculated at each point of the discrete scheme in the bulk flow as well as in the boundary layer using appropriate correlations presented in Appendix A.

The prediction of the overall performance of the module element results from a combination of the performance data of each individual increment Δy along the brine flow path. The general process variables characterising the overall performance were determined in the following way :

- Total permeate flow :

$$Q_{P\,ave} = \frac{\left(\sum_{j=1}^{M} V_{P_{N,j}}\right)}{M} h_P L \qquad (3\text{-}44)$$

- Average permeate concentration:

$$C_{Pave} \approx \frac{J_{2\ total}}{J_{1\ total}} \qquad (3\text{-}45)$$

- Average permeate pressure drop:

$$DP_{P\ ave} = \frac{\sum_{j=1}^{M} P_{P_{1,j}}}{M} - P_{atm} \qquad (3\text{-}46)$$

- Average brine reject concentration:

$$C_{B\ ave} = \frac{\sum_{i=1}^{N} C_{B_{i,M}}}{N} \qquad (3\text{-}47)$$

where $C_{B_{i,M}}$ is the exit brine concentration of the ith grid point along the brine spacer width calcualted from a salt material balance (eq.3-27).

- Average brine reject flow:

$$Q_{B\ ave} = \frac{\left(\sum_{i=1}^{N} V_{B_{i,M}}\right)}{N} h_B W_B \qquad (3\text{-}48)$$

- Average brine pressure drop:

$$DP_{B\ ave} = P_{BF} - \left(\frac{\sum_{i=1}^{N} P_{B_{i,M}}}{N}\right) \qquad (3\text{-}49)$$

Once proved successful, the application of the SP program will be very useful since one of its prime advantages is that quantitative information on the various parameters can be obtained at any point in the SPW module element. Indeed, in addition to the overall performance prediction, provision was made in the SP program to present, at each axial increment, the local variables variation in one of the two following ways:

- Successively from the outer to the inner grid point around the spiral path.

- At each incremental angle, from the innermost to the outermost grid point.

This form of presentation, in turn, allows the fine assessment of the parameters variation in order to pinpoint areas which might cause poor performance. For example, such areas could be those where excessive salt concentration might occur leading to membrane fouling which can have a disastrous effect on the element's performance.

A simplified block diagram describing the basic overall structure used in both programs is shown in Fig.8. All the computational work was performed on an ICL 3980 at the University of Glasgow.

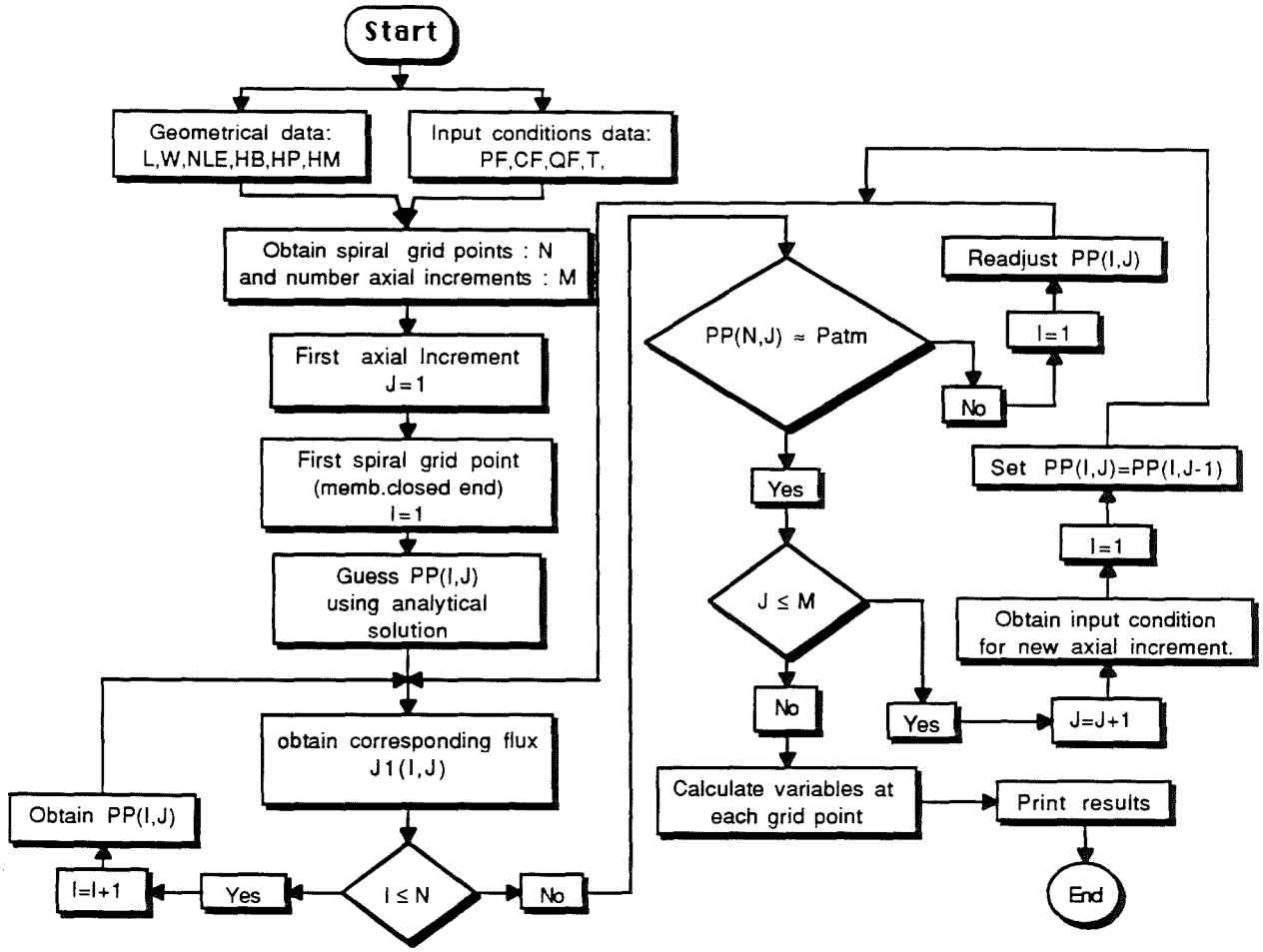

FIG.8: Simplified block diagram for both models.

III-7- Closure.

In this chapter, consideration was first given to illustrate the general features of the two models. Some of the phenomena of the SPW RO process were next interpreted and the difference between the mathematical models were also discussed. This was followed by a mathematical characterisation of the two models using FD formulation. Due to its relevance to the present work, additional attention was paid to the SP model for which a numerical solution was illustrated.

However, before a solution can be determined, the computer modelling is still lacking several membrane and module parameters (such as water and salt permeabilties, spacers friction parameters). As it will be seen in Chapter IV, these parameters are very much dependent on the order of magnitude of the operating conditions. Therefore, the accuracy of the relationships, defining the variation of the parameters, is a major factor in the success or the failure of the solution.

The next chapter will discuss the experimental apparatus and the methods used to evaluate membrane and module parameters.

CHAPTER FOUR

EVALUATION OF THE MAJOR MODEL PARAMETERS.

IV-1- Introduction.

In the last chapter, it was recognised that proper simulation analysis requires the acquisition of membrane and module characteristics data over a wide range of controlled hydrodynamic conditions. These parameters, designated by the " five parameters" are as follows :

- Membrane water permeability, k_1.
- Membrane salt permeability, k_2.
- Brine spacer friction parameter, E_B.
- Permeate spacer friction parameter, E_P.
- Mass transfer coefficient, k.

Unlike previous simulation procedures, all concerned with the Roga type module, where the assumption of constant membrane parameters was acceptable to some extent, it was felt that a more sensitive approach is needed for the FT30 module. Indeed, the relatively restricted range of the Roga module operating conditions is to be contrasted with the wider experimental data range of the FT30 module. Therefore, it was decided to undertake an experimental investigation aimed at defining the FT30 parameters in terms of the variables most likely to affect their variation.

The focus of this chapter is to present the methodology used. We will start by identifying those variables which affect the five parameters, then describe the experimental work in which a certain number of experiments, specially tailored to assess the influence of the different variables, were performed. Finally, the results will be presented and discussed.

Note : It must be pointed out that all the investigations presented here will be specific to the FT30 module type.

IV-2- Selection of variables affecting the membrane and module parameters.

a) Water and Salt permeabilities:

In the literature, there is ample experimental evidence indicating the dependency of both parameters on the operating temperature and pressure. This has been, particularly, emphasised in the work of Sourirajan and Matsuura [17] who performed an extensive experimental investigation using Loeb type cellulose acetate membranes. Their major conclusions were as follows :

- Water permeability :

At a given temperature, the water permeability parameter, k_1, decreases slightly with increase in operating pressure. This may be due to mechanical compaction of the membrane. This change can be expressed by the following equation :

$$k_1 = k_{10}\, e^{-\alpha P} \qquad (4\text{-}1)$$

where : α : constant function of the overall porosity of the membrane.

k_{10} : pure water permeability at zero pressure difference.

They also proposed that, at a given pressure, the temperature dependency of k_1 can be described by the permeate viscosity temperature function. Accordingly, the product of k_1 and permeate viscosity μ is almost independent of temperature i-e :

$$k_{1,\,t_i}\, \mu_{t_i} = \text{constant} \qquad (4\text{-}2)$$

Note : It was stressed [17] that the above correlation (eq.(4-2)) was based on a limited number of experimental data characterised by a restricted temperature range. Consequently, eq.(4-2) cannot always be regarded as being a reasonable approximation.

- Salt Permeability :

Using Sodium Chloride as a feed, they observed that k_2 tends to decrease with increase in operating pressure. They suggested that, at a given temperature, this change may be expressed by the relation,

$$k_2 = k_{2_0}\, P^{-\beta} \qquad (4\text{-}3)$$

where : β : a constant function of the overall porosity of the membrane.

k_{2_0} : a constant at constant temperature.

Regarding the effect of temperature on k_2, they stated that this dependency is very pronounced. At a given pressure, k_2 increases with increase in operating temperature. The following type of equation was suggested to reflect the above dependency :

$$k_2 = A\, e^{(0.005\ T)} \qquad (4\text{-}4)$$

where : A : constant depending on membrane considered.

At this stage, it should be made clear that the above correlations were defined for cellulose acetate type membranes. In this work, the FT30 element is made up of a thin film composite polyamide membrane of which behavior has, to the author's knowledge, not yet been characterised in the published literature. Therefore, it will be interesting to see whether these correlation types do still apply for the FT30 membrane.

b) Friction Parameters :

The driving force for the reverse osmosis process is critically influenced by the pressure drops which occur through both the brine and permeate channels. Therefore, for an accurate prediction of module performance, knowledge about the friction parameter characteristics of these channels is essential. It is well known that the friction parameters, along with the velocity and the geometrical characteristics of the channels are the main variables which affect the pressure drops.

While the brine friction parameter can readily be obtained from the actual FT30 SW module experimental data, the experimental determination of the permeate friction parameter poses more of a problem. In this context, so far only two published experimental techniques have been worked out. The earlier of these [27] consisted of measurements in flat channels whereas in the latter technique [28], direct measurements on the SPW itself were performed. Assuming that the flat channel flow behaviour reflects the flow in a SPW element, it is clear that this type of tests can be very useful in determining the spacer characteristics since the velocity through the spacer is constant and known. This is to be contrasted with the more realistic measurements on the SPW element itself where the velocity is constantly varying from a minimum (i-e V_P=0) at the closed end to a maximum (i-e V_P=V_{Pmax}) at the open one.

Although both methods may be prone to some criticism they do, however, give an

indication of the extent of the pressure drop to be expected and thus, may be used to evaluate and select backing materials. In this work, a different approach will be developed.

c) Mass transfer coefficient :

In concentration polarisation models, an expression giving the mass transfer coefficient, k, is required. Such expression should be able to represent the effect of changing conditions. In the literature, the value of k has, generally, been calculated from Sherwood type relations which are often represented as :

$$Sh = \frac{k\, d_h}{Ds} = p\ Re^q\ Sc^r \qquad (4\text{-}5)$$

where p,q,r are adjustable parameters.

In fact, recently Gekas and Hallstrom [30] revealed the existence of no less than 27 different Sherwood relations for flow in pipes and flat channels. This multitude of relationships makes it impossible to predict which value the mass transfer will have. Further, it should be noted that, most of the above expressions were derived either from non-porous systems or from heat and mass transfer analogies. However, since the brine channel, in SPW modules, is a spacer filled channel the validity of some published expressions may be questioned. Therefore, faced with the uncertainties associated with the determination of the mass transfer coefficient, an attempt to evaluate it experimentally was made.

Considering the available literature on the subject, the variables which are likely to influence the value of the mass transfer coefficient can be expected to be : the spacer geometry, the cross-flow velocity V, the flux J_1, the applied pressure ΔP, the type of solute, the hydraulic dimensions of the module and the characteristics of the membrane.

IV-3- Experimental work.

The most convenient and economical way to determine the intrinsic performance characteristics of a membrane is to perform extensive laboratory tests using small flat coupon samples of the membrane material fitted in a suitably designed RO test cell. Accordingly, the purpose, in this section, is to provide some details about the test cell design as well as the experimental setup and procedure adopted.

IV-3-1- Test Cell Description.

All the experiments were performed in a test cell shown in Fig.9. This design has been arrived at, after considering the requirements necessary for the determination of the process characteristics. The most important considerations being as follows :

- Flow maldistribution must be kept to a minimum.
- Flow path length should be as short as possible in order to minimise the pressure losses.
- Constant cross section to enable the evaluation of the cross flow velocity.
- Possibility of using different brine spacers permitting thus the testing of different turbulence promoters.

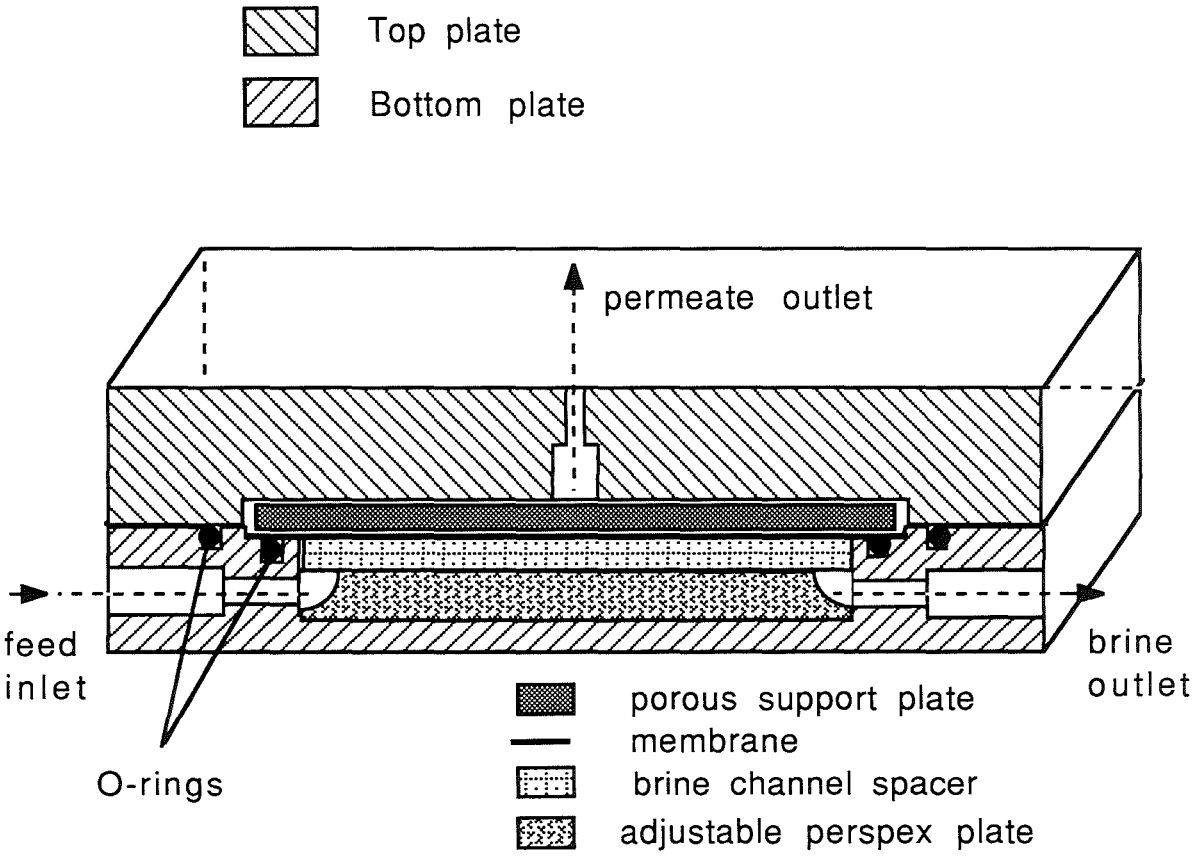

FIG.9:Schematic of Cross Sectional View of Experimental Test Cell.

As shown in Fig.9, the test cell consists of two detachable parts made of 316 stainless steel. The effective area of the membrane in the cell is 8.7x13.7 cm^2. The feed

solution enters the cell at one end of the bottom plate and flows through the brine spacer to the other end where it exits. The permeate, after passing through the membrane and the sintered porous plate, flows out to the product water manifold located on the centre of the top plate. The sintered porous plate offers, practically, no resistance to the fluid flow and its main role is to provide support for the membrane. O-rings were used to ensure proper sealing and alignment of the two plates.

IV-3-2- Experimental Set up and Procedure.

The experimental set up can best be described by referring to the flow diagram in Fig.10. It consists of a closed loop system taking feed from a thermostatic tank and eventually returning the brine, two bypass and permeate streams to the same tank. Initially, the feed tank is filled with 200 l of pure water which is enough to cover the heater and the cooling coil. Then, based on an estimate of the total volume of the system, a known amount of salt (artificial seawater) is dissolved and added to the tank to make a specific feed concentration. In order to mix the liquid trapped in the lines, the LP pump is operated for a few minutes. A 5μ cartridge filter has been placed on the LP line in order to remove any solid particles present in the feed solution. After the filter, the feed goes directly into the high pressure pump which is a Cat reciprocating triplex pump. It is driven by a three phase electric motor. An accumulator, preloaded with nitrogen at a pressure equivalent to 90% of the maximum operating pressure, is attached directly after the pump to smooth pulsations in flow and pressure due to piston reciprocation.

Once, the required temperature was obtained (i-e by using the cooling unit and the immersion heater provided), the desired pressure and brine flow rate were achieved by adjusting the by-pass (relief) valve (B) and reject (flow regulating) valve (C).

As shown in Fig.10, a considerable amount of instrumentation was provided for monitoring and controlling the system in operation. The quantities measured in the experiments included permeate and brine flow rates, permeate and feed concentrations, temperatures and pressures. The permeate flow rates were measured using a graduated cylinder and a stopwatch and the brine flow rates was measured with a rotameter of the "Paddle Wheel" type. The concentrations of the feed and the permeate were determined by measuring the electrical conductivity with a conductivity meter properly calibrated by using standard solutions in the concentration range of interest. Standard thermometers and pressure transducers were used to determine brine temperatures and operating pressures.

It is believed that the maximum deviation in any of the above measurements was no greater than 5%. The rotameter and the conductivity cell both have a stated accuracy of ± 1%. Temperatures were read within 0.5 °C, and pressure readings were within 0.1 bar.

The calibration procedure of the instrumentation is presented in Appendix E.

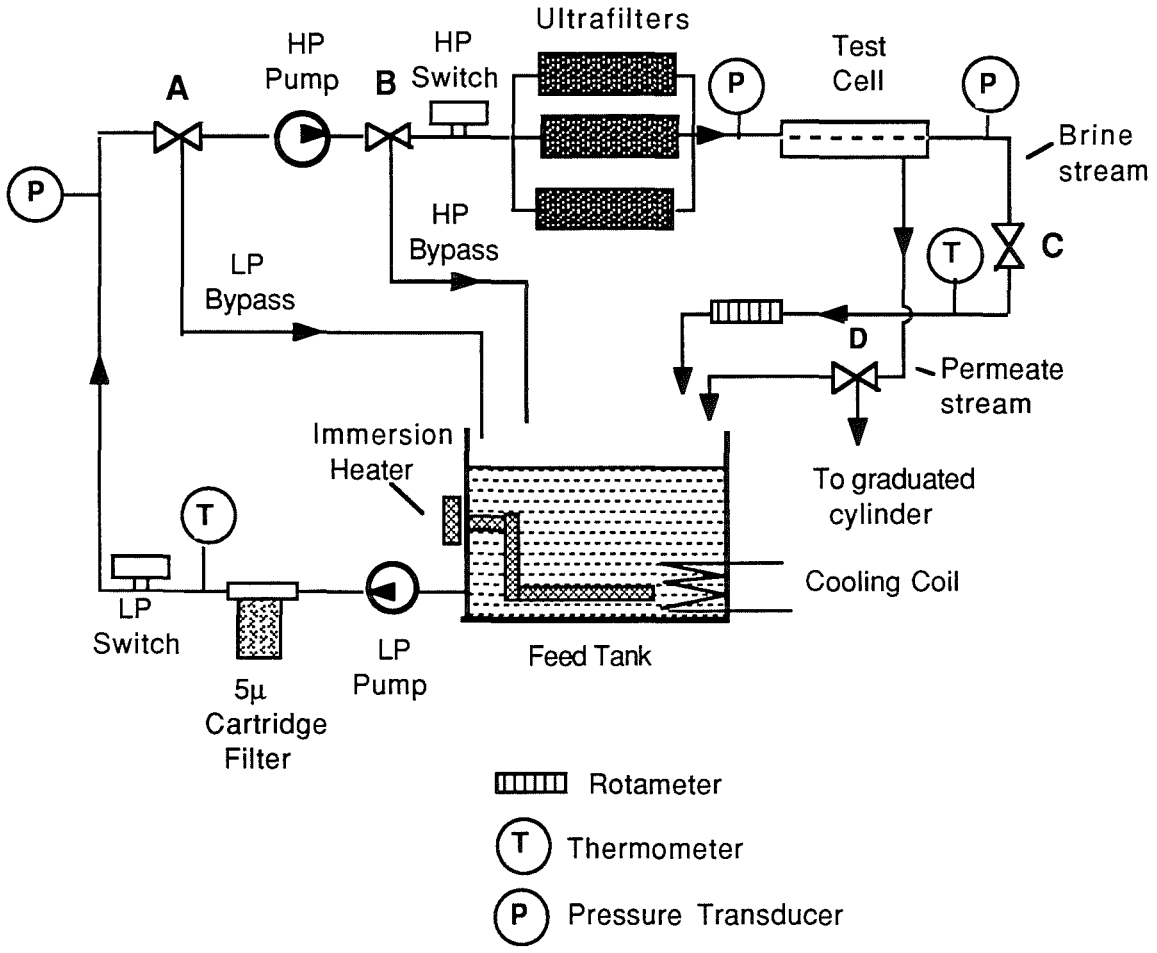

FIG.10: Experimental Setup.

Note : The presence of the ultrafilters as well as as the low and high pressure switches is due to the fact that the test cell was incorporated in the rig which was usually used for experiments performed on standard full scale modules.

IV-4- Test Conditions, Results and Discussions.

- Water Permeability Coefficient.

In this case, pure water was used as feed solution. The aim being to evaluate the variation of the water permeability coefficient with both temperature and pressure, it was therefore decided to maintain the feed flow rate constant throughout at a value $Q_F \approx 18.6$ [cc/s] corresponding to a velocity of approximately 27.8 [cm/s]. The measurements were made for different pressures (namely : 15,19,22,30,35 and 40 [bar] respectively) and for

temperatures from 20°C to 35°C with intervals of 5°C.

For each operating condition, a measurement of the permeate flux was performed and the corresponding value of the water permeability coefficient was evaluated using the following equation :

$$k_1 = \frac{J_1}{P_F - P_{atm}} \qquad (4\text{-}6)$$

A plot of the variation of k_1 with the applied pressure for different temperatures is shown in Fig.11. Prior to any comment, it should be mentioned that excellent straight lines are obtained at all levels of temperatures as witnessed by the correlations coefficient which was in all cases greater than 0.95. This indicates that a nearly perfect fit to a straight line is achieved.

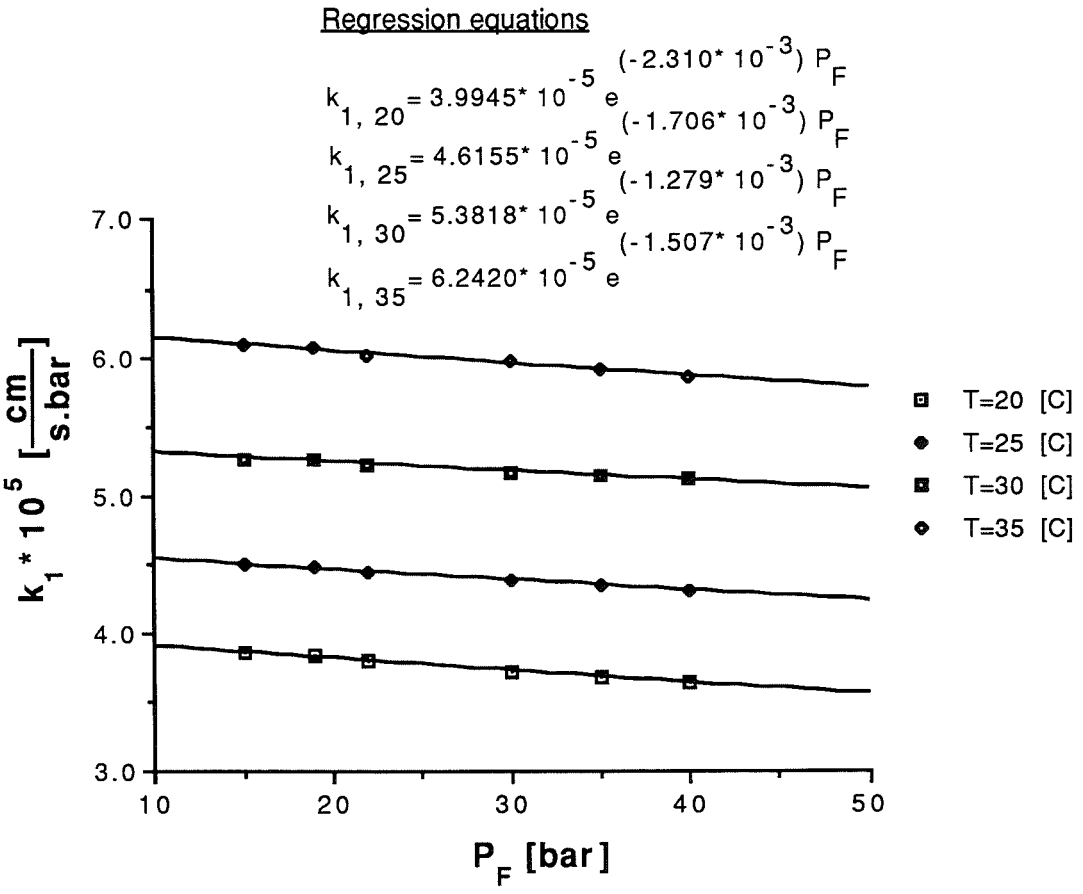

FIG.11: Variation of k_1 with the feed pressure for different temperatures.

The effect of membrane compaction is clearly depicted with a steady decrease in k_1 as the operating pressure increases. This tendency is in agreement with corresponding

published results from reverse osmosis experiments [8,17,29]. Also shown in the same figure are the regression equations which were obtained using a $\ln(k_1)$ versus P_F plot. By identification with equation.(4-1), we see that a is roughly constant having an average value a $=1.7\text{x}10^{-3}$.

Concerning the value of k_{10} in eq.(4-1), it is seen that this latter is primarily dependent on temperature. This dependence is illustrated in Fig.12.

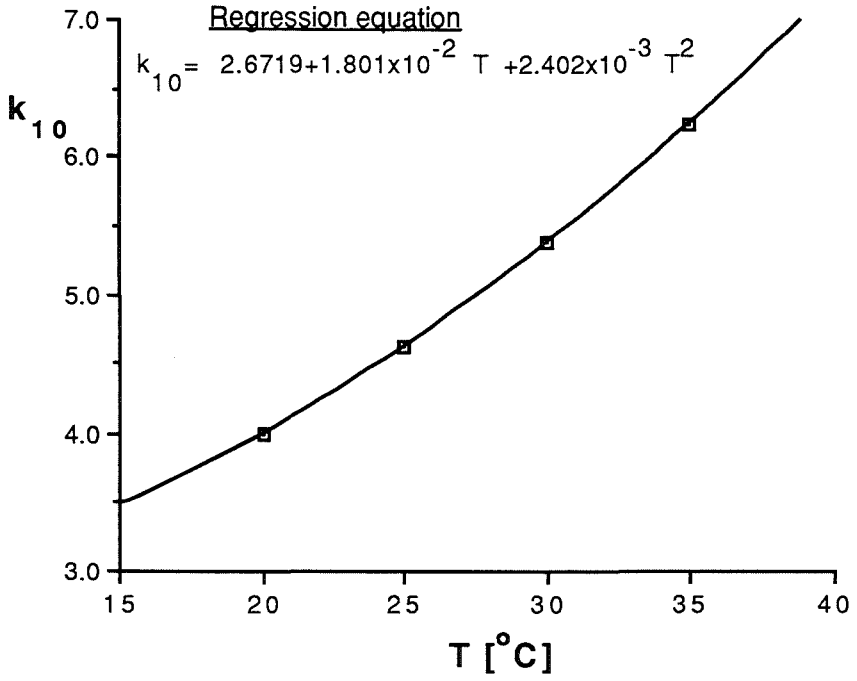

FIG.12: Variation of k_{10} with temperature.

It was found that the effect of temperature on the value of k_{10} can best be correlated using a second order polynomial as follows :

$$k_{10} = (2.6719 + 1.801\text{x}10^{-2}\ T + 2.402\text{x}10^{-3}\ T^2)*10^{-5} \qquad (4\text{-}7)$$

Therefore, the water permeability coefficient, k_1, may be obtained, for this membrane, for any arbitrary operating temperature and pressure, by using the following relation :

$$k_1 = k_{10}\, e^{-1.7\text{x}10^{-3}\ P_F} \qquad (4\text{-}8)$$

where k_{10} is given by eq.(4-7).

Referring to the applicability of eq.(4-2), Fig.13 shows the variation of the product $k_1\mu$, for different pressures, as a function of temperature. It is seen, that at a given pressure, the product $k_1\mu$ increases slightly with increasing temperature. Therefore these plots show that eq.(4-2) cannot be considered as accurate but represents a good estimate for the water permeability coefficient in situations where insufficient data is available.

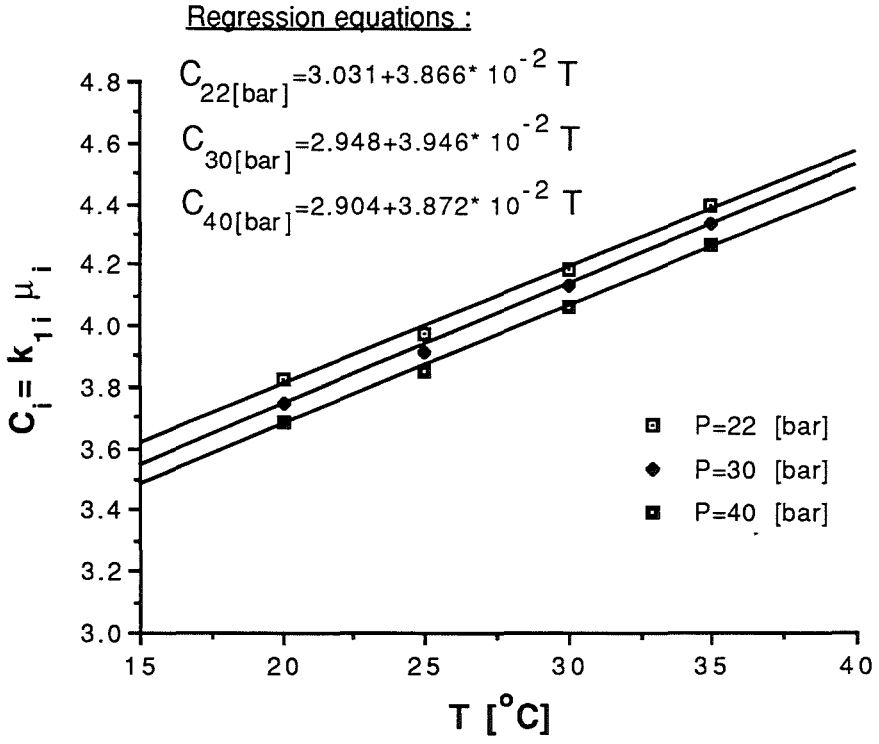

FIG.13: Variation of $k_1\mu$ with temperature for different operating pressures.

In addition to the above experiments, another set of similar tests were performed on a membrane sample originating from a second FT30 membrane element. The purpose of these tests was merely to assess the methodology used to evaluate the permeate spacer friction parameter since permeate pressure drops data on the second membrane were available [28]. The development of the method requires, among other things, knowledge of the water permeability characteristic of the membrane. Details of this method as well as the results will be presented later. Here, the results will be presented in the same fashion as for the first membrane. Fig.14 shows these results. It is seen that similar trends to those in Fig.11 are obtained.

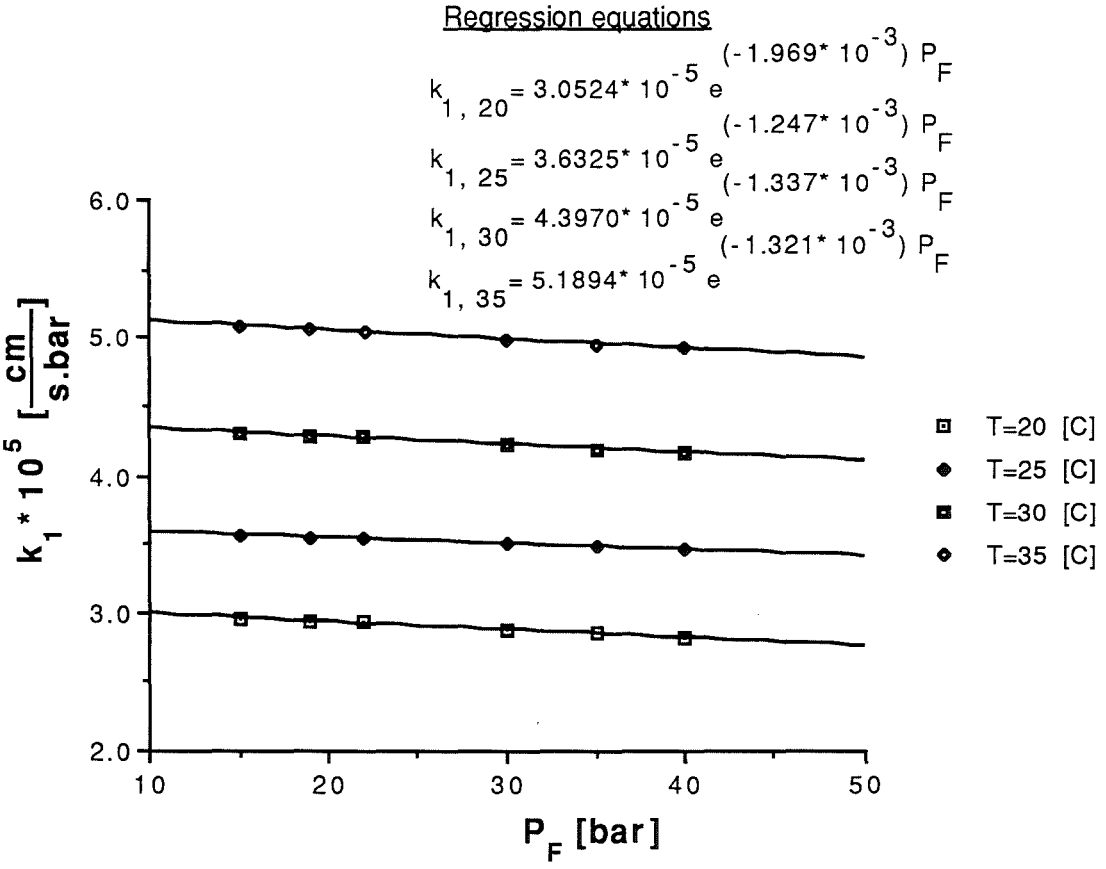

FIG.14: Variation of k_1 with the feed pressure for different temperatures (2^{nd} membrane).

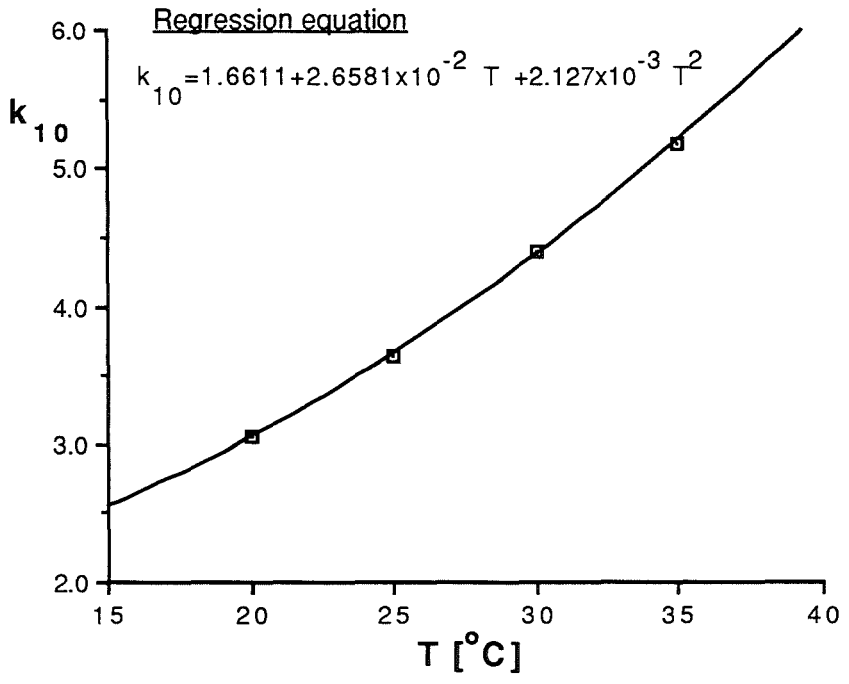

FIG.15: Variation of k_{10} with temperature (2^{nd} membrane).

However, it is clear that the intrinsic water permeability for the second membrane is about 20% lower than that of the first. This considerable variation between the two membranes (or between their samples) may be attributed to the way these were prepared and manufactured. In fact, most membrane manufacturers acknowledge this aspect of non-uniformity from membrane to membrane by allowing a margin of productivity expectations in their membrane specifications.

Considering both Figs.14 and 15, the correlations characterising the water permeability for the second membrane are as follows :

$$k_{1\,(2^{nd}\text{memb.})} = k_{10\,(2^{nd}\text{memb.})}\, e^{-1.47\times10^{-3} P_F} \qquad (4\text{-}9)$$

where :

$$k_{10\,(2^{nd}\text{memb.})} = (1.6611 + 2.6581\times10^{-2}\, T + 2.127\times10^{-3}\, T^2)*10^{-5} \qquad (4\text{-}10)$$

- Salt permeability :

In section IV-2, it was seen that the main variables affecting the salt permeability, k_2, were the operating pressure, temperature and possibly concentration. To this effect, experiments were conducted at two level of feed concentrations, i-e 19300 and 30900 ppm, and for the same temperature range as in the pure water experiments. Also, the applied pressure was varied from 35 to 60 [bar] in steps of 5 [bar] and feed flow rate was maintained constant at 18.6 [cc/s]. The measured parameters were the permeate flux and concentration. For each test condition, the value of k_2 was estimated using the general relationships specific to the Solution-Diffusion model as follows :

$$J_1 = k_1\, (\Delta P - b(C_{BW} - C_P)) \qquad (4\text{-}11)$$

A rearrangement of the water flux equation, i-e eq.(4-11), gives the following relation for the value of the brine wall concentration :

$$C_{BW} = \frac{\Delta P - \frac{J_1}{k_1}}{b} + C_P \qquad (4\text{-}12)$$

In the above equation, all the parameters on the right hand side are known making it possible to derive k_2 from the solute flux equation i-e :

$$k_2 = \frac{J_1 \, C_P}{C_{BW} - C_P} \qquad (4\text{-}13)$$

The tests results are displayed in Fig.16 where the variation of k_2 with temperature, for both set of concentrations used, is plotted. Also shown, in the figure, are the relevant empirical relations specifying the temperature dependence of k_2.

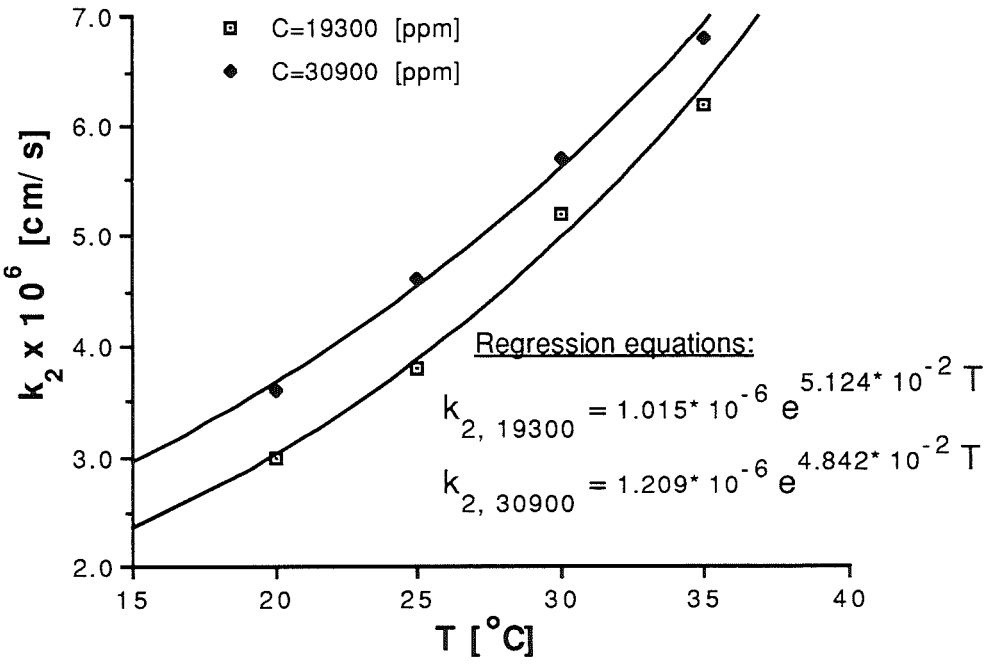

FIG.16: Variation of k_2 with temperature for different feed concentrations.

It is seen that there is some evidence of k_2 dependence on concentration particularly at the lower temperatures. However, since the experiments were conducted at only two feed concentrations, a relationship describing the effect of concentration on k_2 could not be derived. Further, it has been suggested that k_2 tends to decrease with increase in

operating pressure. Such tendency has not been detected in these experiments, as shown in Fig.17 where it can be observed that the variation of k_2 with pressure is rather random.

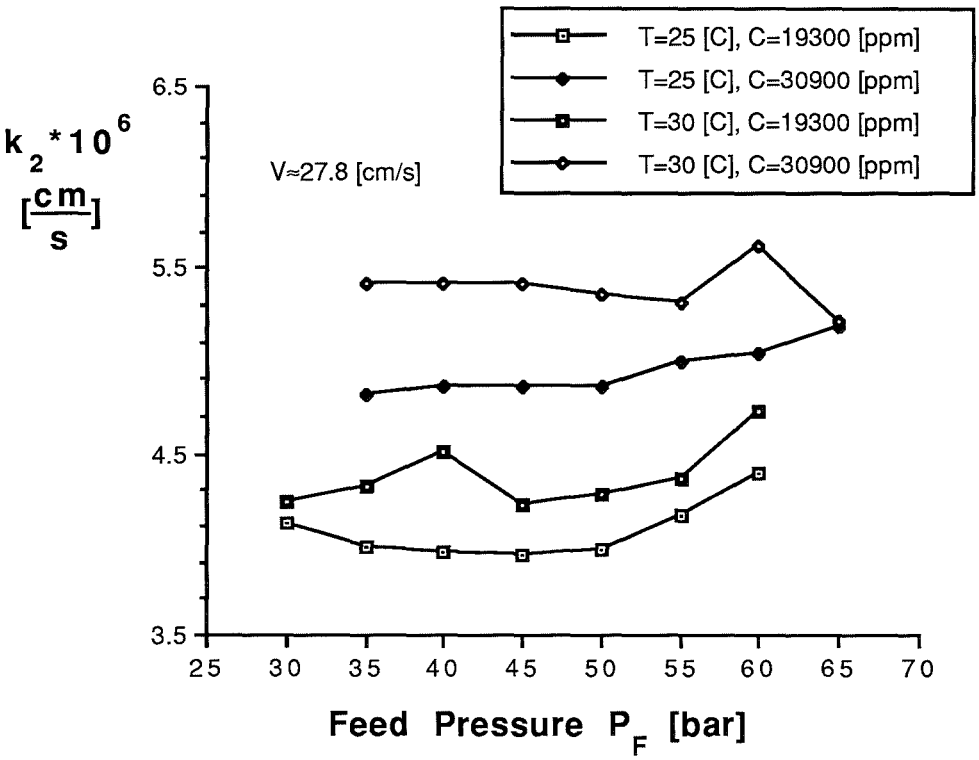

FIG.17 : Variation of k_2 with feed pressure for different temperatures and concentrations.

Therefore, k_2 may be considered, practically, as independent of operating pressure. Consequently, an averaged correlation describing the variation of k_2 with temperature can be deduced as follows :

$$k_2 = 1.112 \times 10^{-6} \, e^{4.983 \times 10^{-2} T} \qquad (4\text{-}14)$$

Note : It is worth noting that the exponent coefficient on the resulting correlation is close to that found for cellulose acetate membranes (eq. 4-4). This would, perhaps, indicate an analogy between the behaviour of the FT30 membrane and the cellulose acetate membrane of Loeb type.

- **Mass transfer coefficient.**

The objective of this portion of the work is to investigate experimentally the variation

of the mass transfer coefficient. In order to achieve this, a series of experiments were undertaken to evaluate the influence of the following variables :

-a) Cross flow velocity.
-b) Flux.
-c) Concentration.
-d) Temperature.

The range of test conditions included :

- Feed flow rate : Q_F= 18.6, 15.6, 12.6, 9.6, 7.2, 3.8 and 1.9 [cc/s].
- Feed Pressure : P_F= 30, 35, 40, 45, 50, 55, 60 and 65 [bar].
- Feed concentration : C_F= 19300 and 30900 [ppm].
- Operating temperature : T= 25 and 30 [°C].

At each temperature, feed concentration and pressure, the feed flow rate was varied from the highest value (18.6 [cc/s]) to the lowest one (1.9 [cc/s]) and the permeate flux and concentration were measured. The technique used to evaluate the mass transfer coefficient is known as "the osmotic pressure method" where the concentration polarisation phenomenon is described by the film theory (see section I-3-3).

$$k = \frac{J_1}{\ln\left[\frac{C_{BW} - C_P}{C_B - C_P}\right]} \qquad (4\text{-}15)$$

in the above equation, the only unknown is C_{BW} which can be obtained from eq.(4-12) where a correlation has been used in order to evaluate the osmotic pressure coefficient, b, in terms of concentration and temperature (see appendix A).

In the remaining part of this section, the results from the method using the osmotic pressure difference will be given. General tendencies will be shown, as well as the influence of the various experimental circumstances on the calculated mass transfer coefficient. Further, an attempt will be made to obtain a correlation for the mass transfer coefficient of the same type as eq.(4-5) with the difference that the possible effect of flux could be included. Therefore, such correlation would be of the following form :

$$Sh = \frac{k\, d_h}{Ds} = p\, Re^q\, Sc^r \left(\frac{J_1}{J_0}\right)^m \qquad (4\text{-}16)$$

where J_0 is the unit flux included only for homogeneity purposes.
Plots will be generated to investigate the effect of each of the variables (i-e: Re, Sc and J_1) separately on the Sherwood number Sh in order to evaluate the value of p,q,r and m in eq.(4-16).

The details of the experimental findings will be given next starting with the effect of the cross flow velocity. To this end, the variation of Sh with Re is plotted in Fig.18. For each curve, characterised with a constant value of Sc (i-e constant temperature and concentration), the flux was maintained approximately constant at a value of $J_1 \approx 1.1 \times 10^{-3}$ (cm/s).

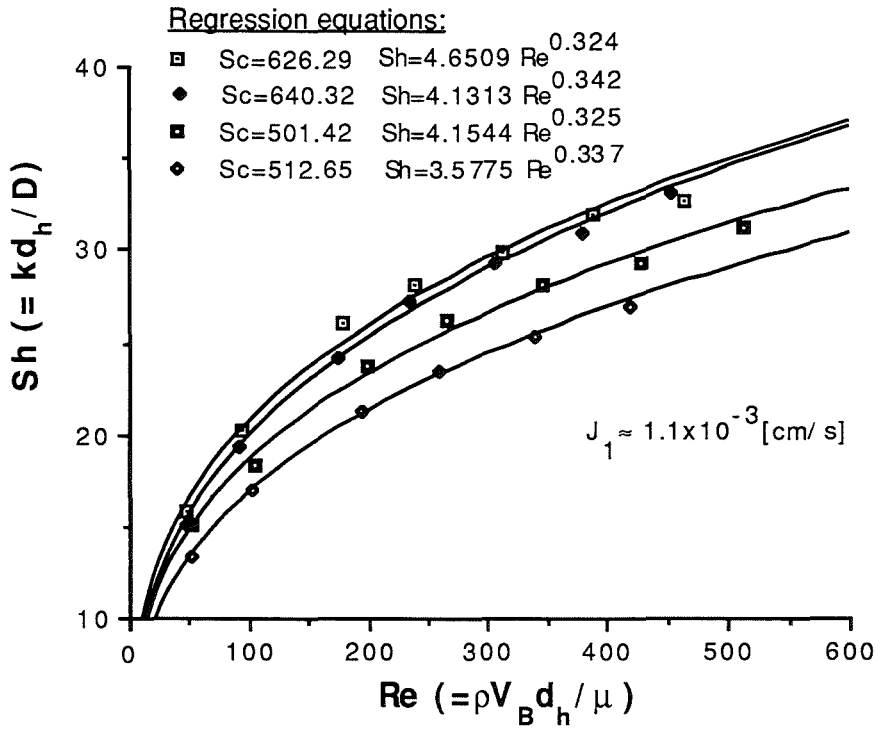

FIG.18: Variation of Sh number with Re number for different Sc numbers.

As expected, it is clearly seen that the mass transfer coefficient is velocity dependent. A closer look at the correlating equations, displayed on the same plot, reveals that the exponent on the Reynolds number is reasonably constant having an averaged value of q = 0.33. Therefore, it can be stated that the variation of Sh with Re is of the type:

$$Sh \propto Re^{0.33} \qquad (4\text{-}17)$$

Figure 19 reports on the variation of Sh with the flux J_1. Each curve represented corresponds to a constant Schmidt number and Reynolds number. All curves show similar trends suggesting that Sh is flux dependent. It is particularly clear that as the flux increases, the mass transfer coefficient decreases. This tendency, although not taken into account in any of the published correlations, seems quite realistic. It is natural to think that, while maintaining feed temperature, concentration and velocity constant, a change in flux (due to a change in applied pressure) will result in a corresponding change in the mass transfer coefficient since the establishment of a new equilibrium at the membrane solution interface will be required.

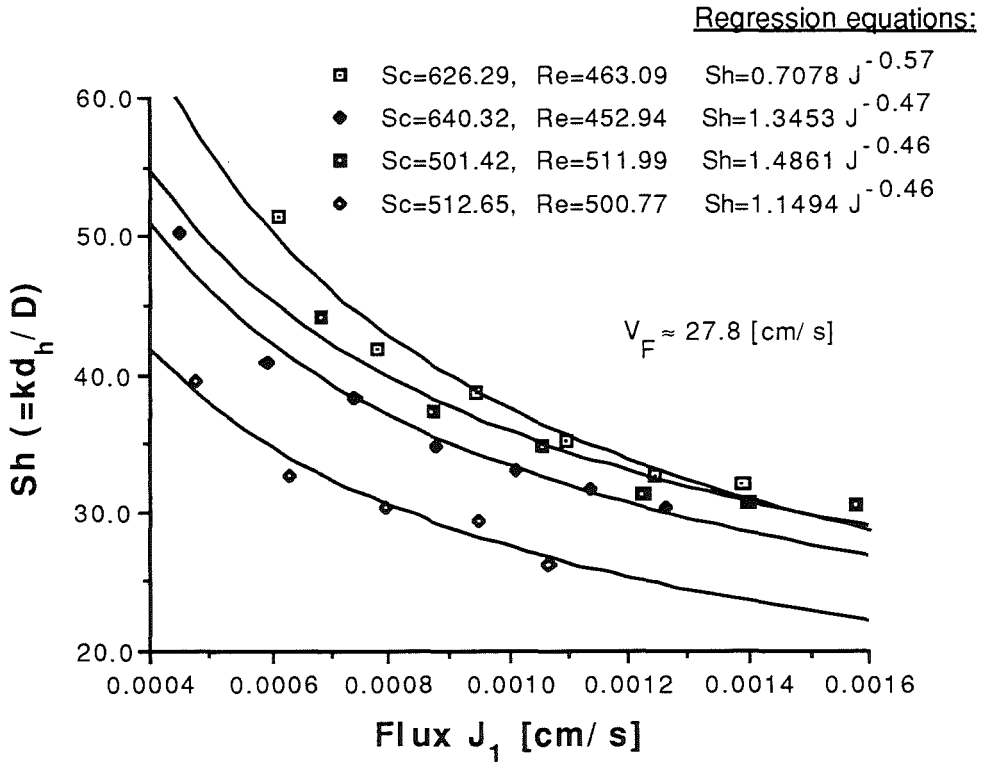

FIG.19: Variation of Sh number with Flux as a function of Re and Sc numbers.

Also, incorporated in the same graphs are the different correlating equations giving the variation of the Sh number as a function of the flux J_1 only. It is seen that, with the exception of one case, i-e at Sc=626.29, the exponent on the flux is relatively constant,. Therefore, an average constant value could be taken which would give a Sh number dependency on the flux of the following type :

$$Sh \propto \left(\frac{J_1}{J_0}\right)^{-0.46} \qquad (4\text{-}18)$$

Finally, in order to evaluate the values of the coefficient p and the exponent r on the Sc number in equation (4-16), a graph of ($Sh\ Re^{-033}\ (J_1/J_o)^{0.46}$) versus Sc is plotted in figure 20. It should be noted that, because the tests were carried out at only two different operating temperatures and concentrations, the reliability in the determination of p and r is consequently entirely dependent on the accuracy of the experimental results. To reduce effectively the uncertainties, a wider range of temperatures and feed concentrations should have been included initially in the experimental programme.

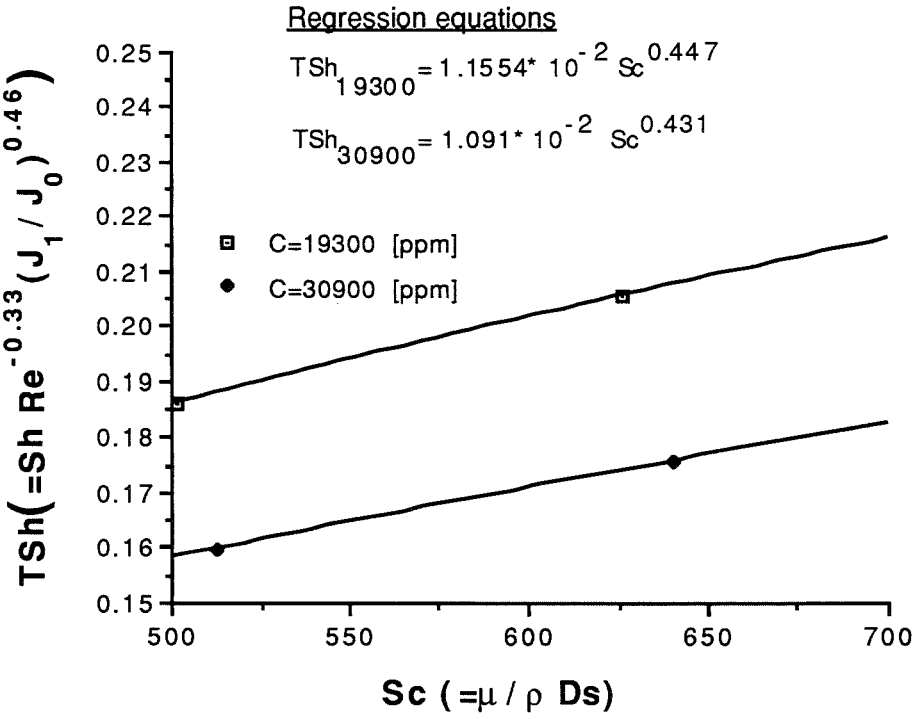

FIG.20 : Variation of TSh with Sc number at different feed concentrations.

From Fig.20, the reported regression equations, obtained through a logarithmic curve fitting type equation, would suggest that the p and r values are somewhat dependent on the .feed concentration. However, with regards to the scarcity of experimental data, no definitive trend can be deduced. This problem therefore needs further investigation. Consequently, it was decided to neglect the possible effect of feed concentration and to consider p and r as constants equal to an average value between the data, i-e:

$$TSh = Sh\ Re^{-0.33}\left(\frac{J_1}{J_0}\right)^{0.46} = 0.0112\ Sc^{0.44} \qquad (4\text{-}19)$$

A rearrangement of eq.(4-19) yields the following expression for the variation of the

Sh number in terms of the variables discussed above :

$$Sh = 0.0112\ Re^{0.33} Sc^{0.44} \left(\frac{J_1}{J_0}\right)^{-0.46} \qquad (4\text{-}20)$$

- Brine Friction Parameter.

The brine friction parameter was determined using the experimental data on the actual SPW element and the Darcy equation, eq.(3-5), related to the flow through porous media. Therefore, here, it is assumed that the brine spacer behaves as a porous material. In fact, the brine spacer is a mesh which serves two purposes :

- To provide a space for the brine flow by separating two membrane surfaces.
- To promote turbulence to reduce the thickness of the concentration boundary layer.

Unlike most previous published work, inlet and outlet pressure losses in the SPW element were eliminated in these experiments by using two pressure transducers to which two fine probes were connected and placed at the extreme ends of the brine spacer so as to bypass the pressure losses in the fittings and the tubing connected to the element pressure vessel. The location of the two probes connected to the pressure transducers is sketched in the figure below, Fig.21.

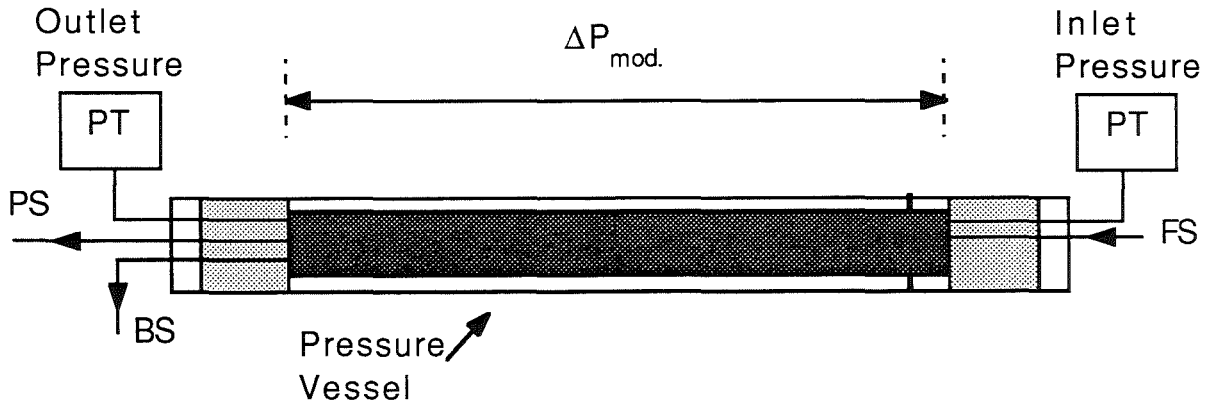

FIG.21 : Position of the pressure transducer probes for the brine flow pressure drop measurements.

A wide range of feed velocities were used. In any case, it was found that the brine pressure drop was quite low even at the highest recommended feed flow rate where these losses were less than 1 [bar]. This behaviour is in agreement with the experimental results of Shock and Miquel [27].

For each operating condition, the brine friction parameter E_B was evaluated from a modified form of the discretised equation for the brine pressure drop, i-e eq.(3-25), in which the whole module length was considered as a single increment. This equation took the following form:

$$\Delta P_{mod.} = -\mu\, E_B\, L\, V_{B_{Ave.}} \qquad (4\text{-}21)$$

At this stage, it should be mentioned that, for accuracy purposes, only data from experiments at low recovery (Rec.<5%) were considered so as to minimise the effect of permeation through the membrane. Further, for the same reason, an average brine velocity, $V_{B_{ave}}$, between the feed and the brine exit was used for the calculations. Fig.22 reports the variation of E_B with the brine velocity for different temperatures.

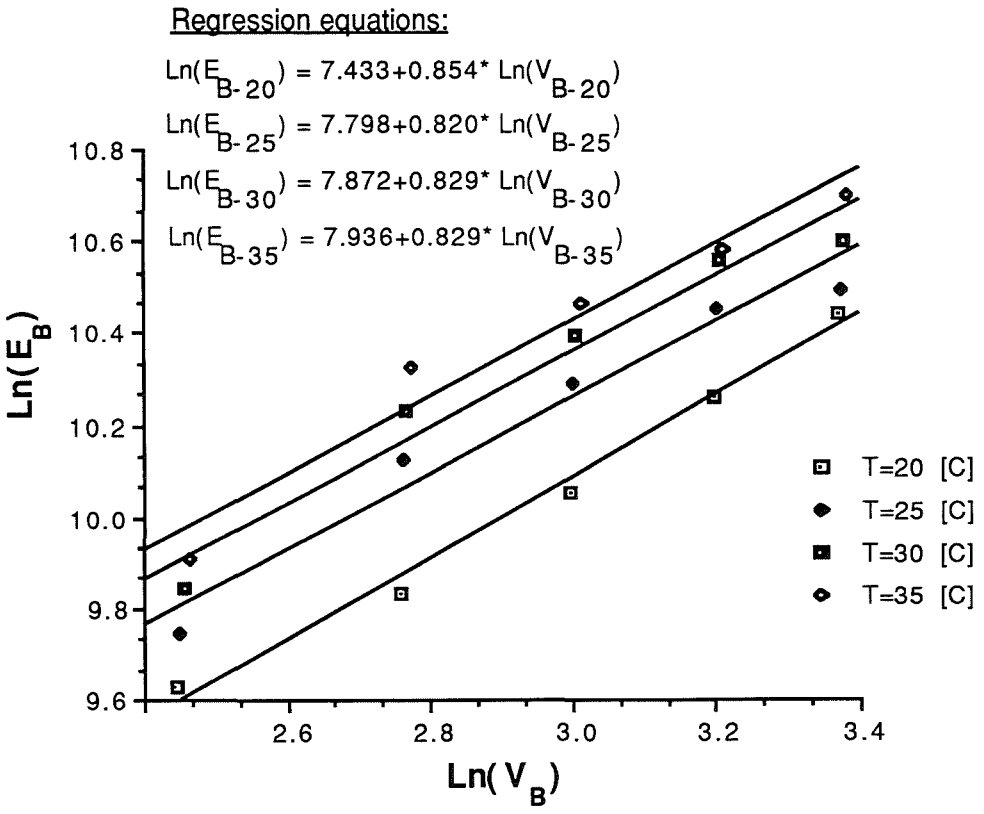

FIG.22 : Variation of $Ln(E_B)$ with $Ln(V_B)$ for different temperatures.

Also, included in the same figure, are the correlations resulting from a curve fitting. These correlations reveal that the exponent on the velocity in the Darcy's equation for the brine pressure drop is greater than 1.

From the results in Figure 22, it may be seen that the pressure drop is proportional to the average brine velocity to power 1.82. Therefore, Darcy's equation, in this situation, should be modified as follows :

$$\frac{\delta P_B(x,y)}{\delta x} = -\mu E_B V_B^{1.82}(x,y) \qquad (4\text{-}22)$$

In the above equation, the brine friction parameter is slightly dependent on temperature. This dependency can be expressed with a fairly good approximation as :

$$E_B\mu \approx \text{const.} \qquad (4\text{-}23)$$

In this respect, Fig.23 shows that, within the experimental uncertainties, ($E_B\mu$) is fairly independent on temperature.

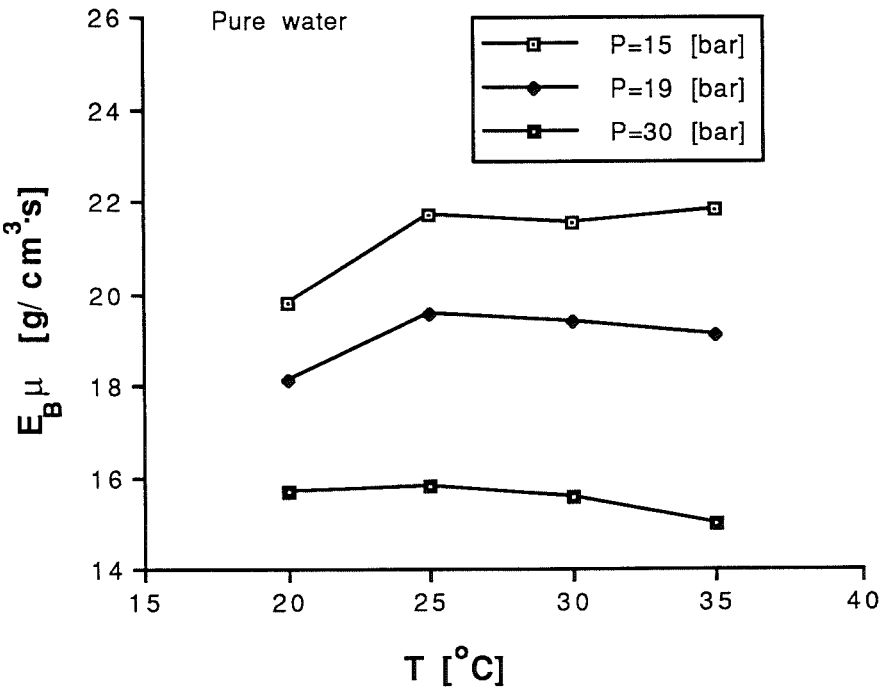

FIG.23 : Variation of ($E_B\mu$) with temperature for different feed pressures.

This is in accordance with the experimental results in which the brine pressure drop appeared to be independent of temperature.

Roughly, it was found that, for the whole range of operating conditions used,the brine friction parameter varied from a minimum value of 17000 [cm^{-2}] to a maximum of 33000 [cm^{-2}] which corresponded to a maximum brine pressure drop of around 0.8 [bar]. This brine pressure loss is not very great so that an averaged brine friction parameter at $\mathbf{E_B=25000\ [cm^{-2}]}$ could be assumed without a significant loss of accuracy.

Note: In evaluating the brine velocity from the feed flow, the brine spacer width (in the spiral direction) was used instead of the permeate spacer width which was used in previous analyses [26,28].

- Permeate Friction Parameter.

The determination of the permeate friction parameter poses some serious problems. As mentioned in section IV-2-b, two different experimental techniques have been worked out for measuring pressure drop in the permeate channel. The first one [27] made use of a flat channel whereas in the latter [28] direct measurement on the actual SPW element was achieved. In this last technique, a special fine tube was inserted into the inter-membrane space at the closed end of the permeate channel. When the module was in use, the pressure drop in the backing material was determined directly by measuring the pressure at the closed end.

In this work, direct experimental determination of the permeate friction parameter, E_p, using the test cell was not possible. Therefore, a different approach had to be sought. The method used consisted in developing a semi-analytical solution predicting the performance of a SPW element using pure water as feed. In this way, with the aid of pure water experiments data on the actual SPW element, the value of the permeate friction parameter can be evaluated. To achieve this, knowledge of the operating conditions as well as the permeate flow are required. Details of this analysis are presented in appendix C.

It should be stressed that the use of this procedure does not allow one to derive a relationship for the permeate spacer similar to that of the brine spacer (i-e eq.(4-22)) since, due to the permeation through the membrane, the permeate velocity is constantly changing along the permeate channel. Therefore, the remaining alternative is to assess the effect of temperature and pressure on E_p. In this regard, the results are plotted in Fig.24 where the variation of E_p with feed pressure, for different temperatures, is reported. It is apparent, from Fig.24, that the permeate friction parameter is dependent on both the temperature and the pressure.

However, since an increase in either the temperature or the applied pressure result in a corresponding increase in permeate flow, it is therefore quite difficult to form a judgement as to whether this apparent dependency is due to the fact that the exponent on the permeate velocity was taken as unity (whereas it might be different) or whether these variables affect truly the permeate friction parameter. To provide a sound answer requires careful tests such as those performed by Shock and Miquel [27] in which both the permeate velocity and pressure drop are obtainable. At this stage, we can only speculate that the variation of E_p with pressure might be due to a decrease of the permeate channel thickness as the applied pressure increases.

In any case, it was observed that, over the tested operating conditions, E_p varied from a minimum of around 900,000 [cm^{-2}] to a maximum of about 1400,000 [cm^{-2}]. This variation, although quite large, seems to have a small effect on the final result : indeed some preliminary computer simulation runs revealed that a 30% variation in E_p resulted in less than 3% variation in the predicted permeate flow. Therefore, it is reasonable to assume a constant value of E_p taken as an average as $\mathbf{E_p=1200000\ [cm^{-2}]}$. The impact of such assumption is thus expected to be not very significant.

This method may not sound attractive but, considering the alternatives, seemed the most efficient. Many researchers have been using the same approach for years [20,22,26].

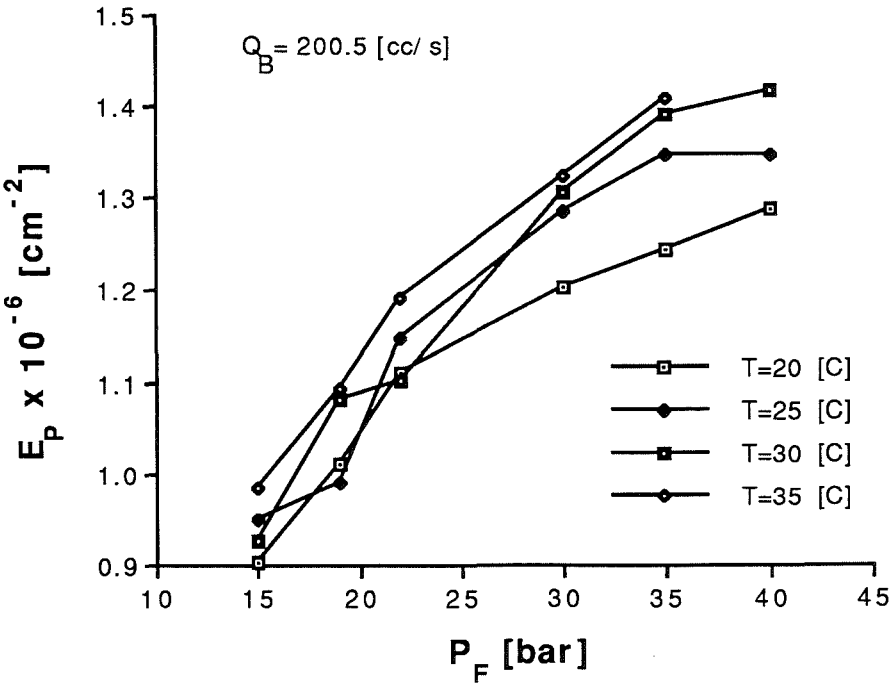

FIG.24 : Variation of E_p with feed pressure for different temperatures.

IV-5- Closure.

In this chapter, by the use of the above simple tests with the cell, it has been possible to correlate the experimental results in order to determine the module and membrane parameters over a wide range of operating conditions. However, the reliability of these correlations in predicting the performance of the actual FT30 SPW element has yet to be demonstrated. This aspect will be examined in the next chapter. At this stage, it should be stressed that the determination of such correlations from independent measurements, if proved successful, would be very useful from the point of view of specifying membranes and predicting element performances under different operating conditions.

CHAPTER FIVE

VALIDATION AND COMPARISON OF THE MODELS.

V-1- Introduction.

In this chapter, we turn our attention to the real test of our numerical models, i-e the prediction of actual experimental results. To be useful, the computer programs must give realistic quantitative predictions over a sufficiently wide range of operating conditions. In this context, a particularity of this work is that the assessment of the models is based on, by far the most extensive set of data ever compiled, for Spiral wound elements, in the literature. Indeed, the experimental data used included both sets typical of brackish and sets typical of sea water desalination. They were supplied from two different types of SPW modules:- these were the Roga-4160HR and the Filmtec FT30SW2540 modules respectively.

Unlike the Roga data [29] which were published some time ago and have been used by various RO researchers, the FT30 data utilised here, were provided from an extensive experimental programme performed, recently, at Glasgow University. These experiments made use of simulated sea water, i-e "Instant Ocean", feed solutions which have to be contrasted with the dilute NaCl feeds used in the Roga tests. A detailed description of the experimental set-up and procedure together with the results can be found in [28].

For the computational calculations, information regarding the SPW element geometry is needed. For the Roga element, the geometrical information was readily obtainable [29]. In contrast, the FT30 element geometrical characteristics were collected after dismantling and measuring the element. In any case, the "destruction" of the FT30 element was necessary in order to obtain the membrane coupon samples needed for the experiments described in the previous chapter.

The relevant geometrical information for both SPW elements is presented in Table 5-1. The required characteristic parameters for their membranes and spacers are reported in Table 5-2.

Table 5-1 : Geometrical data of the modules.

		4" ROGA 4160-HR	2.5" FT30
Number of leaves :	NLE	3	1
Membrane spiral length (cm):	W	143	110
Membrane axial length (cm):	L	88	85.4
Membrane thickness (cm):	h_M	0.01	0.014
Brine channel height (cm):	h_B	0.07	0.077
Permeate channel height (cm):	h_P	0.03	0.041
Brine channel spiral length (cm):	W_{BS}	-	133

Table 5-2 : Membranes and Spacers characteristics.

		4" ROGA[(a)] 4160-HR	2.5" FT30
Water permeability (cm/s):	$k_1 x\ 10^5$	2.085	eq.(4-8)
Salt permeability (cm/s) :	$k_2 x 10^5$	1.444	eq.(4-14)
Permeate friction parameters (cm^{-2}):	E_P	744444	1200000
Brine friction parameter (cm^{-2}):	E_B	183673	25008

(a) : taken from ref.[20]

The general approach used to assess the veracity and feasibility of the computational models is based on the following steps:

1- Using the SP program, investigate the sensitivity of the solution to the variation of each the five parameters (i-e k_1, k_2, k, E_P, E_B). It was felt that this analysis would be very useful in identifying the key parameters most likely to influence the results.

2- By comparison with the Roga and the FT30 experimental data, check the adequacy of the models and of the values of the five parameters determined experimentally in the previous chapter.

3- Compare accuracy of prediction of both the "Slit" and the "Spiral" models.

V-2- Sensitivity of predictive solution to the variation in membrane and module parameters.

In this portion of the work, the influence of the variation of the SPW parameters (

i-e the "five parameters"), on the SP model predictions, is assessed. In this analysis, the range of a parameter's variation used is often hypothetical but, nevertheless, does cover values corresponding to what is common or considered quite possible in current practice. Therefore, the numerical values of the different input parameters and the corresponding output results must be considered as guidelines only. These would, however, provide a useful information regarding the extent of uncertainties that can be attributable to the parameters.

Further, at this stage, for the purpose of this analysis, it is anticipated that the SP computational model is applicable. Thus, the significance of this analysis is meaningful as far as the method employed in the derivation of the SP model is correct. But, as will be seen later, confidence in the structural aspects of the SP model applicability is demonstrated.

In the following, unless otherwise stated in the figures, the value of the different parameters utilised in the calculations are those reported in Table 5-2 and are specific to the FT30 type membranes. In addition, the mass transfer coefficient was evaluated using the Winograd correlation, eq.(3-1), the validity of which has been tested in previous work [32].

Effect of the water permeability coefficient :

Figs.25-a and 25-b show, for different operating conditions, the effect of the water permeability coefficient, k_1, on the permeate flow and concentration respectively.

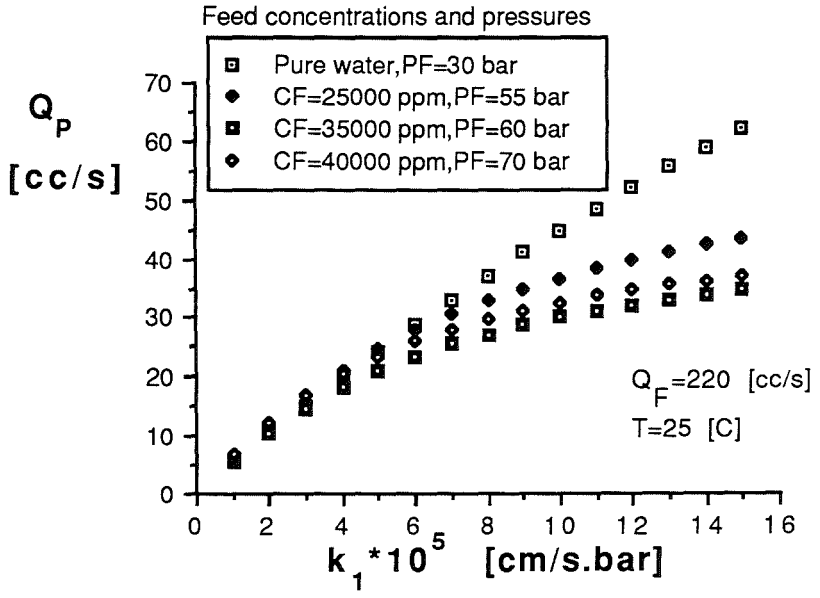

Fig.25-a : Variation of FT30 element productivity with the water permeability coefficient

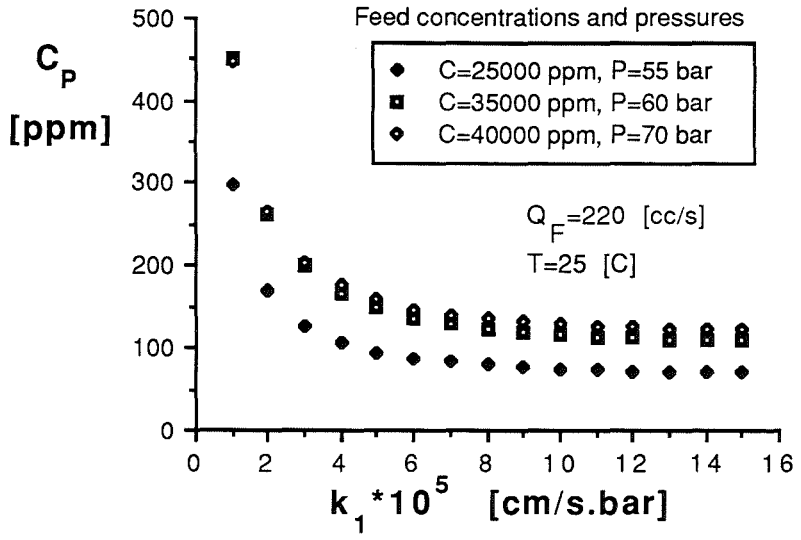

Fig.25-b : Variation of FT30 element permeate concentration with the water permeability coefficient

Judging from these figures, it is seen that the variation of k_1 affects considerably the productivity and the product quality of the SPW element. It should be noted that the water flux dependency on k_1 is not linear since the product flow increase with k_1 slows down as k_1 increases. This is valid whether pure or salt water is used as a feed and due to two facts :

(i)- Increase of permeate pressure drop as the permeate flow increases.

(ii)- Concentration polarisation increase due to higher solute convection toward the membrane and, in the extreme case, to the reduction in brine flow velocity owing to a higher recovery.

Disregarding the possible event of membrane fouling, it is clear, from the above figures, that the increase in k_1 is beneficial for the permeate flux and quality up to a certain point (where the product quality curves, in particular, tend to become asymptotic) above which a higher value of k_1 will hardly improve the average permeate quality and only slightly improve the flux.

Effect of the salt permeability coefficient :

The predicted variation of the module element productivity and product quality with the salt permeability coefficient is displayed in Figs. 26-a and 26-b. These figures reveal that, while the effect of the variation of k_2 on the permeate flow is negligible (Fig.26-a),

the same variation will affect substantially the product quality (Fig.26-b). In fact, the product concentration increases linearly with the increase in k_2.

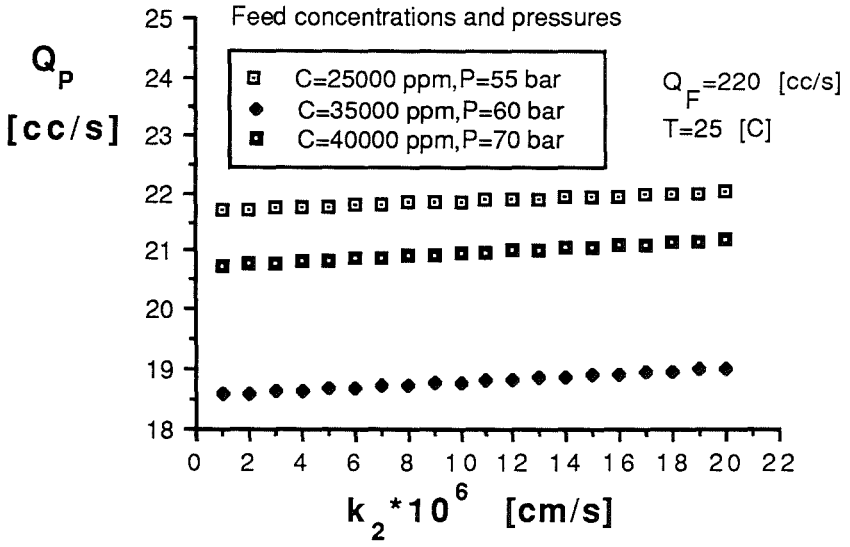

Fig.26-a : Variation of the FT30 element productivity with the salt permeability coefficient.

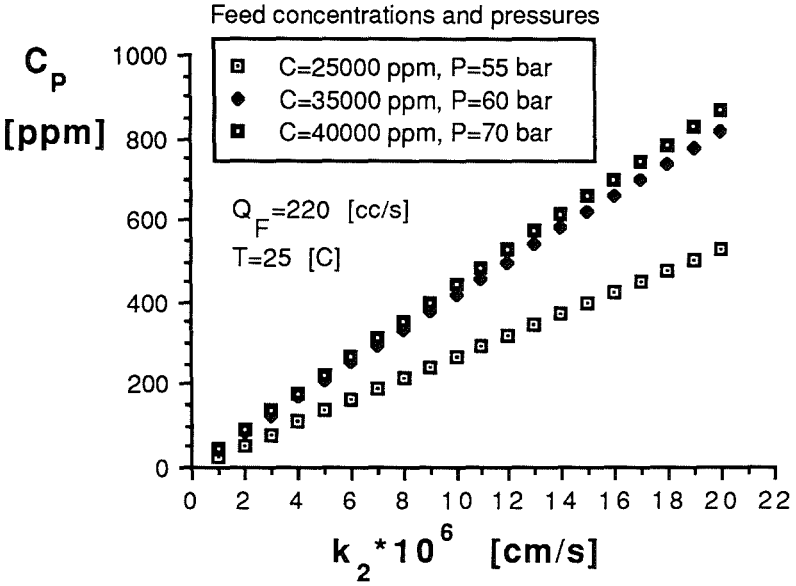

Fig.26-b : Variation of the FT30 element permeate concentration with the salt permeability coefficient.

Effect of the brine spacer friction parameter :

The effect of the brine friction parameter, E_B, on the membrane performance is plotted in Fig.27. As expected, the variation of E_B has an insignificant effect on the

permeate concentration (Fig.27-b). As concerns the permeate productivity, it is clear from Fig.27-a that a small effect is discernible only at extreme values of E_B. It is concluded that, for the type of brine spacer used in the FT30 element, the effect of brine pressure drop on flux is negligible, hence, that this need not be a major consideration.

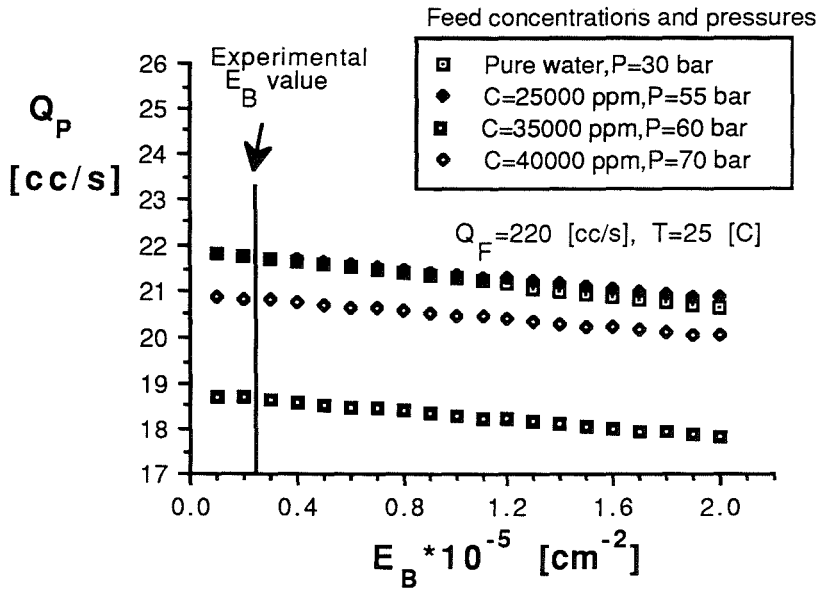

Fig.27-a : Variation of the FT30 element productivity with the brine friction parameter.

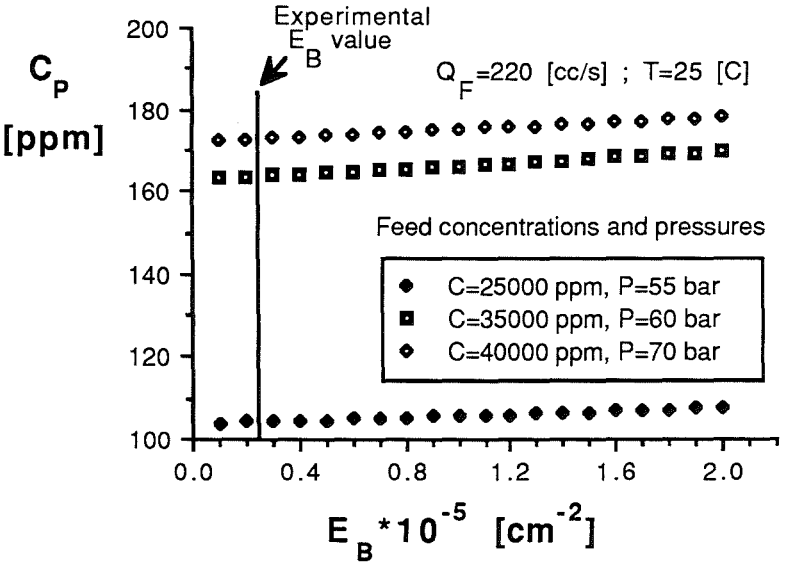

Fig.27-b : Variation of the FT30 element permeate concentration with the brine friction parameter.

For ease of comparison, the following table gives a quantitative evaluation of the effect of the variation of E_B on the module performance.

Table 5-3 : Percentage deviation of predicted element productivity,for different values of E_B, as compared with those obtained when $E_B=E_{BN}^*$.

	ΔQ_P[%]	
Operating conditions	$E_B=0.5E_{BN}^*$	$E_B=2E_{BN}^*$
Pure water, P_F=30 [bar]	+0.45%	-0.7%
C_F=25000 [ppm], P_F=55 [bar]	+0.34%	-0.6%
C_F=35000 [ppm], P_F=60 [bar]	+0.37%	-0.66%
C_F=40000 [ppm], P_F=70 [bar]	+0.32%	-0.55%

* E_{BN}= 25008 [cm^{-2}]

Referring to Table 5-3, it is evident that considering the brine friction parameter as constant, within the experimental range of E_B variation, is very unlikely to cause any major deviations in the prediction capability of our model.

Effect of the permeate friction parameter :

The effect of a variation of the permeate friction parameter, E_P, on the module performance is illustrated in Figs.28-a and 28-b. It is seen that while the E_P variation does not affect the permeate quality, its effects on the module productivity is considerable and much more pronounced than the effect of the brine friction parameter.

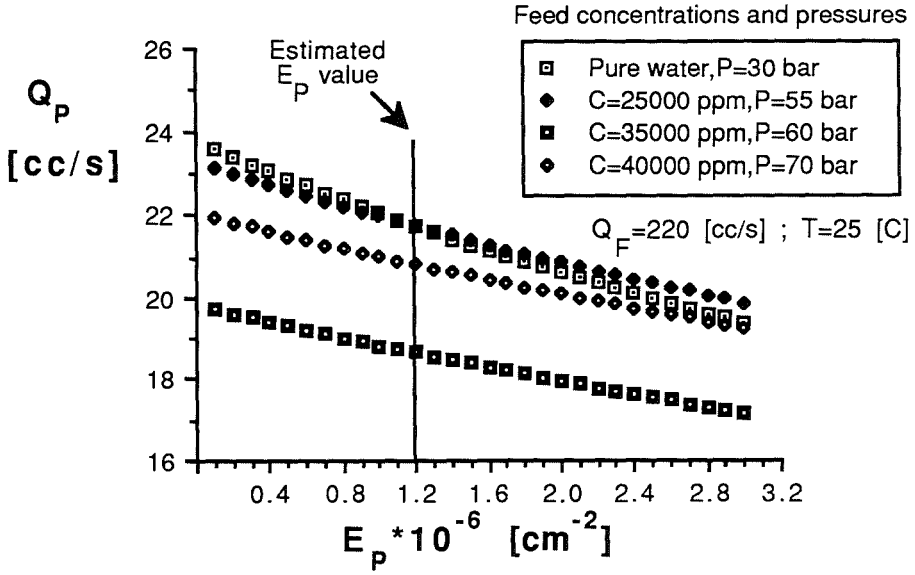

Fig.28-a : Variation of the FT30 element productivity with the permeate friction parameter.

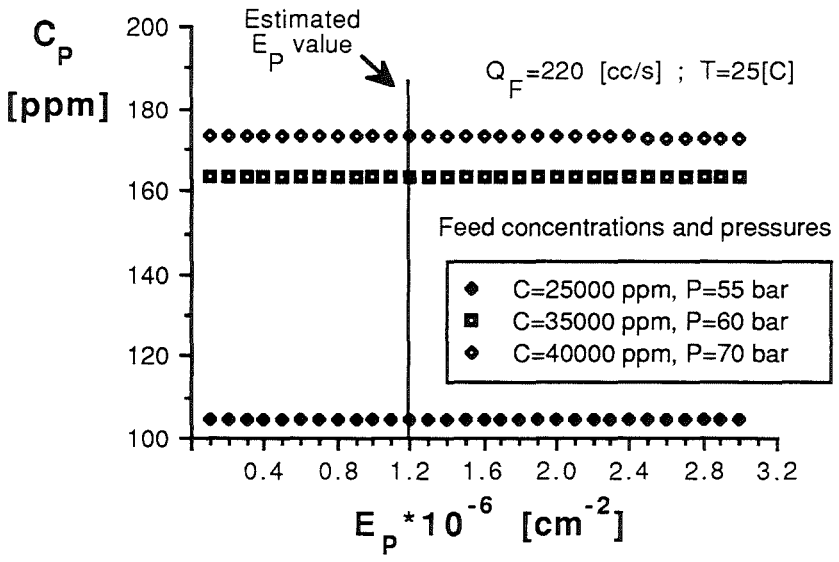

Fig.28-b : Variation of the FT30 element permeate concentration with the permeate friction parameter.

For a clearer picture, Table 5-4 gives some quantitative insight into the effect of the variation of E_P on the predicted results.

Table 5-4 : Percentage deviation of predicted element productivity, for different values of E_P, as compared with those obtained when $E_P=E_{PN}^*$.

	ΔQ_P [%]	
Operating conditions	$E_P=0.5E_{PN}^*$	$E_P=2E_{PN}^*$
Pure water, P_F=30 [bar]	+4.4%	-7.6%
C_F=25000 [ppm], P_F=55 [bar]	+3.3%	-6.0%
C_F=35000 [ppm], P_F=60 [bar]	+3.5%	-5.0%
C_F=40000 [ppm], P_F=70 [bar]	+3.0%	-5.1%

*E_{PN}=1200 000 [cm^{-2}]

Again, it is clear from Table 5-4 that, the assumption of a constant E_P is very reasonable specially if we note that the experimental variation range of E_P, determined in the previous chapter (range), was much smaller than the one represented in the above table.

Effect of the mass transfer coefficient :

The effect of the variation of the mass transfer coefficient, k, on the average flux and permeate concentration is shown, for different operating conditions, in Figs.29-a and 29-b. It is seen that the magnitude of concentration polarisation has a direct influence on the flux and permeate quality : the lower k, the higher the concentration polarisation and the lower the flux and permeate quality. The effect of k on the module performance becomes less significant at high k values.

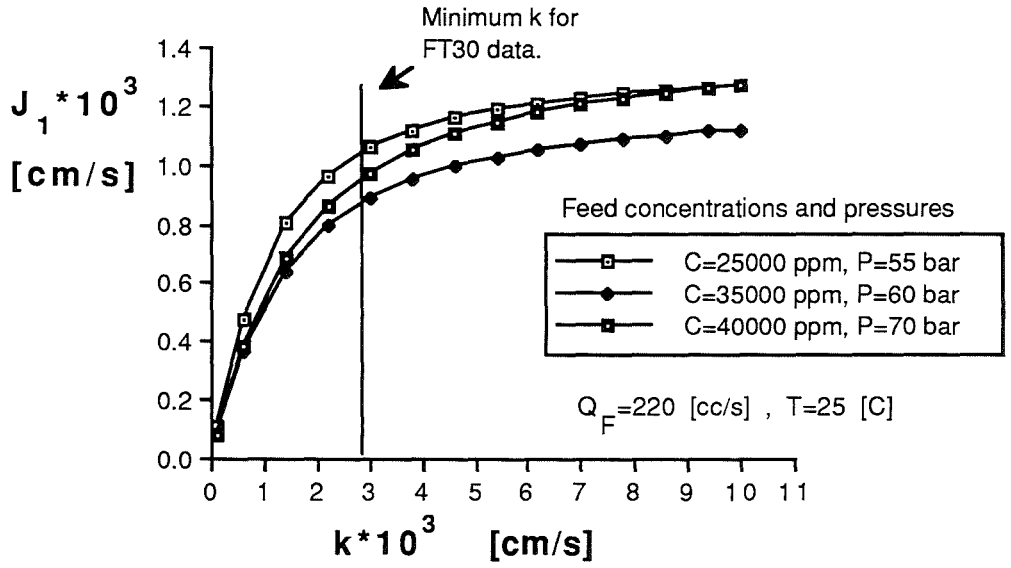

Fig.29-a : Variation of the FT30 element productivity with the mass transfer coefficient.

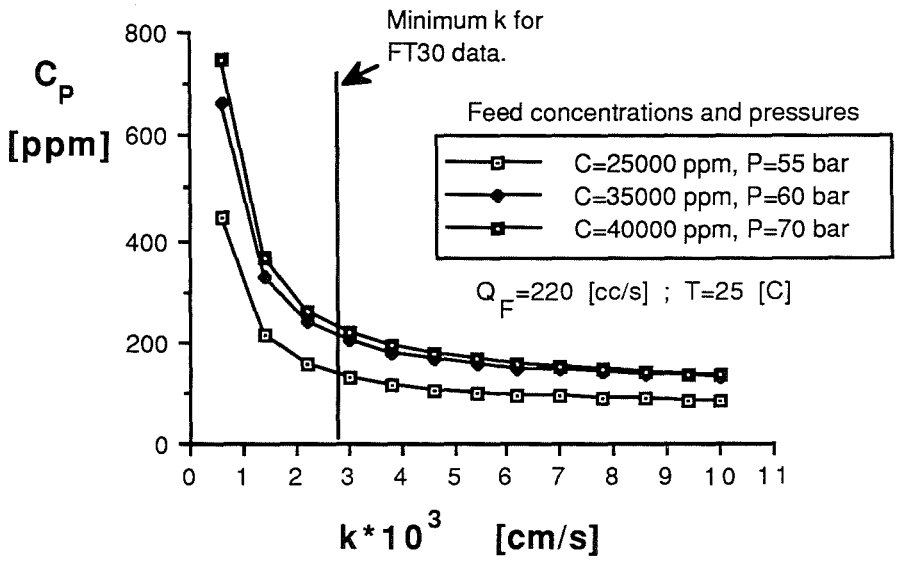

Fig.29-b : Variation of the FT30 element permeate concentration with the mass transfer coefficient.

An additional plot representative of the Roga type data is shown in Fig.30. This figure was included to show that the effects of concentration polarisation are much less significant for brackish waters of low salinity than in desalination of brines of high salinity (as shown in Fig.29). In this connection, it is not surprising that the authors of a previous work [25] obtained a good agreement with the Roga type data using a model that neglects completely the concentration polarisation phenomenon.

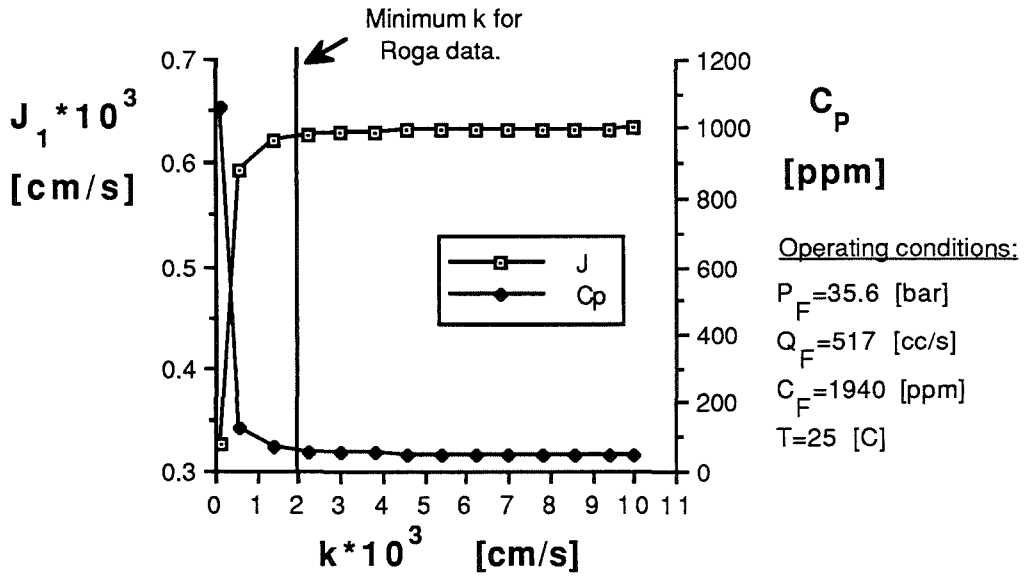

Fig.30 : Variation of the Roga element performance with the mass transfer coefficient.

Therefore, it is clear that it is not valid to derive or assess a correlation for the mass transfer coefficient using data from tests carried out solely with dilute solutions as feeds.

The main purpose of the above analysis was to assess the sensitivity of the model prediction to the variation in the "five parameters" in order to identify those parameters likely to affect the predictive accuracy of the model. At the same time, this analysis indicated good consistency of the SP model results as compared to the qualitative trends that would be expected.

From this investigation, and as far as the FT30 element is concerned, the water permeability, k_1, the salt permeability, k_2, and the mass transfer coefficient, k, emerge as the critical factors upon which accuracy the success of the models predictive capability largely depends.

The next section is devoted to the assessment of our models with actual experimental data.

V-3- Analysis of the Models Predictions.

V-3-1- Introduction.

Throughout this section, the different models will be tested for their ability to simulate actual module performance. Starting with the Spiral model, a detailed analysis will be presented. This will be followed by a comparative study of the Spiral and Slit models which will emphasise their merits and drawbacks..

Here, it should be pointed out that the accuracy of the numerical method, used in the models, is dependent on choosing sufficiently small mesh steps in both the radial and axial directions (see Figs.6 and 7). These were reduced until the predicted results did not change in the first three significant digits. The mesh step sizes used were :

- In the axial brine flow direction : 10 mesh steps for both models.

- In the radial flow, these were dependent on the model considered, i-e an incremental angular step of 30° (degrees) for the Spiral model and 20 equi-distant mesh steps for the Slit model.

The selection of these steps gave a sufficiently fine mesh and allowed for numerical stability to be achieved.

V-3-2- Predictive accuracy of the Spiral Model.

In a previous section, it was seen that the accuracy of the empirical relationships, describing the variation of the module parameters with operating conditions, is a key factor in establishing confidence in the predicted results. Consequently, considering the uncertainty associated with the applicability of these relationships, it was decided to adopt the following procedure for assessing their reliability as well as of the basic structure of the computational models:

- Compare experimental data with the predicted ones for tests using only pure water as a feed. This will allow to test the suitability of the equations defining the water permeability constant and the friction parameters.
- Compare the predictions with the more interesting case of salt feed solutions.

Due to the very close agreement obtained and for clarity, the plots displayed in the comparative figures will be generated in terms of relative errors. The relative errors are

defined as follows :

$$\Delta = \frac{\text{experimental - predicted}}{\text{experimental}} * 100\% \qquad (5\text{-}1)$$

The comparisons between the experimental and the predicted results were consistent and similar accuracy trends were exhibited at all brine reject flows. Because of this, plots at a single constant brine exit flow rate of Q_B= 200.5 [cc/s] are presented in this section. A detailed summary of the main experimental and predicted results can be found in Appendix D.

The first comparison is displayed in Fig.31 which shows the variation of the relative error on the module productivity versus the applied pressure for different operating temperatures. It is seen that the agreement is very satisfactory with an estimated maximum deviation related to the experimental results of just about ±5%. This agreement, although having a limited utility in practical situations, is very important since it contributes in :

- Adding credibility to the experimental procedure adopted for the determination of the water permeability correlation.
- Establishing confidence in the structure of the program prior to attempting to compare its prediction with salt water data.

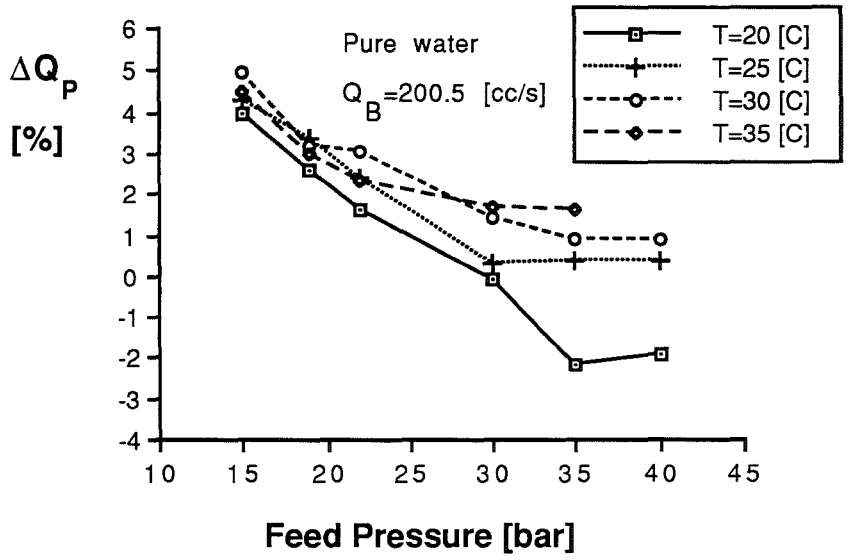

Fig.31: Variation of the relative error on the FT30 element productivity for pure water data using the SP model.

At this stage, since additional experimental data on the permeate pressure drop for the 2nd FT30 element were available [28], it was thought that it would be interesting to compare them with our model predictions. This allows a practical assessment of the choice of a constant permeate friction parameter (E_p=1200000 cm^{-2}) as well as the adequacy of the Darcy expression (i-e eq.(3-2)).

It should be noted that the permeate friction parameter is a spacer property rather than a parameter linked to the membrane characteristics. Therefore, it is clear that for the 2nd FT30 membrane, although its intrinsic properties are different from the first one (see IV-4), should, nevertheless, possess the same friction parameter. In fact, it was for this purpose that some tests, aimed at the determination of the intrinsic water permeability for the 2nd FT30 membrane, were performed. This comparison is presented in Fig.32-a where all the data necessary to generate the plots made use of eq.(4-9), i-e the water permeability correlation specific to the 2nd FT30 membrane, to predict the change of the water permeability with operating conditions.

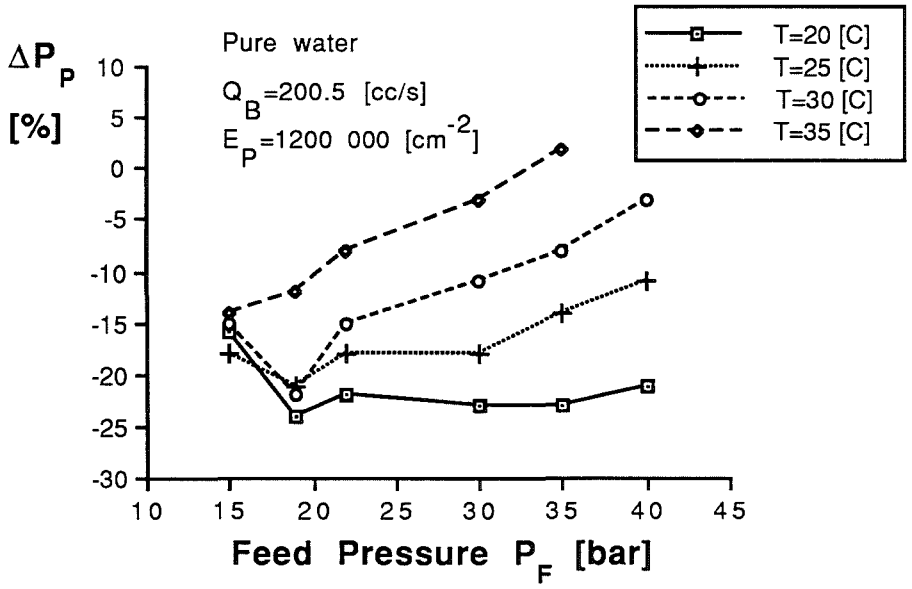

Fig.32-a : Variation of the relative error on the permeate pressure at the membrane closed end for the 2nd FT30 element using the SP model.

From Fig.32-a, it is seen that the relative error of the predicted values for the permeate pressure is quite considerable especially at the low temperatures and feed pressures where the maximum deviations reached 25%. To some extent, these discrepancies were expected and might be attributed to one or to a combination of the following factors :

- Experimental uncertainties : as stressed previously (see section IV-2), permeate pressure measurements on the actual element are very difficult to perform and therefore, are prone to some degree of errors.

- The permeate friction parameter, E_P, was taken as a constant equal to an average value over the range of operating conditions and obtained through a semi-analytical procedure (see Appendix D). This procedure made use of Darcy's relationship for flow through porous media, i-e :

$$\frac{dP_P}{dx} = -\mu E_P V_P^{n_P}$$

in which the exponent, n_P, on the permeate velocity was assumed to be 1. This was necessary as the true value of n_P could not be found since V_P varies constantly along the channel due to permeation. Therefore, this assumption (i-e n_P=1) would result in a corresponding error in the prediction of the permeate pressure.

However, as seen in section V-2 (Fig.28-a), the variation of E_P should not have a great effect on the prediction of the module productivity. In this context, Fig.32-b shows the corresponding relative errors on the module productivity predictions, obtained for the same data as those displayed in Fig.32-a.

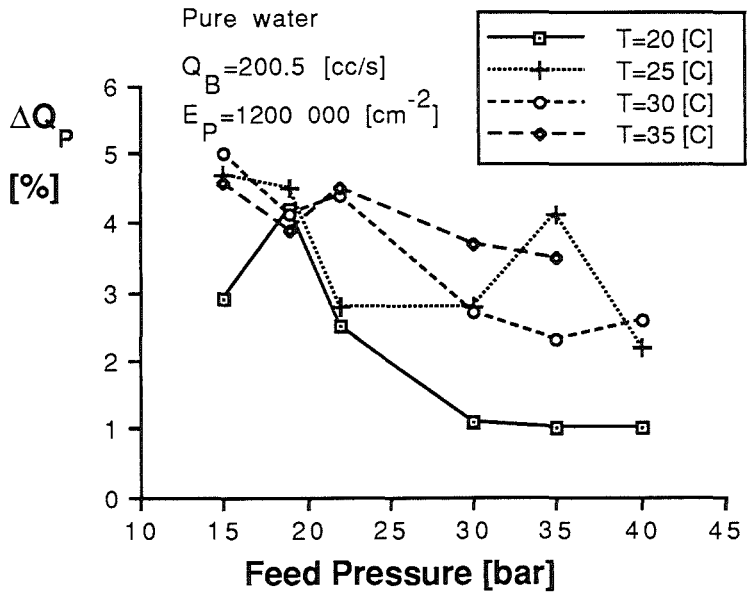

Fig.32-b: Variation of the relative error on the 2nd FT30 module productivity for pure water data using the SP model.

Judging from the above figure, Fig.32-b, it is seen that the module productivity predictions were reasonably accurate, considering the wide range of variables tested and the fact that pressure drop is very sensitive to flow distribution.

In an attempt to see whether the permeate pressure prediction can be improved, Figs. 33-a and 33-b display the results obtained when making use of a correlation giving the permeate friction parameter in terms of feed pressure, i-e $E_P=f(P_F)$, at constant temperature. Such correlations were obtained from a curve fitting using the data in Fig.24 (see chapter IV).

It must be stressed that this procedure is not strictly correct and applicable for the present data where the feed pressure varied up to 80 bar. However, it was though that such correlations would be useful to show if an improvement can be obtained.

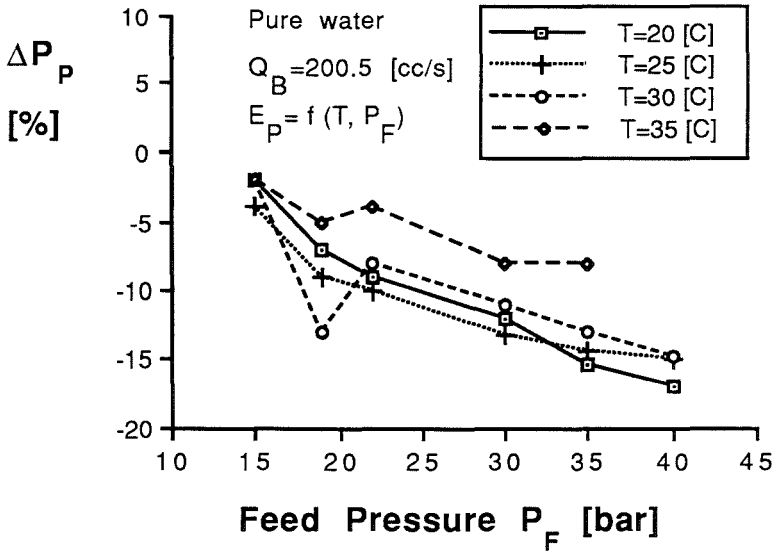

Fig.33-a: Variation of the relative error on the permeate pressure at the membrane closed end for the 2nd FT30 element using the SP model and a varying permeate friction parameter.

From Fig.33-a, it is seen that by using a variable permeate friction parameter an improvement on the permeate pressure drop prediction, although modest, is certainly obtainable. The corresponding improvement in the element productivity predictions is shown in Fig.33-b.

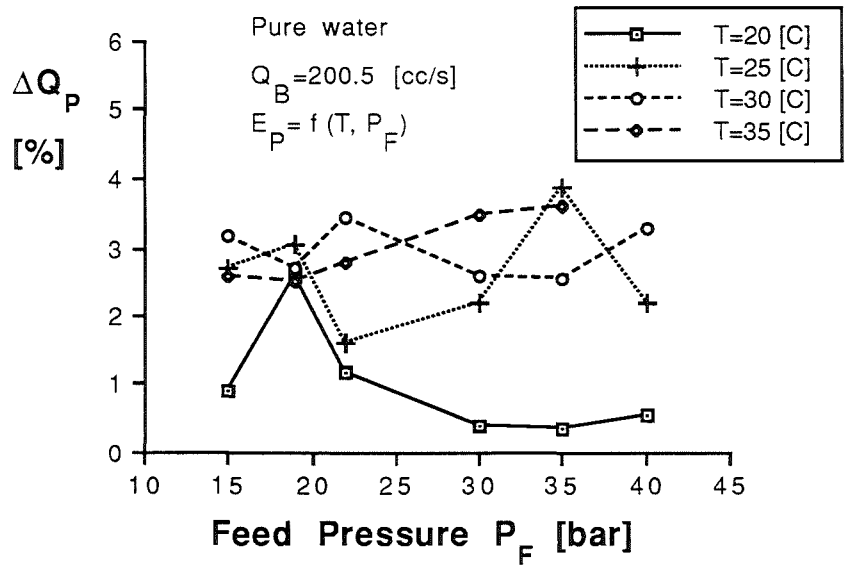

Fig.33-b: Variation of the relative error on the 2nd FT30 element productivity for pure water data using the SP model and a varying permeate friction parameter.

This investigation reveals that a specific weakness in the present treatment lies in the assumption of a constant permeate friction parameter. Without detailed experimental data obtained from constant flow in flat channels, it is difficult at this stage to adopt a better estimate for E_P. However, considering Figs 32-b and 33-b, it is seen that the effect on module productivity is fairly small.

The remaining part of this section is devoted to the more practical aspect of this analysis, i-e the performance simulation on brine feeds. This will be achieved by comparing the experimental data with the SP model predictions. By doing so, the accuracy of the empirical relationships, related to the mass transfer coefficient and salt permeability, will be assessed also.

Fig.34 illustrates such a comparative test. The different plots were carried out at only one level of feed concentration, i-e C_F=35000 [ppm], as this condition represented fairly well the general trends of the performance predictions. This figure shows clearly that, in this case, the discrepancies are more pronounced than when only pure water data were compared. The maximum deviations were of about 14% with respect to module productivity and up to 34% with respect to permeate concentration.

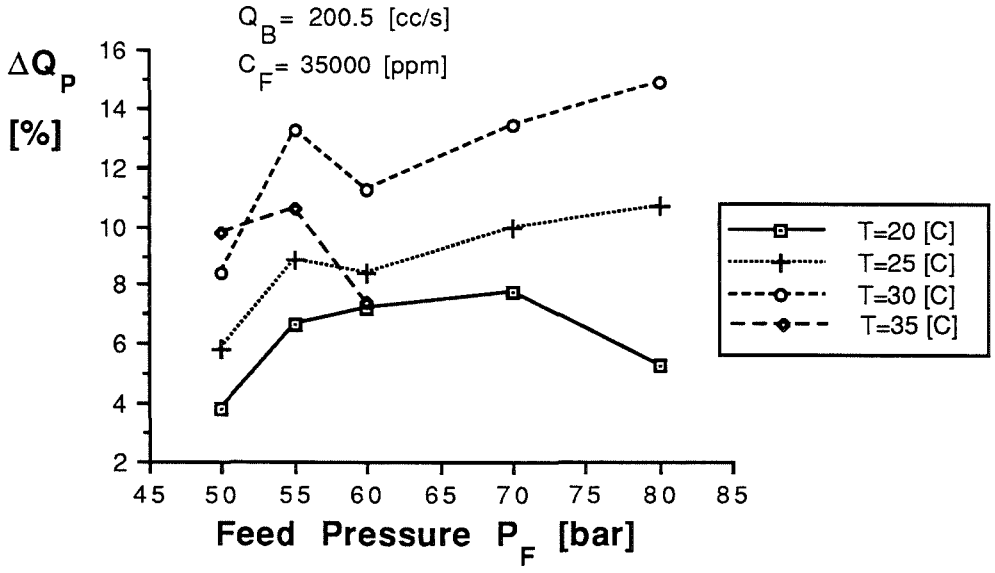

Fig.34-a : Variation of the relative error on the FT30 element productivity when eq. (4-20) is used in the SP model.

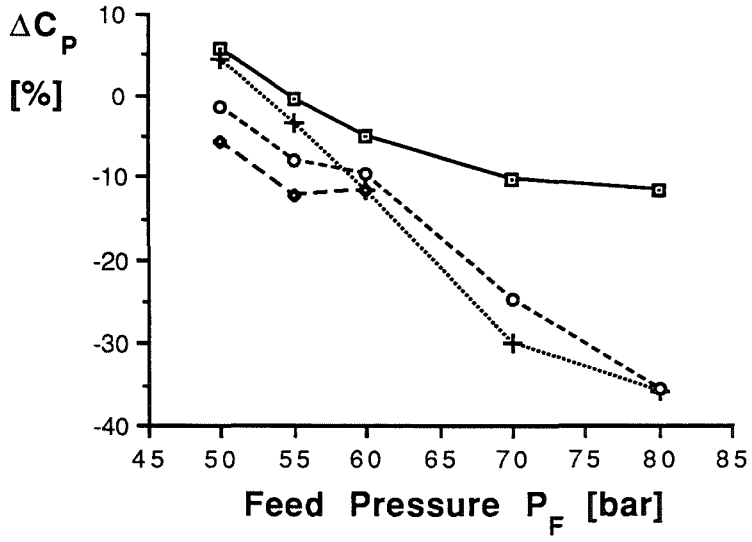

Fig.34-b : Variation of the relative error on the FT30 element permeate concentration when eq. (4-20) is used in the SP model.

A comparative analysis of Figs.31 and 32-a reveals that the factor mainly responsible for the rather poor agreement obtained in Fig.34-a is the use of our empirical relationship concerning the variation of the mass transfer coefficient, eq.(4-20), defined in the previous chapter as:

$$Sh = 0.0112\ Re^{0.33} Sc^{0.44} \left(\frac{J_1}{J_0}\right)^{-0.46} \qquad (4\text{-}20)$$

Seemingly, this correlation has a very limited aptitude in describing correctly the concentration polarisation phenomenon taking place in the module. At this stage, one can only speculate on the reasons at the origin of this failure and, in this context, two distinct possibilities are suggested as follows:

One is, perhaps, due to the restricted range of temperatures and concentrations tested. This might have a particular effect on the evaluation of the true exponent on the Schmidt number (eq.(4-20)). The other lies in the way the data were calculated and represented by the osmotic pressure method which is very sensitive to changing parameters. This, in turn, might have magnified significantly the apparent dependency of the mass transfer coefficient on the flux. Therefore, probably the osmotic pressure method is not particularly suited for the experimental determination of the mass transfer coefficient. A similar conclusion was reached by Gekas et al [33] and an in depth discussion of the problems associated with this technique may be found in this reference.

It should be noted that the above causes are only possibilities. A complete resolution of this matter awaits an investigation which would include detailed measurements of the local brine wall concentration. To this end, direct measurements of the concentration profile using microelectrodes and/or optical devices are, perhaps, best suited. This would make it possible to derive a quantitative mathematical relationship describing the concentration polarisation phenomena. Until such work is done, an alternative is to use one of the current published mass transfer correlations. Among these, the Winograd correlation [24], i-e eq.(3-1), defined in chapter III as :

$$k = 0.753 \left(\frac{KB}{2\text{-}KB}\right)^{1/2} \frac{D_s}{h_B}\ Sc^{-1/6} \left(\frac{Pe\ h_B}{MB}\right)^{1/2} \qquad (3\text{-}1)$$

emerges as the more appropriate since, unlike most others, it was not derived from heat and mass transfer analogies. This correlation has been incorporated in the SP computational model. The resulting comparison is given in Fig.35 where the same experimental data as in Fig.34 were used.

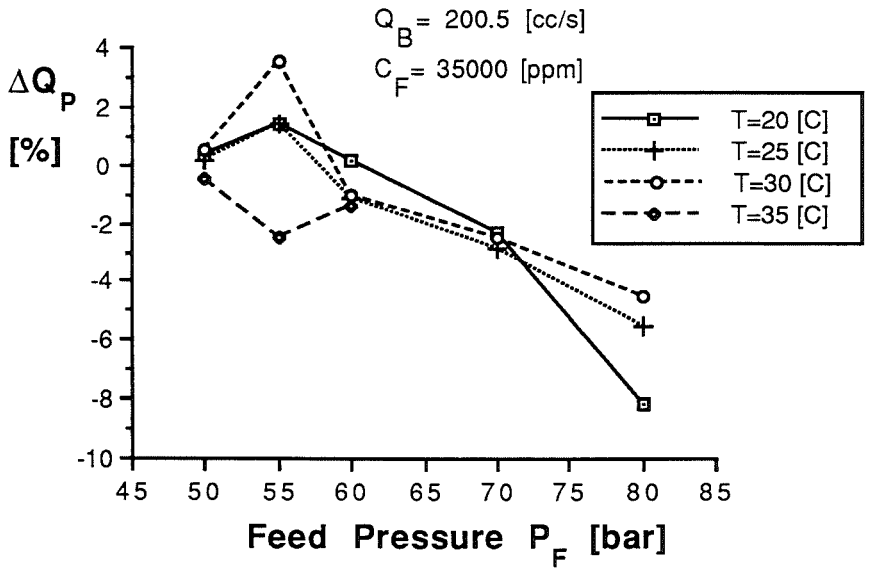

Fig.35-a : Variation of the relative error on the FT30 element productivity when eq. (3-1) is used in the SP model.

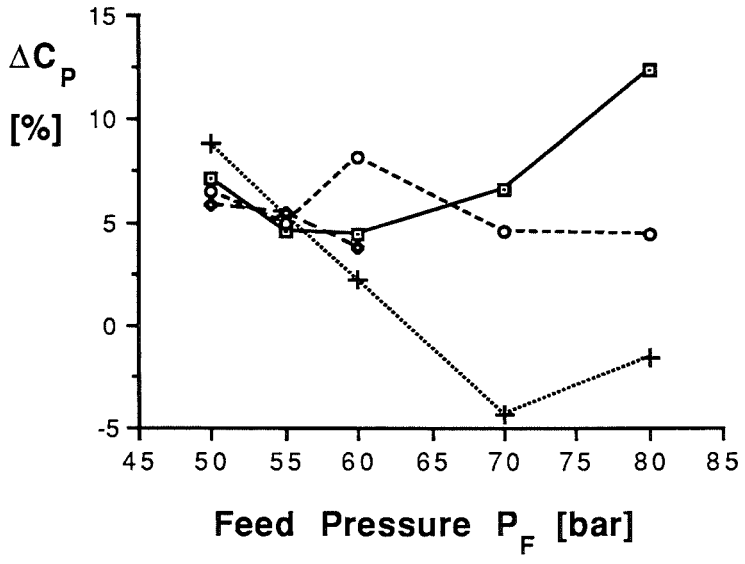

Fig.35-b : Variation of the relative error on the FT30 element permeate concentration when eq. (3-1) is used in the SP model.

First of all, it is noticed that, by using the Winograd correlation, an improved prediction is obtained. Indeed, within the accuracy of the experimental data, it is clear from Fig.35 that the deviations of the predicted results are much smaller than the ones implemented in Fig.34. For the whole range of the FT30 experimental conditions tested (Appendix D), typical deviations were, with the exception of some isolated cases, of about ±6% for the module productivity and of the order of ±10% for the permeate concentration. The relatively larger deviations observed in the permeate concentration can

be explained by the fact that the average permeate concentration depends on the relative amounts of solute and solvent fluxes. Therefore, a small deviations in either of these fluxes will inevitably affect the prediction of the permeate concentration. Another possibility could be associated with the transport mechanism, i-e the Solution diffusion model, adopted in this work. Therefore, it is suggested that, in the future, it would certainly be worthwhile to use 3-parameter models or a model of the Solution diffusion imperfection type to see whether the prediction of the permeate concentration can be improved.

A similar comparison has been carried for lower feed pressures and concentrations specific to the Roga module data. The results are reported in Fig.36.

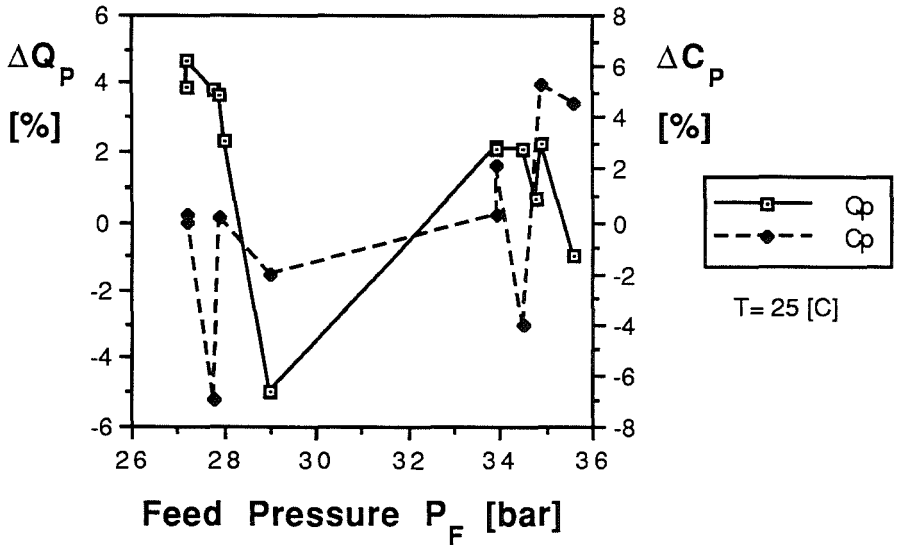

Fig.36 : Comparison of the SP model predictions with the Roga element experimental data.

Again, as for the FT30 results, it is seen that for the Roga data the agreement is good with a maximum deviation being of just 5% with respect to permeate flow and less than 7% for the permeate quality. It should be noted that these results were obtained despite that the calculations were performed with characteristic parameters, for the membrane and spacers, borrowed from a previous investigation (see Table 5-2). These were estimated through their particular procedure and therefore can not be taken for granted. In this connection, some of the discrepancies may be attributable to these parameters.

As a closure to this section, it was seen that, for the whole range of experimental conditions, the agreement is good with respect to both product rates and salt separation indicating the validity and practical utility of the prediction technique used in the SP model.

On the other hand, a major contribution of this analysis was the validation of the Winograd correlation which, to the author's knowledge, has, for the first time, been tested against data typical of sea water desalination.

V-3-3- Slit versus Spiral Model.

In this section, a comparative analysis of the SP and SL models will be presented. The accuracy of the SL model will be tested progressively by using, as a first step, the Roga module data which are characterised by low feed pressures and concentrations. This will be followed by an assessment of the SL model predictions against the more severe feed conditions of the FT30 data.

Fig.37 presents the results of the SL model predictions as compared with the Roga element data.

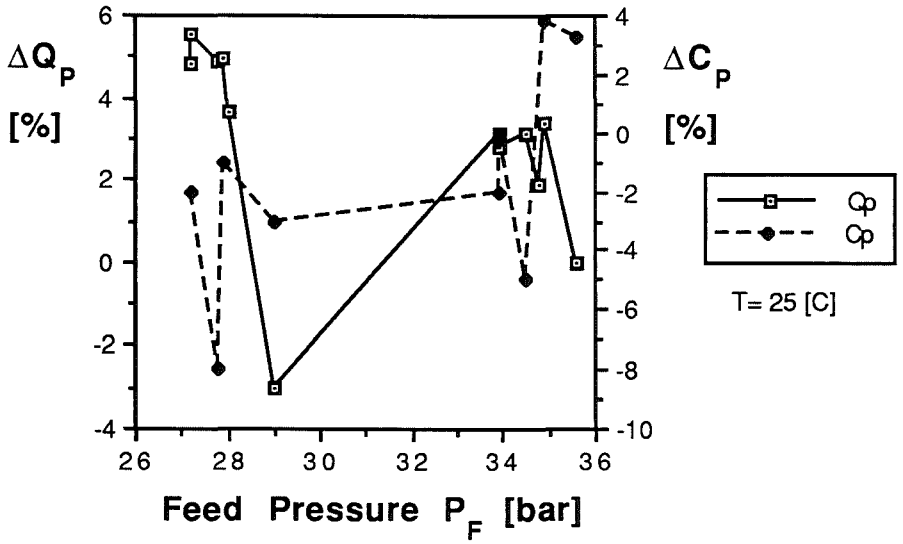

Fig.37 : Comparison of the SL model predictions with the Roga element experimental data.

From the above figure, it is seen that the agreement between the calculation and experiment is good with typical deviations of less than 6% for module productivity and less than 9% with respect to permeate concentration. A comparison of Fig.36 with Fig.37 reveals that there is no significant differences in the predictive accuracy of the SL and SP models. However, this could be expected since it was shown earlier (see section V-2) that for the Roga type data the level of concentration polarisation cannot be considered as significant. Therefore, a rigorous comparison of the model's capabilities would be more appropriate when the FT30/seawater data are used. Such comparison is shown, for both models, in the following table, Table 5-5.

Table 5-5 : Comparison between experimental and predicted results for FT30 module with Q_B=246.22 (cc/s) and C_F= 35000 (ppm).

T (C)	P_F (bar)	Q_F (cc/s)	ΔQ_P(%)		ΔC_P(%)	
			SP*	SL**	SP*	SL**
20	50	258.50	0.1	0.3	5.1	3.5
20	55	260.90	0.2	0.4	4.1	2.4
20	60	262.90	-1.8	-1.6	3.4	1.3
20	70	267.18	-2.6	-2.4	9.0	7.5
20	80	269.85	-9.5	-9.3	17.8	15.5
25	50	259.90	-0.3	-0.1	10.7	9.1
25	55	262.60	-0.2	0.0	4.6	3.1
25	60	267.18	-2.6	-2.3	1.2	-0.6
25	70	269.55	-3.8	-3.5	-3.0	-5.2
25	80	273.72	-6.0	-5.7	0.0	-2.5
30	50	260.70	0.9	1.1	8.1	6.6
30	55	264.22	-2.2	-1.9	2.3	0.5
30	60	266.97	-3.2	-2.9	7.7	5.8
30	70	272.25	0.7	1.0	3.6	1.2
30	80	276.88	-7.0	-6.7	0.0	-2.8
35	50	263.10	-1.4	-1.1	7.4	5.8
35	55	266.15	-3.2	-2.9	7.4	5.9
35	60	269.55	-2.7	-2.4	0.9	-1.3
35	70	275.72	-3.6	-3.3	6.6	4.0
35	80	281.05	-5.8	-5.5	-1.2	-3.7

* : using Spiral Model.

** : using Slit Model.

It is clear from the above table that, for both models, a very good agreement of the predicted values for permeate flow rates and concentrations is obtained. It is, particularly interesting to note that no appreciable discrepancies are encountered when the prediction capability of the models is compared. Additional results supporting the trends shown in Table 5-5 are reported in Appendix D. These results would suggest that the effect of model geometry is not as significant as implied by our initial qualitative comparison of the two models presented in section III-2-2. Indeed, the agreement outlined in this section appears to validate the SL model for the whole range of experimental conditions used in

this work which cover most cases in current desalination practice.

It should be mentioned that, unlike the traditional SL model [20, 23], the one presented here is quite different since it takes into account :

(i)- The fluid variation properties at every location (i-e in the bulk flow as well as in the boundary layer).

(ii)- Characterisation of membrane and spacers.

(iii)- The calculation of the feed velocity was based on the brine spacer spiral length.

All of the above factors contributed to the apparent success of our SL model prediction capability. The importance of the first two is evident. The last factor has often been neglected and a comment stressing its significance is believed worth mentioning at this stage. It indicates that the feed velocity evaluation should be based on the brine spacer spiral length, W_{BS}, rather than on the membrane spiral length, W_M, as physically implied by the SL model. This is because, in practice, the brine spacer is wider than the membrane leaf. For example, for the FT30 element, we have W_{BS} = 133 [cm] whereas W_M = 110 [cm] : therefore an evaluation of the cross sectional area, available for the feed flow, based on W_M will introduce in this case an overestimation on the feed velocity of the order of 21% as compared with the actual value calculated from W_{BS}. This, in turn, would result in a considerable effect on the mass transfer coefficient. Incidentally, such problem does not arise when making use of the SP model since it includes a procedure which evaluates W_{BS} with a very good approximation.

At this stage, it is concluded that, while the difference in modelling approaches was certainly worthy of further investigation, the Spiral model does not seem to yield any advantage when compared to the SL model. Further, a computer program based on the SP model must carry out all the indexing and calculations related to the various mesh lengths and grid locations which are not as straightforward as those implemented in the SL model. Consequently, a main disadvantage of the SP model, as compared with the SL model, is the greater amount of computer time required. Indeed, for the "optimum" mesh step sizes reported in section V-3-1, both programs were run under similar feed conditions on an ICL 3980 computer: the SL program was on average more than 20 times faster than the SP program with typical execution times of 5s and 90s of CPU time respectively.

V-4- Parametric study of the effects of the operating variables.

The validity of the simulation procedure adopted, in the models developed, has been determined in the previous sections. Here, the main purpose is to establish the consistency of the models by studying the effect on the predicted permeation flux and quality due to changes in operating conditions. Basically, there are four operating conditions which influence the performance of the reverse osmosis process.

These are :

- The applied pressure.
- The feed flow rate or feed velocity.
- The feed solution concentration.
- The operating temperature.

In the following, the influence of the above variables will be investigated separately. The results of this parametric study will include some plots of the local values of flux and brine wall concentration, expressed as dimensionless quantities, axially along the SPW element. These were judged necessary for a clearer understanding of the physical mechanisms and to help explain the characteristic effects of the operating conditions on the SPW element performance. The dimensionless quantities considered are defined as follows :

- $(J_1/J_O)_{Ave.}$: ratio of local flux to initial flux (at the membrane inlet) averaged over the spiral length of the membrane.

- $(C_{BW}/C_F)_{Ave.}$: ratio of local brine wall concentration to feed concentration averaged over the spiral length of the membrane.

Note: in the literature, the value of (C_{BW}/C_B) is usually plotted, however in this work we felt that a better indication of C_{BW} would be to plot (C_{BW}/C_F), to allow the reader to deduce the actual value of C_{BW}. Because C_B is changing with position, C_{BW} cannot be readily computed from (C_{BW}/C_B) data.

The effect of the applied pressure on the FT30 element performance is displayed in Fig.38.

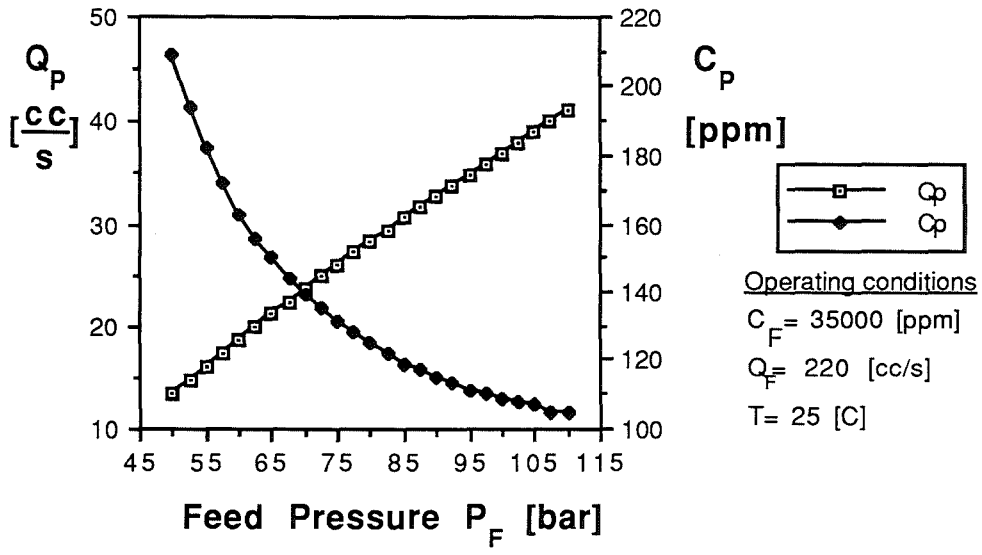

Fig.38 : Effect of the applied pressure on the FT30 element performance.

From the above figure, it is seen that as the applied pressure increases, the flux increases and the permeate concentration decreases. However, the flux increase is not proportional to the increase in applied pressure. This behavior is due to the increased effect of concentration polarisation which tends to increase as the flux increases (due to a higher salt convection towards the membrane) and thus results in higher osmotic pressures. This is illustrated in Figs.39-a and 39-b which show, for different applied pressures, the axial variation of $(J_1/J_0)_{Ave.}$ and $(C_{BW}/C_F)_{Ave.}$ respectively.

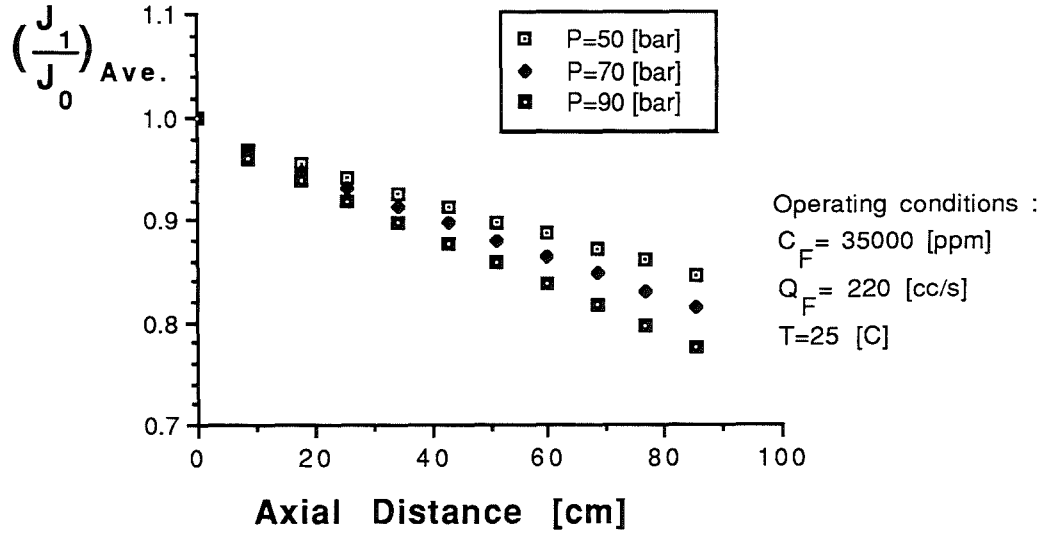

Fig.39-a :Variation of $(J_1/J_0)_{Ave.}$ along the membrane length as a function of the applied pressure.

Fig.39-a shows that the flux decreases with axial position. This is due to an increase in the brine wall concentration as shown in Fig.39-b. In this figure, it is clearly depicted that as the applied pressure increases, the increase of $(C_{BW}/C_F)_{Ave.}$ tends to be sharper because the value of the bulk concentration $(C_B)_{Ave.}$ increases with position due to recovery. Thus, we can see that the majority of the rise in C_{BW} is due to recovery : the higher the recovery (applied pressure), the sharper the increase in bulk concentration, (C_B), and the higher the wall concentration (C_{BW}). For example, for P_F=90 [bar] and at an axial distance x=47 [cm] from the element inlet, we have $(C_{BW}/C_F)_{Ave.}$=1.64. The corresponding value of $(C_{BW}/C_B)_{Ave.}$ is 1.43 which is lower.

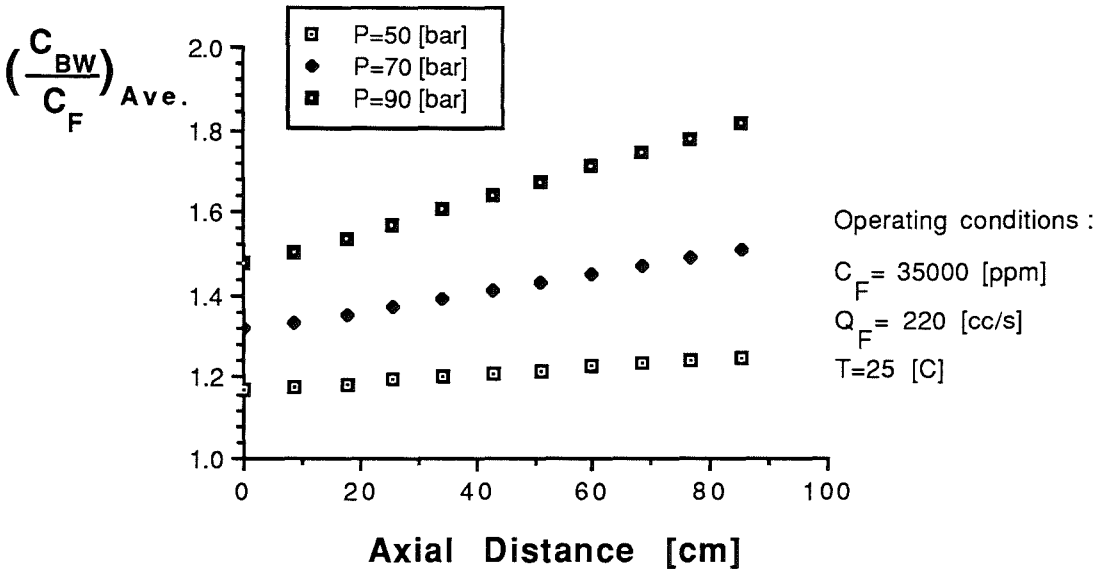

Fig.39-b :Variation of $(C_{BW}/C_F)_{Ave.}$ along the membrane length as a function of the applied pressure.

As concerns the permeate quality, the decrease in permeate concentration with increase in applied pressure, P_F, is due to the rise in water flux. However, at high P_F values, this decrease tends to slow down due to an increase in the value of the brine wall concentration (Fig.39-b) which results in higher salt fluxes.

The feed flow rate or brine crossflow velocity affects considerably both the module productivity and permeate quality. This is clearly shown in Fig.40.

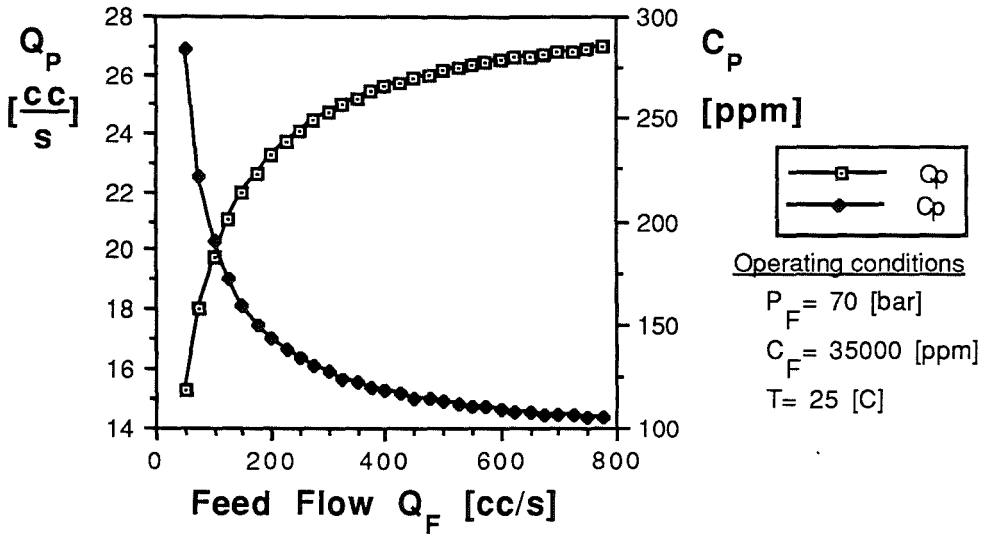

Fig.40 : Effect of the feed flow rate on the FT30 element performance.

As the feed velocity increases, the permeate flow increases and the permeate concentration decreases. This is because a high velocity generates shearing forces and/or turbulence which in turn limits the thickness of the boundary layer by increasing the mass transfer coefficient and reducing thus the concentration polarisation effects. A more detailed vision of this phenomenon can be seen from Figs.41-a and 41-b which show, respectively, the axial variation of the "spirally averaged" values of the flux and of the brine wall concentration for different feed flow rates.

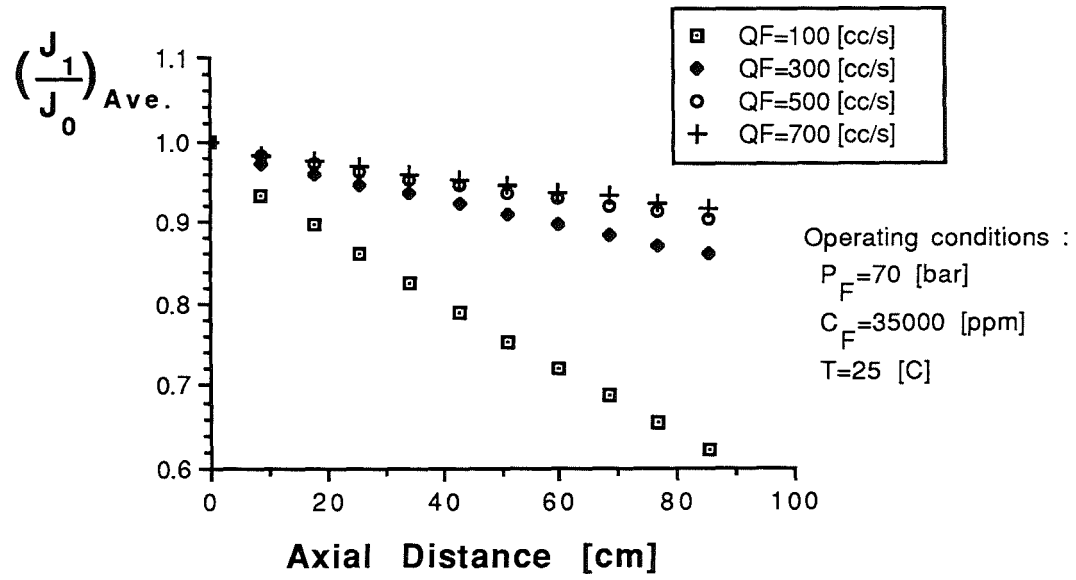

Fig.41-a :Variation of $(J_1/J_0)_{Ave.}$ along the membrane length as a function of the feed flow rate.

From Fig.41-a, we see that the flux decreases with axial position along the membrane length. This flux decline increases as the feed flow rate decreases due to a rise in the brine wall concentration as shown in Fig.41-b.

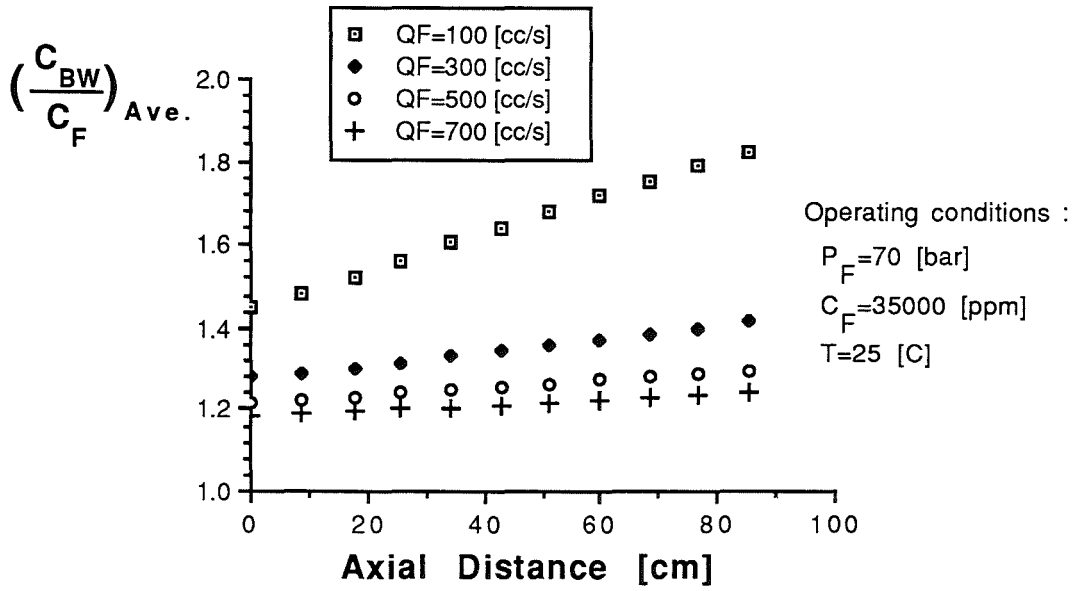

Fig.41-b : Variation of $(C_{BW}/C_F)_{Ave.}$ along the membrane length as a function of the feed flow rate.

From the above figure, it is clear that at decreasing feed flow rates, corresponding to increasing recoveries, the concentration gradient along the membrane increases.

It was computed that, at an axial distance x=47 [cm] from the element inlet, as the initial feed flow rate was increased from 100 [cc/s] to 500 [cc/s], the dimensionless wall concentration, $(C_{BW}/C_F)_{Ave.}$, decreased from 1.64 to 1.25. This difference was increasing as the element exit end was reached due to recovery.

On the other hand, it should be noted from Fig.40 that, at high feed flow rates, the productivity and permeate quality reach an asymptotic value. This is because at such brine velocities, the effect of concentration polarisation becomes less significant, (Fig.41-b), and the main limiting factor becomes the pressure drops in both the permeate and brine channels.

Fig.42 demonstrates that the SPW element performance is considerably affected by the feed concentration.

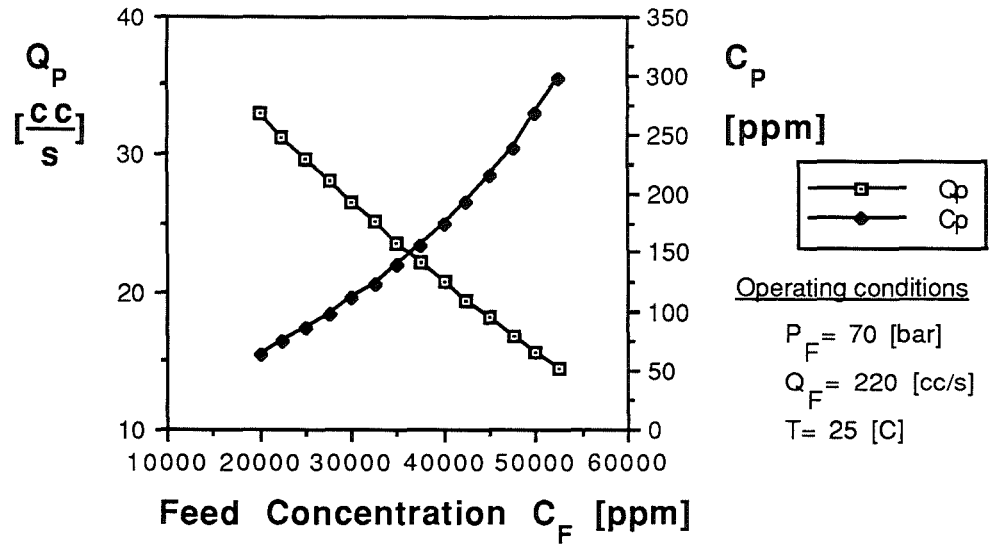

Fig.42 : Effect of the feed concentration on the FT30 element performance.

As expected, it is seen that an increase in feed concentration results in a decrease in both water productivity and salt rejection. These variations are not linear : the flux drop and the permeate concentration rise are steeper as the feed concentration increases due to higher osmotic pressures which reduce the effective driving differential pressure across the membrane. This is clearly observed in Figs. 43-a and 43-b which show the actual axial variation of the flux and wall concentration, respectively, along the membrane length.

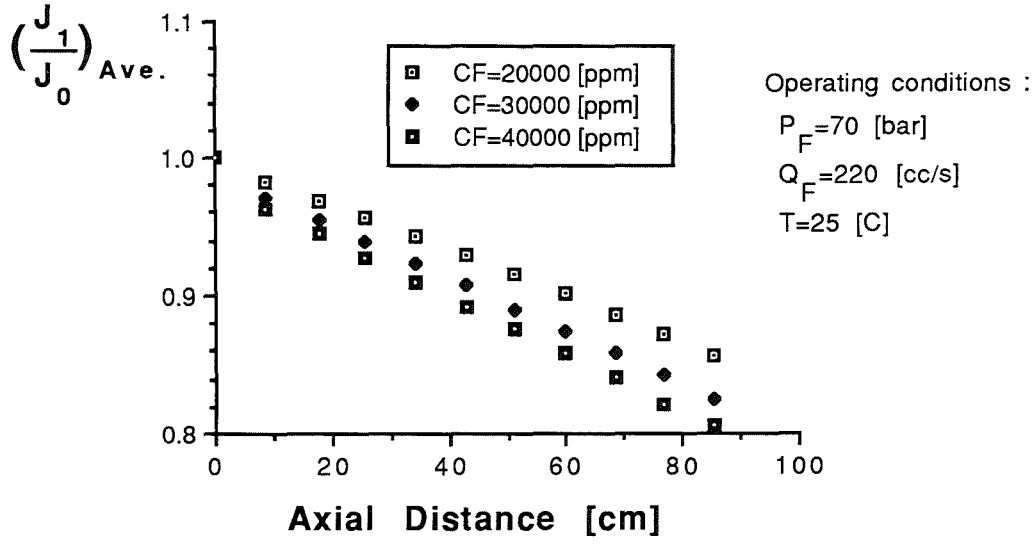

Fig.43-a :Variation of $(J_1/J_0)_{Ave.}$ along the membrane length as a function of the feed concentration.

In Fig.43-a, it is seen that the flux decline, along the whole membrane length, increases from 15% to 20% as the feed concentration increased from 20000 [ppm] to 40000 [ppm]. This is due to an increase in recovery and thus in the wall concentration as shown in Fig.43-b.

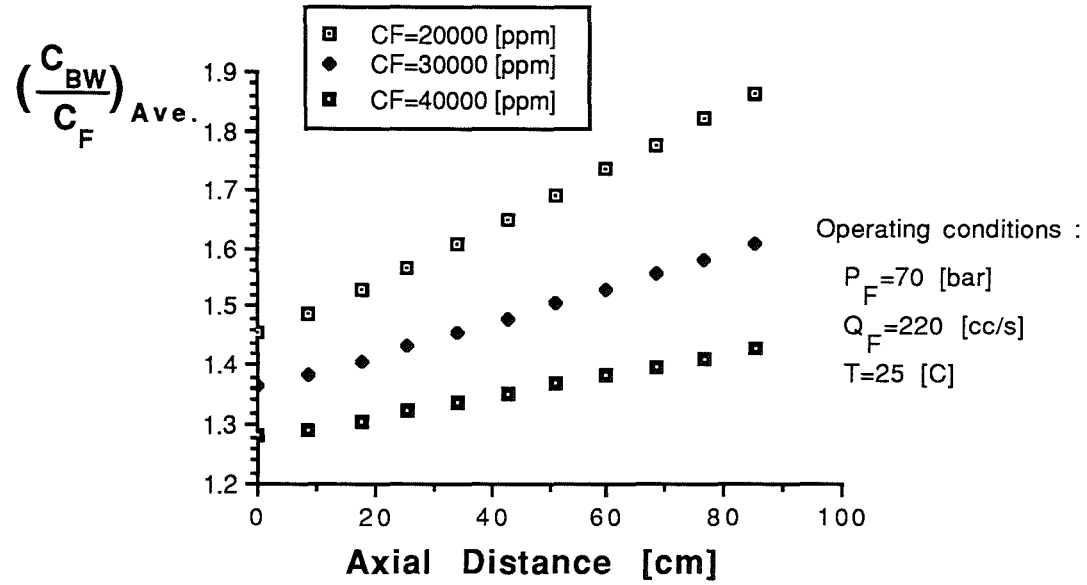

Fig.43-b : Variation of $(C_{BW}/C_F)_{Ave.}$ along the membrane length as a function of the feed concentration.

Concentration polarisation increased for lower feed concentrations, showing therefore that higher water fluxes result in an increase in solute convection towards the membrane and hence increased flux drop along the membrane length.

The effect of the variation of the operating temperature on the SPW element is exhibited in Fig.44. As expected, it is seen that the flux and the permeate concentration increase with temperature. This variation is not linear since a variation in temperature has contradictory effects on several parameters.

Temperature affects the flow conditions through and parallel to the membrane resulting in a two fold effect on membrane performance. The flux increases with temperature on account of lower viscosity. An increase in temperature also results in an elevation in the osmotic pressure (Π). The diffusitivity, Ds, also increases with temperature. This increase in Ds should result in a decrease in the wall concentration, C_{BW}, due to an increase in solute back diffusion. This would also result in an increase of flux, which would increase solute convection toward the membrane. Thus, most of the above contradictory effects will tend to cancel each other out to some extent. This was indeed the case as shown in Figs. 45-a and 45-b.

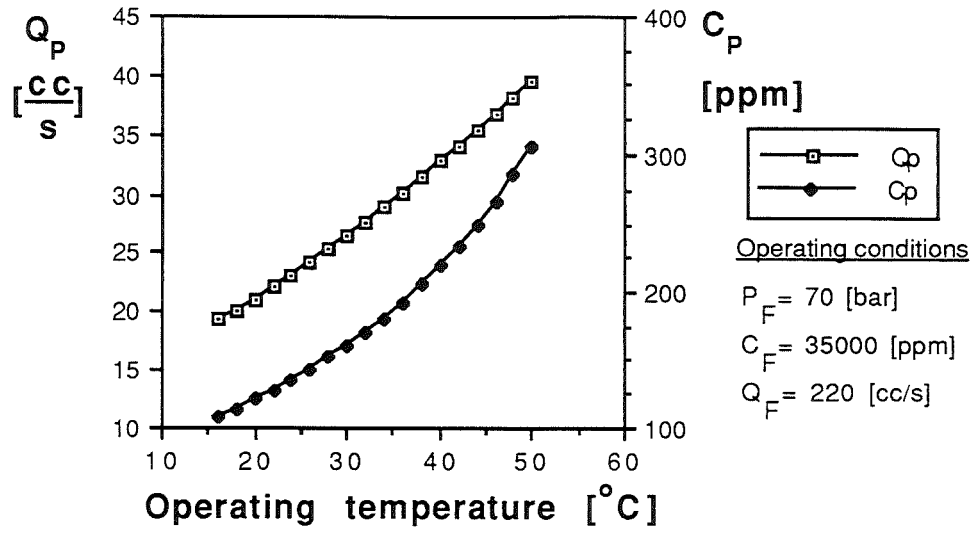

Fig.44 : Effect of the operating temperature on the FT30 element performance.

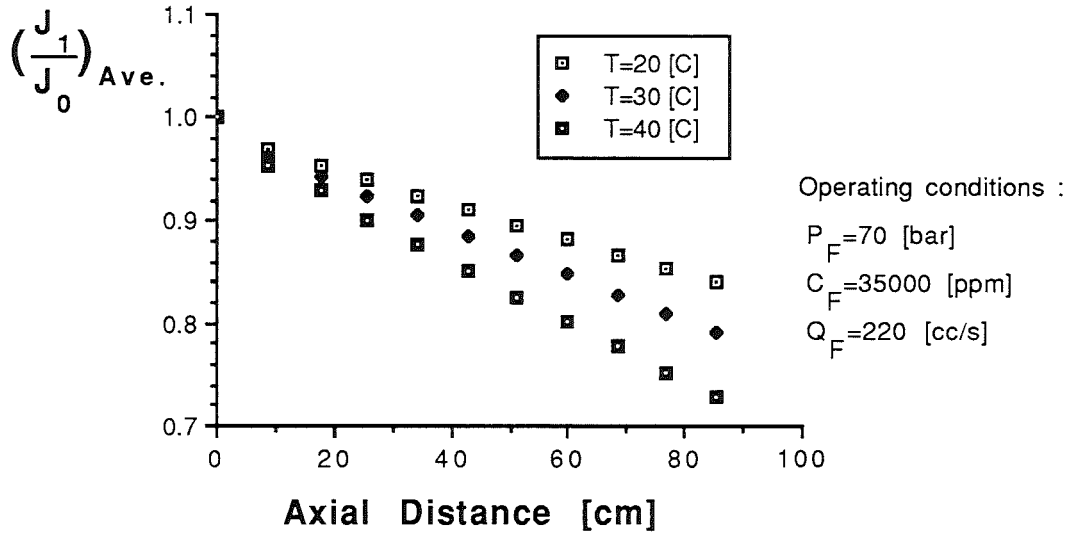

Fig.45-a :Variation of $(J_1/J_0)_{Ave.}$ along the membrane length as a function of the operating temperature.

From the data in Fig.45-a it was computed that, for the given operating conditions, as temperature increased from 20 to 40 [°C], the flux decline along the membrane, i-e from inlet to outlet, increased from 18% to 30.5%. This is due to the higher brine wall concentration gradient, as shown in Fig.45-b, (which increased from 15% to 20% respectively) resulting in increased osmotic pressure.

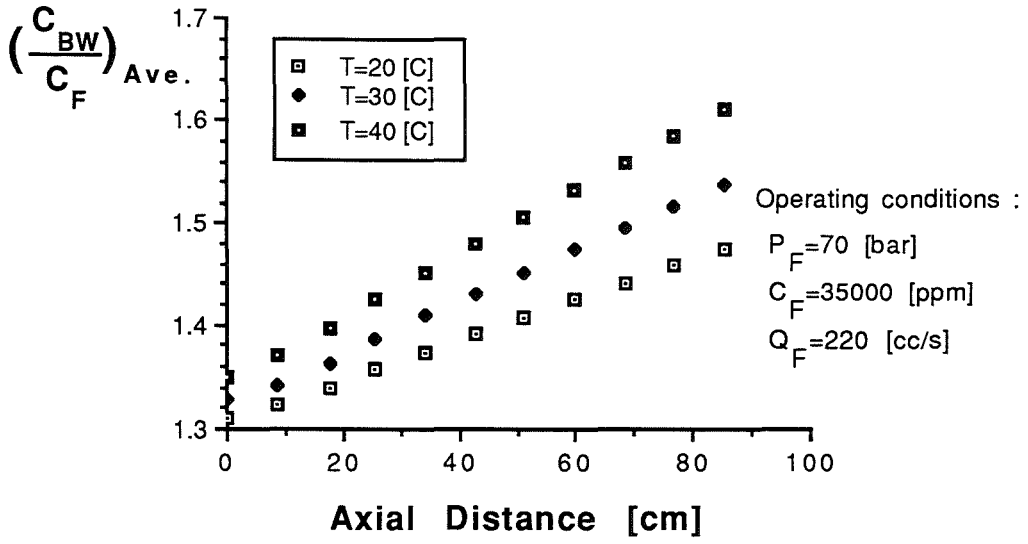

Fig.45-b :Variation of $(C_{BW}/C_F)_{Ave.}$ along the membrane length as a function of the operating temperature.

As compared with the 20 [°C] run, the 40 [°C] run had an initial average flux (J_O) 64% higher but the osmotic pressure (Π_O) was 12.7% higher with this difference becoming more pronounced as the wall concentration increases.

On the other hand, it is clear from Fig.44 that as the temperature rises the increase in the permeate concentration is steeper than for the flux. This is due to the combined effect of increasing brine wall concentrations and salt permeability coefficient (see eq.(4-14)).

From a scaling and/or chemistry point of view, one is interested in knowing the value of the maximum brine concentration that occurs in the SPW element for different operating conditions. It is clear that the maximum brine concentration occurs at the membrane interface boundary layer due to concentration polarisation (CP). Apart from increasing the osmotic pressure, and thus reducing the driving pressure for the filtration process, excessive CP might have other negative consequences as follows :

> If the brine wall concentration reaches the saturation concentration, precipitation on the membrane surface will take place (scaling). This in turn increases the risks for changes in composition of the membrane material due to chemical reaction which would result in a corresponding change in the membrane separation characteristics.

Therefore, for the safe design of RO SPW elements, it would be desirable to attain

some degree of fouling (scaling) control through optimisation of the operating conditions. In this context, the models developed represent a useful guiding tool. As an illustration of such exercise, Fig.45 displays quantitatively the variation of the maximum brine concentration, C_{BWmax}, as a function of operating temperature and feed pressure.

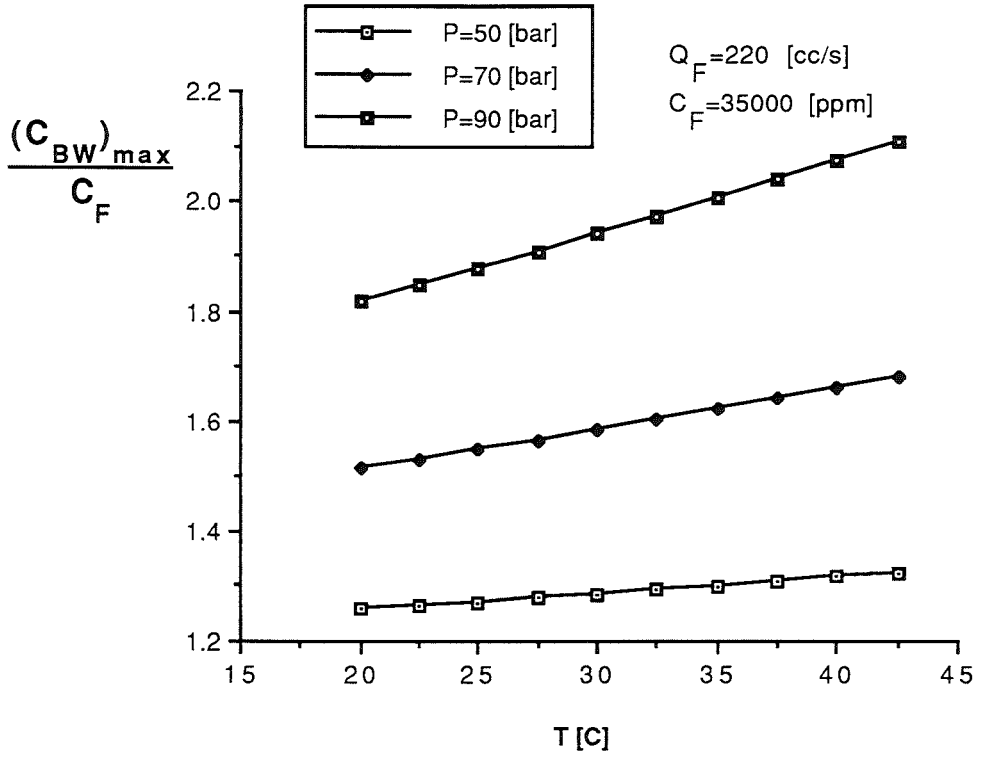

Fig.45 : Variation of the maximum brine concentration as a function of operating temperature and pressure.

From the above figure, it is seen that C_{BWmax} increases with both temperature and feed pressure as expected.

V-5- Closure.

Before passing to the next chapter, it is interesting to recapitulate the main points which resulted from this analysis as follows:

-1) Both the SP and SL models developed in this work proved to be successful in predicting, reasonably, the spiral wound element performance over a wide range of operating conditions.

-2) Permeate concentration predictions were less successful. Possible reasons were identified. Particularly, it was suggested that the use of a model which takes into account the coupling between the water and salt fluxes, Solution diffusion imperfection model, would, perhaps, result in a better estimate of the permeate concentration.

-3) It was shown that no significant discrepancies were encountered between the SL and SP models predictions, at least for the type of operating conditions most likely to be met in practical situations. This was not expected and can be attributed to the degree of sophistication of our SL model. Indeed, the major difference between the models is that the SP model considers, at a given brine location, the asymmetrical nature of the flux referred to in section III-2-2. Consequently, it is concluded that this difference is one of detail and not of essence.

-4) The analysis highlighted the need for a thorough experimental characterisation of the membrane and module parameters. In this respect, it was shown that the use of simple scale down experiments on membrane samples was adequate. However, the experimental determination of the mass transfer coefficient proved to be less satisfactory and it was concluded that more sophisticated mass transfer coefficient measurement techniques might be required.

-5) One important contribution of the work was the extension of the range of validation of the Winograd correlation for the prediction of the mass transfer coefficient variation with operating conditions.

With regard to the above conclusions, it is clear that the validity of the simulation procedure has been established. This result is important since the success of the simulation stage is a prerequisite to any in-depth investigation concerning the main parameters governing the practical design of spiral wound systems. In this context, the next chapter is devoted to the applicability of this analysis for the optimisation of spiral-wound elements.

CHAPTER SIX

SPIRAL WOUND ELEMENT OPTIMISATION.

VI-1- General Remarks and Objectives.

It is evident that, for the successful application of any SPW element, the use of a suitable membrane is essential. Besides this, other factors such as the economic and hydrodynamic aspects are at least of equal importance. Indeed, the efficiency of SPW elements depends not just on the membrane properties but also on the flow conditions within the element. In this chapter, our efforts are directed at examining the design features of elements using the FT30 SW membrane. As mentioned previously, this membrane was conceived for sea water desalination. A similar investigation concerning the brackish water application of the Roga type SPW element was carried out in a previous work [32]. Presumably, the designs of both these types of elements were based on either an empirical or semi-empirical approach or any other method specific to the membrane manufacturer. In any case, none of these methods are generally available in the literature for obvious commercial reasons.

The purpose, here is to show that the models developed can be used not only to predict the SPW element performance but also for the element optimisation. In order to apply an optimisation procedure it is, first, necessary to define an objective function, then to identify the variables that affect it and finally to find an equation relating the objective function to the variables. Due to the scarcity of information on module manufacturing and running energy costs, an economic optimisation was not attempted. There is no reason why, given the appropriate data, this analysis could not be used to make an economic optimisation. However, for the purposes of illustrating the use of this analysis in the optimisation of an element design, an objective function maximising the water production per unit element volume per unit applied pressure is chosen. This objective function, termed "the volume specific productivity of the SPW element", (ζ), is defined as follows :

$$\zeta = \frac{Q_P}{V_{MOD} \cdot P_F} \qquad (6\text{-}1)$$

The number of variables against which optimisations may be made is large. Consequently, as an illustrative exercise we shall limit ourselves to the optimisation of the element geometry over a set of operational conditions representative of those for which

the FT30 SPW element was intended. From the design viewpoint, one wishes to know how the volume specific productivity, ζ, will vary as a function of the geometrical variables over which the designer has control. That is:- How do the number of membrane leaves (NLE), the membrane axial length (L), the membrane spiral length (W), the heights of the channels affect the element performance? Are the optimum values of these parameters sensitive to differing operating conditions?

For given typical operating conditions, it will be interesting to see how the computed optimal geometry does compare with the original design used by FilmTec.

Note : In the following, unless otherwise stated, the geometrical data listed in the table below, Table 6-1, were used for the generation of each plot.

Table 6-1 : Geometrical data used in the calculations.

Number of leaves :		NLE	1
Membrane spiral length	(cm)	W	110
Membrane axial length	(cm)	L	85.4
Membrane thickness	(cm)	h_M	0.014
Brine channel height	(cm)	h_B	0.077
Permeate channel height	(cm)	h_P	0.041

In this analysis, the use of the SP model was preferred primarily because it takes account of the difference between the spiral lengths of the brine channel and the membrane which, as shown earlier, can affect considerably the evaluation of the feed velocity. Further, the SP model takes into account the relative shift between the membrane leaves as they wind around the central collector pipe.

VI-2- Optimisation of Spiral-Wound Elements using the FT30 sea water membrane.

This section will start by considering an optimisation of the number of leaves and of the membrane leaf geometric dimensions. To perform such task, it is appropriate first to hold the total membrane area, A_{TM}, constant. For ease of comparison, the chosen value of the total membrane area corresponded to the one used in the actual FT30 SPW element, i-e A_{TM} =1.88 [m^2]. The next step consists in selecting the bases for the estimation of the optimum values. In this context, the following two different possibilities were identified:

1- Membrane axial length fixed and its spiral length allowed to vary.

2- Both membrane axial and spiral lengths varied.

At this stage, there is no clear way of deciding which of these approaches will be more likely to occur as the choice will mainly depend on information related to manufacturing and/or economic constraints. For example, if the choice of the membrane axial length is dictated by practical manufacturing considerations, then the first procedure would be preferred. In any case, both procedures will be considered in this analysis.

Figs.47 and 48 show respectively the influence of the membrane axial length and of the membrane axial-to-spiral length ratio on the volume specific productivity with the number of leaves as a parameter. The curves were all evaluated at a constant channel heights and, therefore, module packing density, of P_D=1370 [m^2/m^3].

At first sight, these figures would suggest that a different optimal number of leaves would be obtained depending on the approach used. However, a detailed analysis of each figure is required for a better understanding of the phenomena involved.

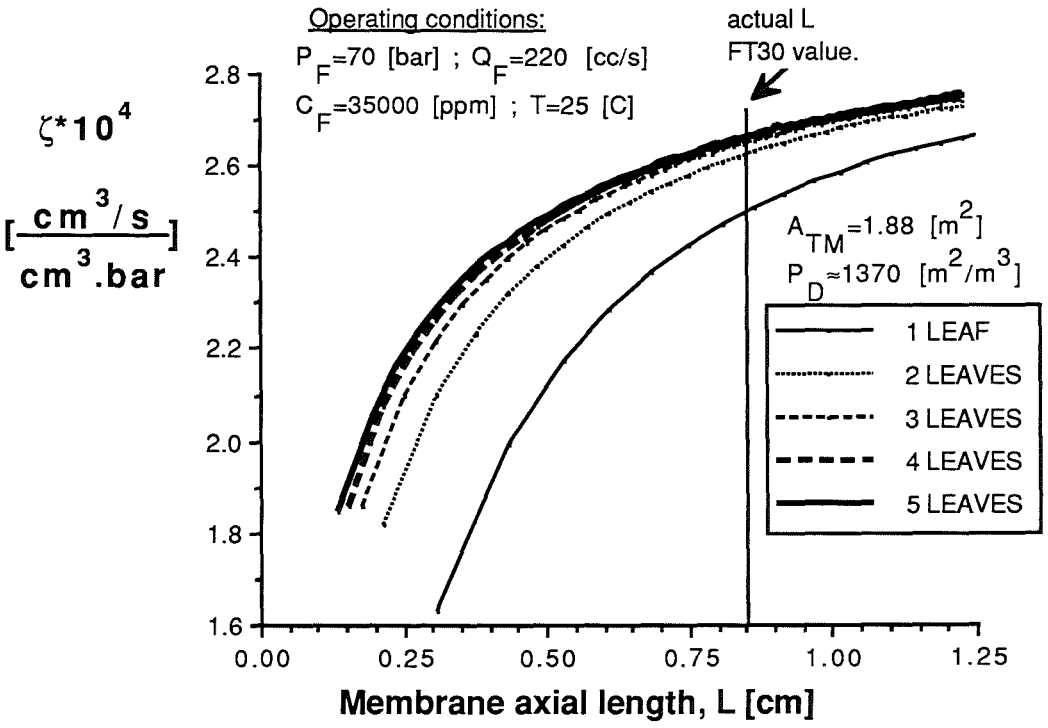

FIG.47: Influence of membrane leaf geometry on module volume specific productivity as a function of membrane axial length.

From Fig.47, it is seen that, to some extent, the specific volume productivity increases with increase in the number of leaves. This was expected since the permeate pressure drop decreases as the number of leaves increases due to the resulting decrease in the spiral length of the permeate channel. This figure shows clearly that, for the range of axial membrane lengths quoted, the advantage of increasing the number of membrane leaves becomes less apparent for a number of leaves NLE>2. Thus, it would appear that the optimum number of leaves is of two leaves. However, it should be stressed that an important factor which was not accounted for in Fig.47 is the effect of the membrane glue line width. This glue line is necessary in practice for protection against possible leakage. In a previous work [32], it was shown that consideration of the glue line width results in a decrease of the SPW element performance due to the reduced effective area of the membrane. This negative effect tends to become more pronounced as the number of leaves increases. Therefore, the apparent gain in performance of a two leaves element as compared to a one leaf would be somehow lesser than the one implied in Fig.47. Consequently, one must ask if the possible increase in the productivity of the two leaves element is high enough to justify any increase which may occur in the manufacturing cost.

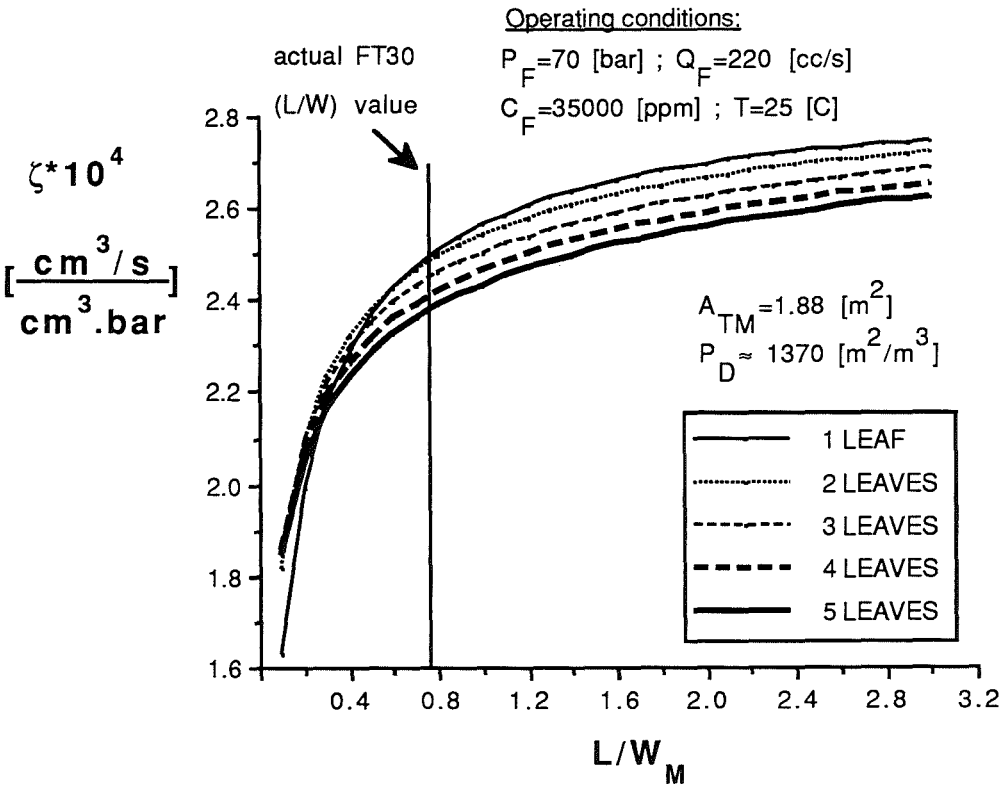

FIG.48: Influence of membrane leaf geometry on module volume specific productivity as a function of the membrane axial-to-spiral length ratio.

The second optimisation approach, where both the membrane axial and spiral lengths were variable, is illustrated in Fig.48. This plot reveals that there is no beneficial effect in increasing the number of leaves since it is clearly seen that the optimum number of leaves is $NLE_{opt.}=1$. This is due to the effect of concentration polarisation (CP) which tends to increase as the cross flow velocity decreases (i-e as the number of leaves increases since the feed flow and the total membrane area were kept constant). Again, as in Fig.47, the effect of the glue line width was not considered; however, in this case, it can be anticipated that such effect will make no difference to $NLE_{opt.}$

Regarding the optimal value of the axial-to-spiral length ratio, it is seen that the calculations did not reveal any sharply defined value; instead, quite independently of the number of leaves considered, there is a critical value of (L/W) starting at about $(L/W)_{crit.}>0.8$ above which the curves become asymptotic. This compares fairly well with the actual value i-e (L/W)actual=0.77.

All curves show, to some extent, a similar pattern highlighting a strong influence of the (L/W) value on the volume specific productivity especially when $(L/W)<(L/W)_{crit.}$. This behaviour can be explained by considering the pressure drop in both channels. In this context, Fig.49 displays these pressure drops as a function of (L/W) at the optimal leaf number $NLE_{opt.}=1$.

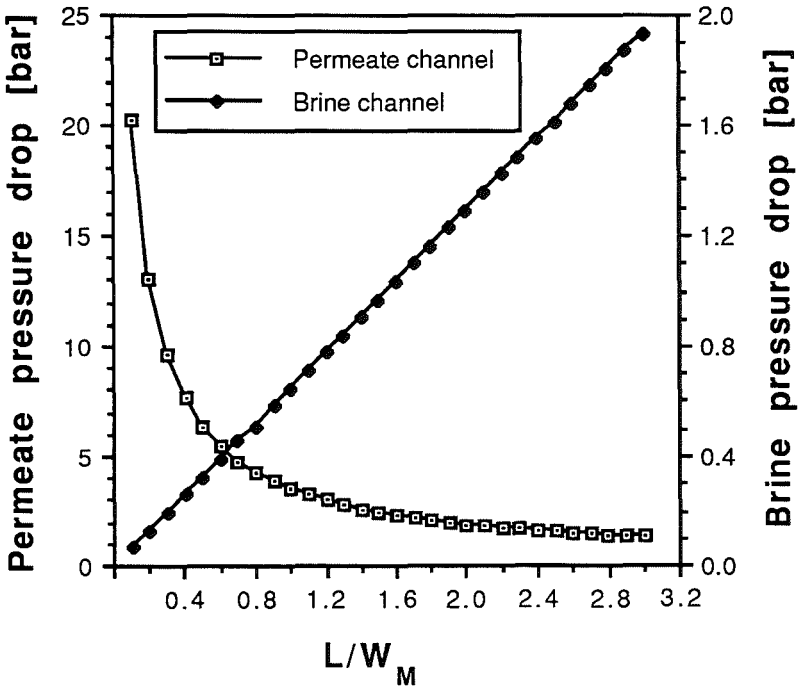

FIG.49: Variation of the pressure losses with (L/W) for a single membrane leaf module.

It is clear from both figures (i-e Figs.48 and 49) that :

- When $(L/W) < (L/W)_{crit.}$, the sharp decrease in the value of ζ, observed in Fig.48, is due to the considerable effect of the permeate pressure drop which results from the excessive spiral length of the permeate channel.

- When $(L/W) > (L/W)_{crit.}$, ζ appears to increase slightly with (L/W). This behaviour is due to the relatively small pressure drop generated in the brine channel, (see Fig.49), and to an increase in cross flow velocity as (L/W) increases (due to a decrease in W as total membrane area was kept constant) which reduces the concentration polarisation effects.

The variation in the permeate quality, corresponding to the element geometrical variation observed in Fig.48 is displayed in Fig.50. As expected, it is seen that a similar pattern is obtained, i-e the "optima" found for ζ are still applicable in this case.

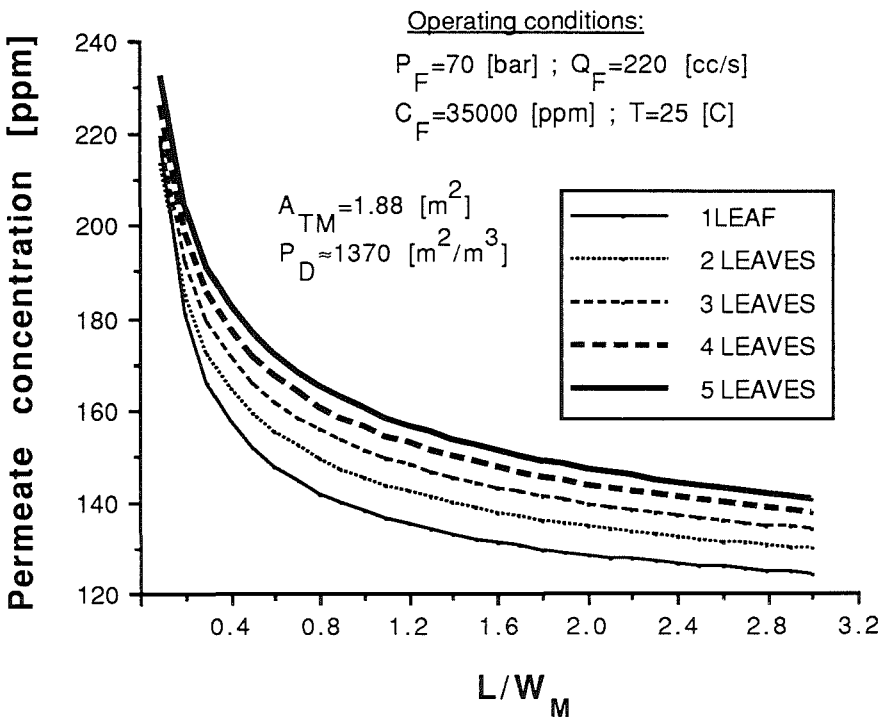

FIG.50 : Influence of the FT30 membrane leaf geometry on the permeate quality.

In definitive, it was seen that, for the case studied, both procedures (i-e used in

Figs.47 and 48) seem to converge reasonably, in terms of the optimum number of leaves, despite the difference in approaches.

Note : Unlike the second method, for a given feed flow rate and membrane axial length the first one presents the advantage of keeping the feed velocity constant independently of the number of leaves considered and allocate the emphasis on the effect of the number of leaves on water productivity per unit volume per unit feed pressure.

Fig.51 shows the volume specific productivity versus the permeate channel height for different membrane spiral lengths. The plot was performed for a single leaf element because it was shown previously that this could well be considered as optimal.

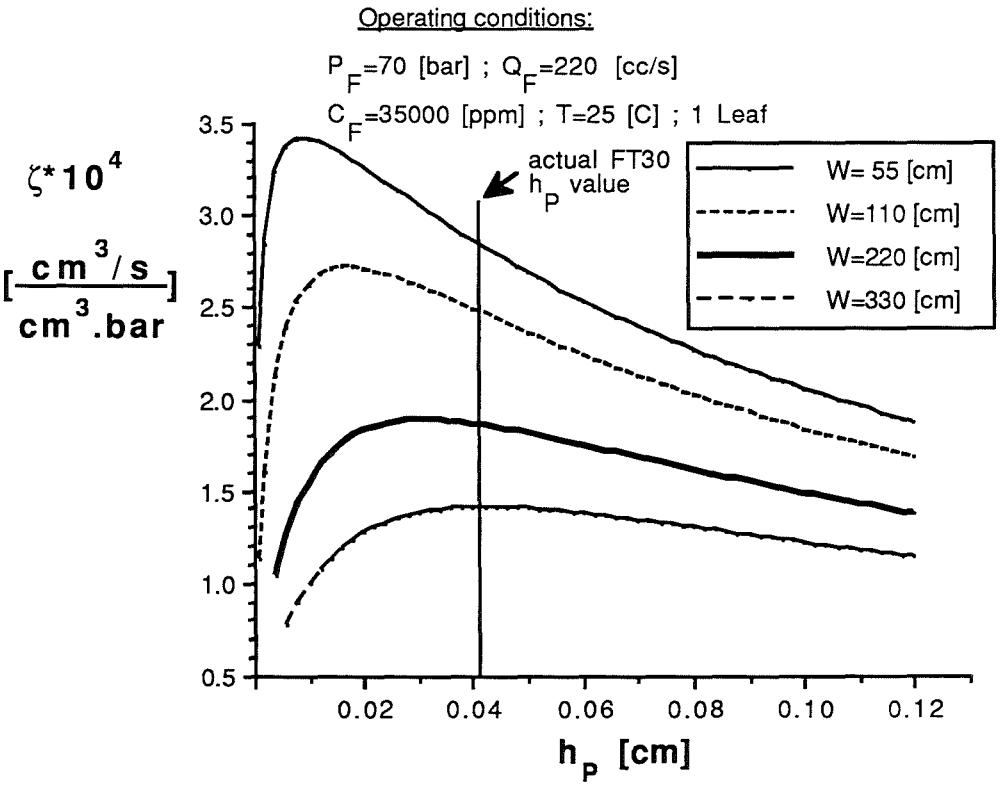

FIG.51 : Module volume specific productivity as a function of height and spiral length of the permeate channel.

All curves have a maximum which shifts towards thicker permeate channels and lower volume specific productivity as the membrane spiral length increases. This behaviour is due to the pressure drop in the permeate channel which, in turn, influence the effective driving pressure. The permeate pressure drop decreases with an increase in the permeate channel height but increases with the membrane spiral length. It is clearly shown that the higher volume specific productivity is obtained at the lower membrane

spiral length. For all the curves, the decrease in ζ at $h_P > h_{Popt}$ is attributed to the increase in the volume of the SPW element (see eq.(6-1)).

Considering the particular membrane spiral length of the FT30 element (i-e W=110 cm), the computed optimal permeate channel height, h_{Popt}, is about 0.24 mm. This computed value is substantially less than that in current use (i-e h_P=0.41 mm) presumably because other factors such as membrane support should be considered. Therefore, when allowance is made for this aspect, the resulting h_{Popt} would be somewhat higher with the additional benefit of a higher productivity at the expense of a lower module packing density (due to increase in element volume).

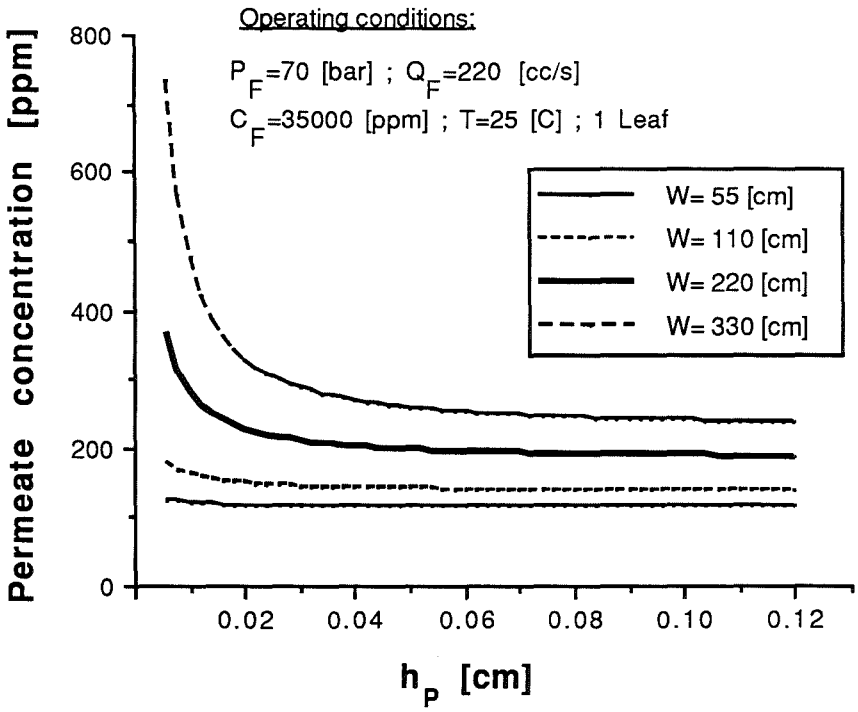

FIG.52 : Permeate quality as a function of height and spiral length of the permeate channel.

The optimal permeate channel height values based on the element productivity result in optimal values for the permeate quality as shown in Fig.52. It is also seen that if, for the reasons mentioned previously, the final permeate channel height is greater than the computed optimum, the resultant permeate quality would not be affected.

The influence of the brine channel height on the volume specific productivity is shown in Fig.53. Optimal thicknesses of the brine channel have been evaluated for the conditions stated on the plot and for different membrane axial lengths.

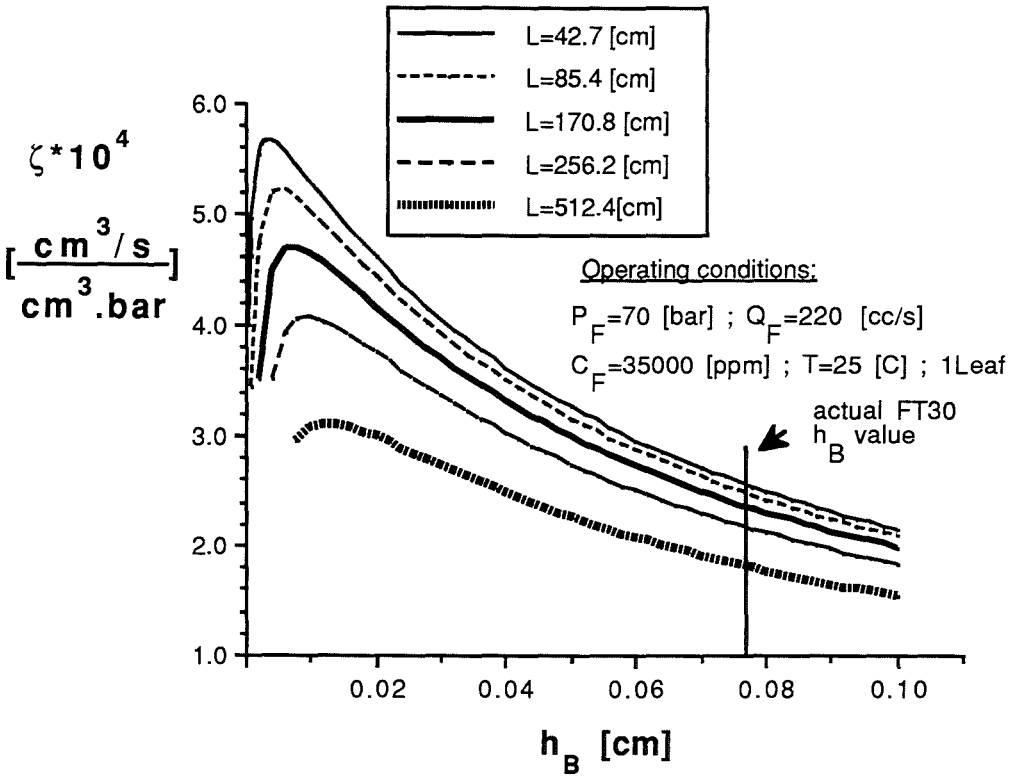

FIG.53 : Module volume specific productivity as a function of height and axial length of the brine channel.

Note : In the above figure, due to brine pressure drop, the starting point for each curve is defined as the minimum value of h_B which would lead to an effective driving pressure for water permeation.

All the resulting curves reveal a well defined optimum for ζ which decreases with increase in module length. This is due to the pressure drop which brings about a reduction of the module productivity. Consequently, this would suggest that thicker brine channels must be used with increase in module length. Beyond the optimums h_B, the drastic decline in ζ with increase in h_B is due to an increase in the element volume and a decrease in the cross flow velocity which results in higher concentration polarisation effect and thus in a reduced driving pressure and productivity. In this context, Table 6-2 gives the predicted quantitative variation of the relevant parameters for different brine channel heights.

Table 6-2 : Variation of element productivity and concentration polarisation with the brine channel height for an membrane axial length of L=85.4 cm and for the operating conditions displayed in Fig.53.

		Brine channel height$\times 10^2$ (cm)		
		1	4	8
Maximum Polarisation :	(C_{BWmax}/C_F)	1.33	1.47	1.55
Element productivity (cc/s) :	Q_P	25.7	24.2	22.7
Permeate quality (ppm) :	C_P	113	134	153

According to Fig.53, the optimum brine channel height, for the particular length of the FT30 module (i-e L=85.4 cm), should be approximately 0.06 mm. This value is much lower than the real one probably because, in current practice, modules are used up to a number of six in series in a single pressure vessel. Therefore, the optimum brine channel thickness should be based on the total length of the modules contained in a pressure vessel. In this context, it is clearly seen in Fig.53 that the optimum brine channel thickness increases as the length of the module increases. The optimal brine channel height, $h_B$opt, for the total length of the six elements in series can be deduced from the curve at L=512.4 cm which does not account for inter-element brine mixing. In this case, $h_B$opt was of the order of 0.12 mm. This value is still much lower than the real one (i-e h_B=0.77 mm).

However, it should be noted that, in practice, maximising ζ is not the only aspect that has to be taken into account when designing a spiral wound element. Fouling tendencies generated by spacers are also important, and very thin brine spacers are more likely to create problems in this respect. Therefore, for safety purposes a "fouling factor" should be included in the evaluation of the optimum brine channel height. This would result in a higher $h_B$opt and consequently in a lesser module productivity and module packing density. On the other hand, the advantage would be a better tolerance to fouling.

In Fig.54 the expected variation in the permeate quality is displayed. It is seen that if a fouling factor is allowed for (i-e at increasing h_B values), the resulting permeate quality would decrease slightly as compared to the one obtained at the computed optimal h_B value. This is due to a combination of a decrease in the module productivity and an increase in the brine wall concentration which increases the salt flux

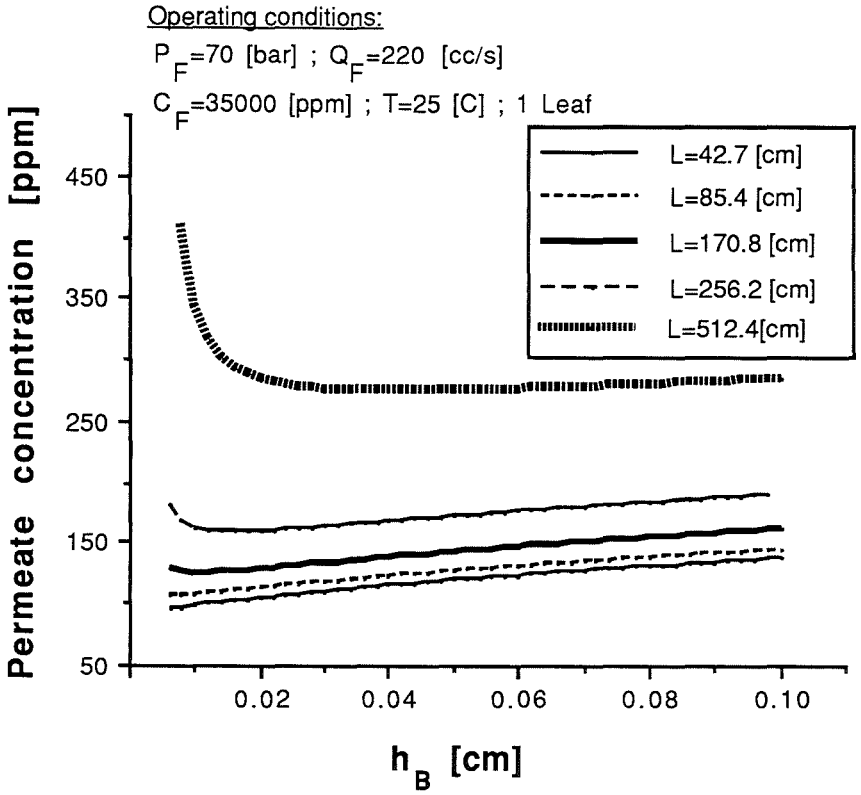

FIG.54 : Permeate quality as a function of height and length of the brine channel.

VI-3- Effect of operating conditions on the element geometrical optimisation.

So far, in this analysis, all the calculations were based on a single set of operating conditions. Further, the assessment of the influence of a particular geometrical parameter on the volume specific productivity, ζ, was performed while the other parameters were kept constant. A change in this procedure may result in different optimal geometrical values. The purpose of this section is to see how the optimal geometrical characteristics determined previously are affected by a variation in some operating conditions.

The optimal number of leaves was found to be of the order of one independently of the considered total membrane area. In Fig.55, the effect of the membrane leaf area, A_M, on both ζ and the axial-to-spiral length ratio is plotted. It is clear from this figure that the highest values of ζ are obtained at the lower values of the membrane leaf area. This is because an increase in the membrane leaf area leads to the combination of the two following negative effects on ζ :

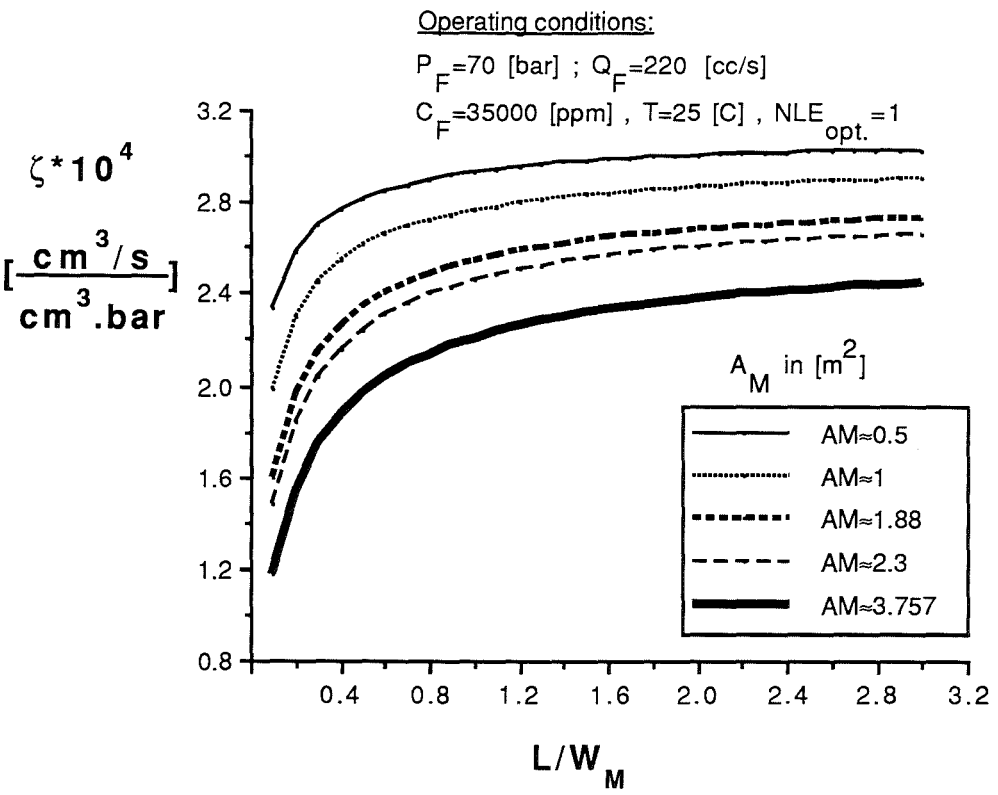

FIG.55: Influence of membrane leaf area on module volume specific productivity as a function of the membrane axial-to-spiral length ratio.

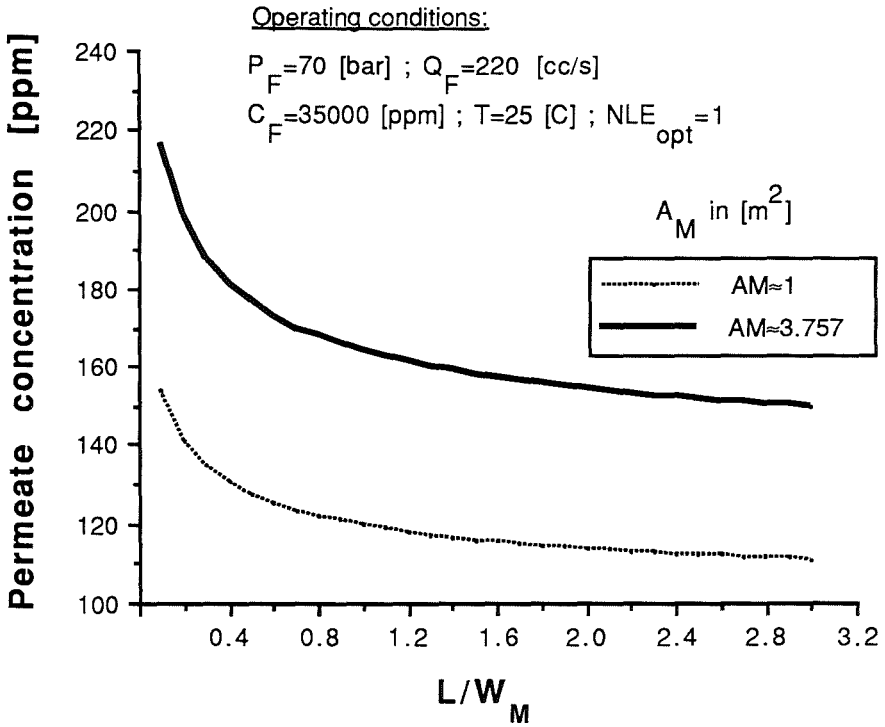

FIG.56: Influence of membrane leaf area on permeate quality as a function of the membrane axial-to-spiral length ratio.

- Increase in volume of the spiral-wound element.
- Greater concentration polarisation due to a reduced cross flow velocity as larger areas are offered to the feed flow.

Also, from this figure, it is seen that the previously defined critical value of (L/W) tends to increase with decrease in A_M. This is due to the increasing permeate pressure drop caused by the higher permeate flow and permeate channel length.

Concerning the permeate quality, Fig.56 shows that similar trends are observed, i-e the lower the membrane leaf area the better the permeate quality.

Fig.57 shows the effect of the feed pressure on ζ and membrane leaf dimensions. According to this figure, $(L/W)_{crit.}$ tends to increase slightly as the feed pressure increases. This is due to an increase in permeate flow which consequently leads to an increase of the permeate pressure drop.

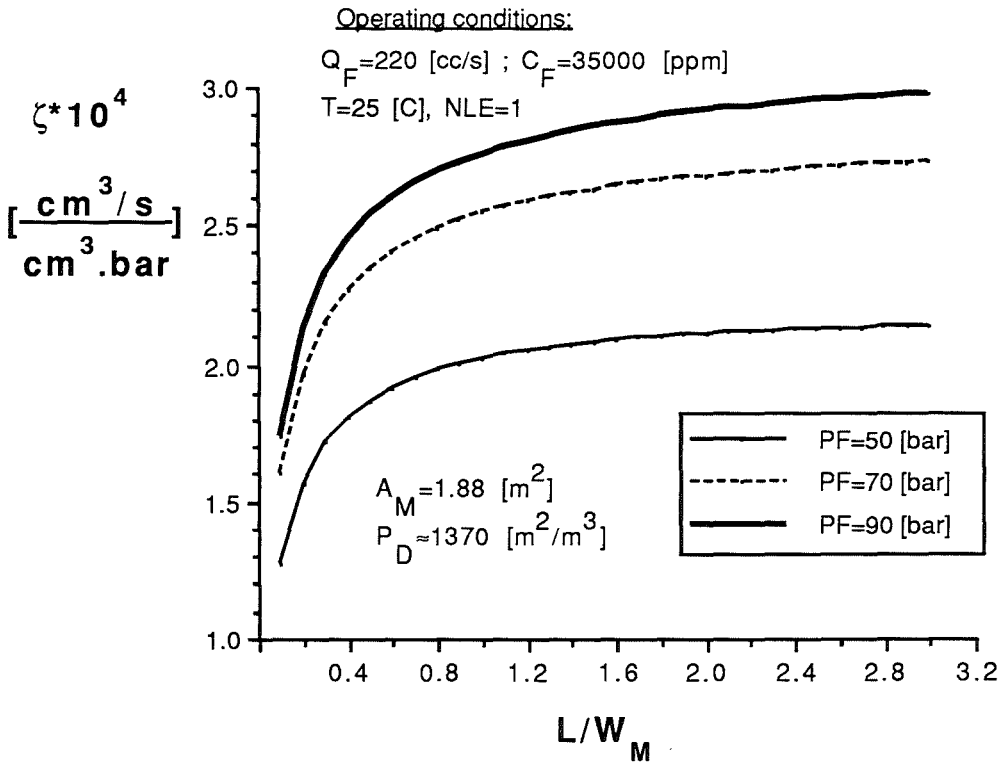

FIG.57: Effect of feed pressure on module volume specific productivity as a function of the membrane axial-to-spiral length ratio.

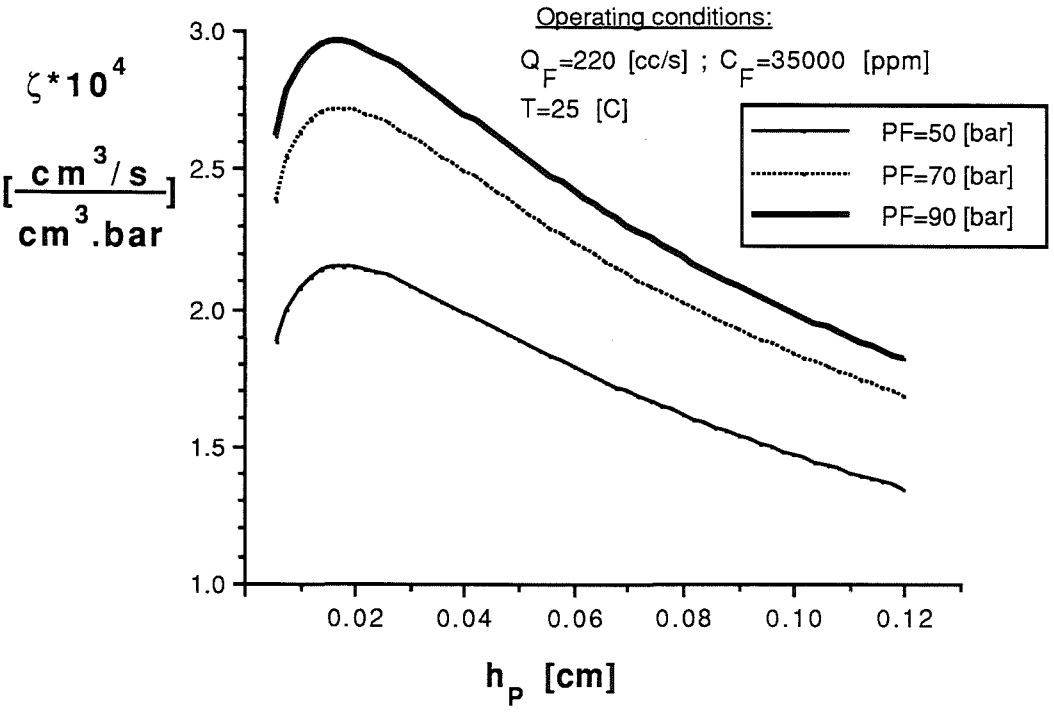

FIG.58: Module volume specific productivity as a function of permeate channel height and feed pressure.

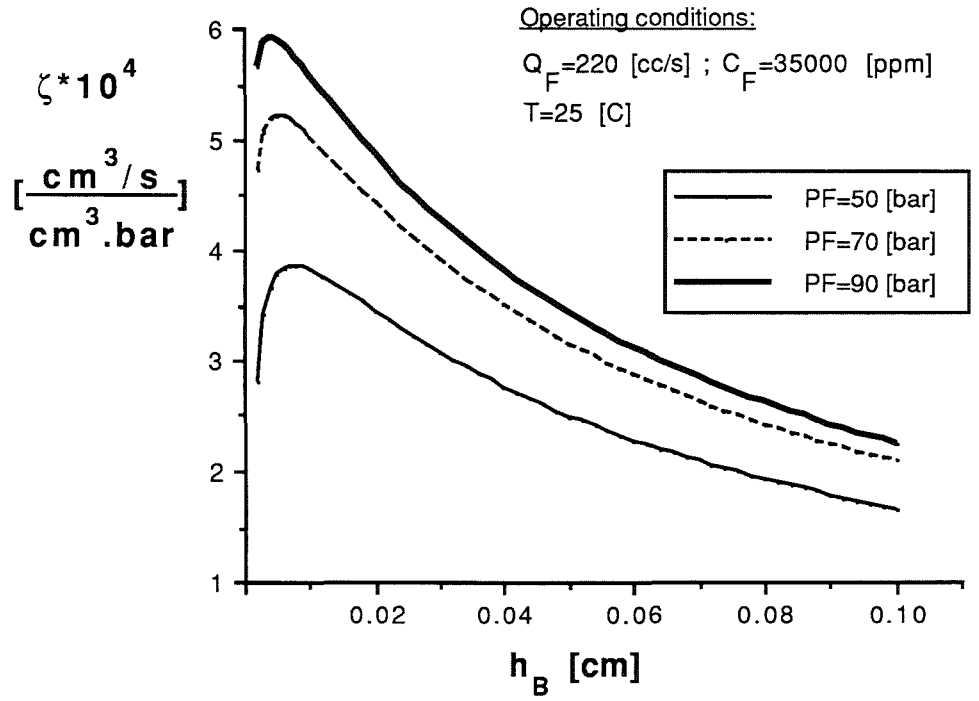

FIG.59: Module volume specific productivity as a function of brine channel height and feed pressure.

Figs.58 and 59 show that the feed pressure, P_F, does not affect the computed optimum values of the permeate and brine channel heights respectively. However, it is clearly seen that a variation in P_F results in a variation of the module productivity which affects significantly ζ.

The effect of the brine channel height on ζ for different feed flows is shown in Fig.60. For all curves an optimum brine channel height exists as represented by a maximum ζ. It is seen that these maxima are obtained at very low brine channel heights. This is due to the beneficial aspect of the brine spacer used which is characterised by low friction losses even at the high cross flow velocities needed to limit the concentration polarisation effects.

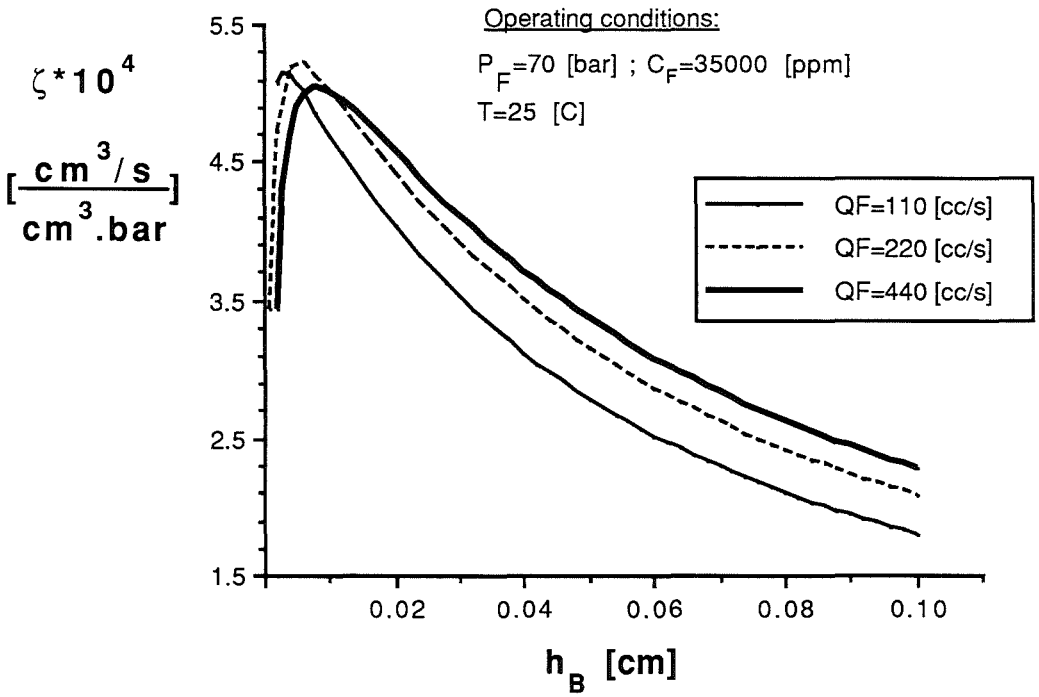

FIG.60: Module volume specific productivity as a function of brine channel height and feed flow.

Concerning the optimum value of h_B, it is seen that this tends to shift slightly towards increasing h_B values as the feed flow increases so as to minimise the brine pressure drop. However, it should be reiterated that the practical value of h_B is usually much greater due to fouling tendencies. Therefore, as h_B increases, the maximum values of ζ are obtained for the highest feed flow. Consequently, this indicates that, in practice,

the effect of concentration polarisation is much more detrimental than the brine pressure drop.

The corresponding variation of the permeate quality is displayed in Fig. 61. For the low height values, the steep increase in the permeate concentration for the highest feed flow (i-e Q_F=440 [cc/s]) is the result of the high brine pressure drop which affects seriously the permeate productivity. For all the curves, as h_B increases beyond the optimal value, it is seen that the permeate quality decrease steadily due to higher effect of concentration polarisation : the higher the feed flow is and the better the permeate quality. This is due to higher productivity and lower brine wall concentrations.

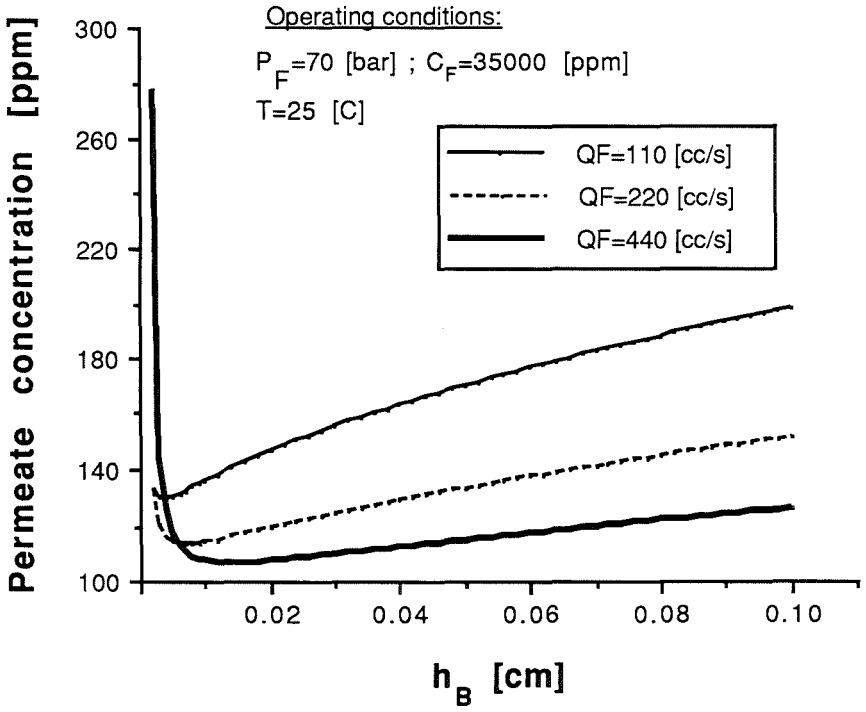

FIG.61: Permeate quality as a function of brine channel height and feed flow.

VI-4- Closure.

The dependence of the module specific productivity on geometrical characteristics and operating conditions has been analysed. It was, particularly, seen that, for sea water applications and for the type of spacers used, the two critical factors governing the geometrical design of SPW elements were the permeate pressure drop and concentration polarisation. The balance of these phenomena determined the shape of the curves from which the optimum can be deduced.

However, it is important to recognise that the task of designing an effective spiral-wound element is more complex than implied by the present investigation : the reported calculations did not include the possible dependence of the channel heights on the membrane axial-to-spiral length ratio. If such dependence proved to be significant, then a lengthy trial and error procedure would be required for their evaluation. Further, factors such as ease of construction, manufacturing and running energy costs, fouling tendencies and allowable module packing density play a major role in the final design optimisation. Clearly in a practical situation such information would be available to membrane manufacturers only and in this respect the procedure used in our analysis can be regarded as a first approach towards the final optimum design.

CHAPTER SEVEN

GENERAL CONCLUSION.

VII-1- Conclusion.

The research project dealt with the modelling of reverse osmosis spiral wound modules. Two different models were developed:- the first was an improved Slit model taking better account of the actual geometry and local variation of solution properties, and the second was a Spiral model accounting fully of the asymmetric nature of the spiral geometry of an element. Despite both models possessing a certain similarity, both were developed in order to produce more precise modelling of spiral wound elements. The two models were compared to assess the benefits of the more complex Spiral model as against the simpler Slit model.

The mathematical modelling made use of the Solution Diffusion model for the description of the water and the salt transport mechanism across the membrane. The governing differential equations, describing the variation in conditions over the membrane surface, were solved using a finite difference technique.

These models could be used for any membrane type providing that its intrinsic characteristics are specified. In this context, it was shown that relatively simple experiments using small membrane samples housed in a test cell were sufficient for the determination of these characteristics. For the thin film composite (TFC) polyamide membrane used in the FT30SW module, these tests suggested that the values of the water and salt permeability coefficients follow similar trends as those observed for the earlier cellulose acetate membranes.

However, it was seen that the same experimental procedure failed to provide a satisfactory mass transfer coefficient correlation. Possible reasons for this failure were given. This led to the use of the Winograd correlation (eq.3-1) which proved to be quite successful in describing the variation of the mass transfer coefficient with changing operating conditions. This result is significant since, in this work, the Winograd correlation has been validated against sea water data for the first time. At sea water concentrations the effects of concentration polarisation are much more significant than in the brackish water data used in the previous studies.

Both models were found to describe fairly well the interactions between the many variables involved. Indeed, the predicted results compared favourably with the experimental data provided from two different commercial spiral wound modules-the Roga 4160 HR [29] and the FT30SW2540 [28]. These data were wide enough in scope to be representative of a realistic span of operating conditions.

Comparison of the Slit and the Spiral models did not reveal significant differences between their predictions. Therefore, it was concluded that while the difference in modelling approach was worthy of investigation, the rather complex algorithm required for the Spiral model did not seem to yield a justifiable improvement. The only argument in its favor appears to be a more realistic and detailed simulation of the interactions taking place in spiral wound modules.

The applicability of this analysis to the practical design of spiral wound modules was illustrated in a case study in which the module geometry was optimised for a given set of operating conditions. The target function was the element volume specific productivity. Although it was recognised that, in practice, the optimum module characteristics would be generally based on combined technical and economical considerations (target functions), the analysis presented in this work is indicative of the techniques that may be used for an economic optimisation.

Finally, an additional use to which such models could be put is for plant performance prediction and/or plant process optimisation since this represents simply a matter of combining single module performance predictions together with water and salt balances over the whole plant.

VII-2- Further Work.

Improvements to the models presented are believed possible. These would be mainly confined to a better characterisation of the pressure losses through the permeate spacer. In this context, it was identified that while pressure measurements on the operating spiral wound element are realistic, these alone would not provide the required information since the permeate velocity is constantly changing due to membrane permeation. It was indicated that flat channel measurements at different constant flow velocities would, probably, more useful

Another possible area for improvement could be the use of a different model for the water and salt transport across the membrane. In this context, while the application of the

Solution Diffusion transport model appeared to be satisfactory, it was suggested that it would be worthwhile to incorporate a 3-parameter type model such as the Solution Diffusion Imperfection model. This would allow a comparison and could, perhaps, lead to better estimates of the permeate concentrations.

Finally, it should be stated that the modelling study did not account for the possible occurrence of membrane fouling. This is because so little is currently understood about this phenomena that it is not yet possible to describe it mathematically. Although, in normal practice, sufficient feed pretreatment is used to minimise membrane fouling, future research should focus on its modelling. The benefits of such work could result in better pretreatment techniques and/or module designs. This in turn, would contribute to the long term implementation of reverse osmosis as a reliable and economical process for water desalination.

APPENDIX A

Correlations for predicting sea water properties.

The following correlations were estimated through the data presented in [33] and were incorporated in the computational programs to calculate the solution properties in the bulk flow as well as in the boundary layer.

* **Viscosity :** μ in [g/cm.s]

$$\mu = \mu_o \, e^{-2.008x10^{-2} T} \qquad (A\text{-}1)$$

where :

$$\mu_o = 1.4757x10^{-2} + 2.4817x10^{-8}C + 9.3287x10^{-14}C^2 \qquad (A\text{-}2)$$

with : $20\ [^oC] \leq T \leq 45\ [^oC]$ and $0\ [ppm] \leq C \leq 10^5\ [ppm]$

* **Osmotic pressure:** Π in [bar]

For the variation of the osmotic pressure, the data were given at 25°C as below :

$$\Pi_{T_{25}} = 0.23745 + 6.748x10^{-4}C + 1.7753x10^{-9}C^2 \qquad (A\text{-}3)$$

with : $C \leq 10^5\ [ppm]$

Using eq.(A-3), the osmotic pressure at any temperature is given by :

$$\frac{\Pi_{T_i}}{T_i} = \frac{\Pi_{T_{25}}}{T_{25}} \qquad (A\text{-}4)$$

It should be noted that, in eq.(A-4), the temperature is expressed in degrees Kelvin.

* **Diffusivity** : Ds in [cm^2/s]

The diffusion coefficient was correlated in terms of the temperature only :

$$D_S = \left(0.72598+2.3087x10^{-2}\ T+2.7657x10^{-4}\ T^2\right)\ x10^{-5} \qquad \text{(A-5)}$$

with : $10\ [^oC] \le T \le 45\ [^oC]$

* **Density** : ρ in [g/cm^3]

$$\rho = \rho_o\ e^{-3.308x10^{-4}\ T} \qquad \text{(A-6)}$$

where :

$$\rho_o = 1.0042 + 7.2924x10^{-4}\ C \qquad \text{(A-7)}$$

with : $20\ [^oC] \le T \le 45\ [^oC]$ and $0\ [ppm] \le C \le 10^5\ [ppm]$

APPENDIX B

Analytical Solution for the Permeate Pressure at membrane closed end.

The purpose of this analysis is to evaluate the pressure profile along the permeate channel flow. This will allow the determination of a reasonably good guess for the value of the permeate pressure at the closed end of the membrane which would speed up the iteration procedure of the numerical method described in chapter III.

This analysis is based on the Slit model and is applicable to salt feed solutions. The assumptions involved are similar to those cited in the formulation of the Slit model (see section III-3-2). The situation is sketched in the figure below, Fig.1-B.

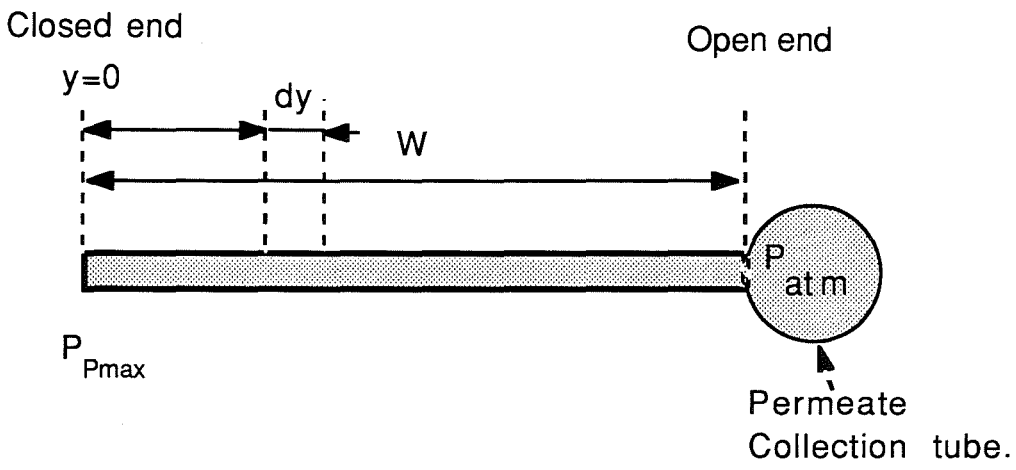

Fig.1-B : Sketch of the Permeate Channel.

Recalling the following governing equations for the permeate flow formulated for the Slit model in section III-3-2, we have :

- Darcy's Law :

$$\frac{dP_P}{dy} = -\mu E_P V_P \qquad \text{(B-1)}$$

- Solvent Material balance :

$$\frac{dV_P}{dy} = \frac{2}{h_P} J_1 = \frac{2 k_1}{h_P} (P_B - P_P - \Pi_B) \qquad \text{(B-2)}$$

Taking the second derivative of eq.(B-1) yields :

$$\frac{d^2P_P}{dy^2} = -\mu E_P \frac{dV_P}{dy} \qquad \text{(B-3)}$$

Substituting eq.(B-2) in (B-3) leads to :

$$\frac{d^2P_P}{dy^2} = - m_P^2 \left(P_B - P_P - \Pi_B\right) \qquad \text{(B-4)}$$

where :

$$m_P^2 = \frac{2 \mu k_1 E_P}{\rho h_P} \qquad \text{(B-5)}$$

Let :

$$Q = - m_P^2 \left(P_B - \Pi_B\right) \qquad \text{(B-6)}$$

A rearrangement of eq.(B-4) with eq.(B-6) gives the following second order differential equation :

$$\frac{d^2P_P}{dy^2} - m_P^2 P_P = Q \qquad \text{(B-7)}$$

The above differential equation is solved with the aid of the following boundary conditions :

$$\text{B.C.}_1 \quad \text{at } y = 0 \; ; \; \frac{dP_P}{dy} = 0$$

$$\text{B.C.}_2 \quad \text{at } y = W \; ; \; P_P = P_{atm} \qquad \text{(B-8)}$$

The solution of eq.(B-7) becomes :

$$P_{P\,(y)} = P_{atm} \frac{ch(m_P y)}{ch(m_P W)} + \frac{Q}{m_P^2}\left(\frac{ch(m_P y)}{ch(m_P W)} - 1\right) \qquad \text{(B-9)}$$

At the permeate channel closed end (i-e y=0), the permeate pressure is given by the following equation :

$$P_{Pmax} = P_{P(y=0)} = \frac{P_{atm}}{ch(m_P W)} + \frac{Q}{m_P^2}\left(\frac{1 - ch(m_P W)}{ch(m_P W)}\right) \qquad \text{(B-10)}$$

In the above expression, the only unknowns are P_B and Π_B which for an axial position at the feed inlet can be given by P_F and Π_F (where Π_F is evaluated in terms of C_F).

APPENDIX C

Semi-Analytical Solution for the Evaluation of the Permeate Friction Parameter.

In this appendix, a semi-analytical solution for the evaluation of the permeate friction parameter is presented. The basic approach which made such analysis possible was that when pure water is used as a feed solution the problems associated with concentration polarisation and osmotic pressure variation along the spiral wound element are not present. The major assumptions considered are summarised as follows :

1- Pure water as feed solution.
2- The Spiral wound element is made up of flat channels (as in the Slit model).
3- Negligible component of the brine and permeate velocities in the y and x directions respectively.
4- The brine pressure is constant along the y direction.
5- The permeate pressure is constant along the x direction.

The figure below, Fig.1-C, shows the volume elements in the brine and permeate channels for which the balances were formulated.

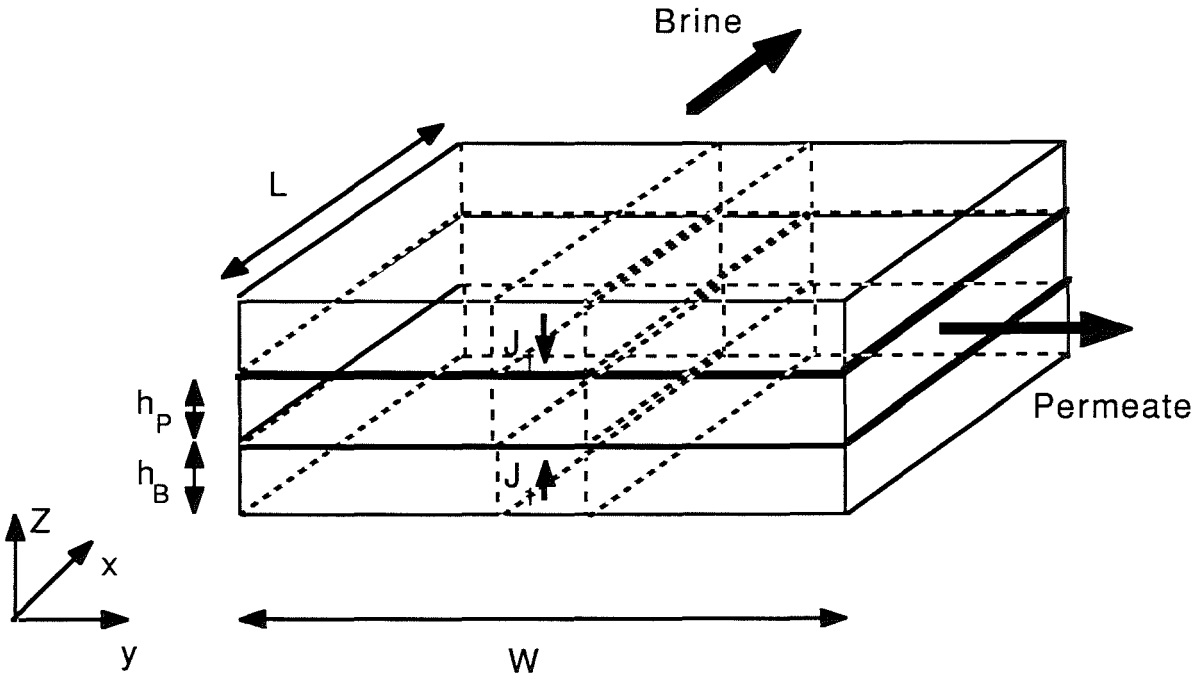

FIG.1-C: Physical Model for the analysis.

The water flux is evaluated using the following well established equation :

$$J_1(x,y) = k_1[\ P_B(x,y)\ -P_P(x,y)\ -\ \Pi_B(x,y)\ +\ \Pi_P(x,y)\ ] \qquad (C\text{-}1)$$

When applied to the case of pure water feed (assumption 1), eq.(C-1) is reduced to the following equation :

$$J_1(x,y) = k_1\ \Delta P_{eff}(x,y) \qquad (C\text{-}2)$$

where :

$$\Delta P_{eff}(x,y) = P_B(x,y)\ -\ P_P(x,y) \qquad (C\text{-}3)$$

and represents the driving pressure at each point (x,y). In the above equation, $P_B(x,y)$ and $P_P(x,y)$ represent the local pressures in the brine and permeate channel respectively.

Permeate channel :

Starting with the permeate channel flow , the following balance's equations are found :

- Darcy's equation :

$$\frac{\delta P_P(x,y)}{\delta y} = -\ \mu\ E_P\ V_P(x,y) \qquad (C\text{-}4)$$

-Mass balance :

$$\frac{\delta V_P(x,y)}{\delta y} = \frac{2}{h_P} J_1(x,y) = \frac{2\ k_1}{h_P}\ \Delta P_{eff}(x,y) \qquad (C\text{-}5)$$

Taking the second derivative of an expression resulting from the combination of eqs.(C-4) and (C-5) gives :

$$\frac{d^2V_P(x,y)}{dy^2} - m_P^2\, V_P(x,y) = 0 \qquad \text{(C-6)}$$

where :

$$m_P^2 = \frac{2\, k_1 \mu\, E_P}{h_P} \qquad \text{(C-7)}$$

Eq.(C-6) has to be solved with the following boundary conditions :

(i)- at $y=0$; $V_P(x,0) = 0$

(ii)- at y ; $\frac{dV_P(x,y)}{dy} = \frac{2\, k_1}{h_P}\, \Delta P_{eff}(x,y)$

The solution of eq.(C-6) is of the following form :

$$V_P(x,y) = C\ ch(m_P y) + D\ sh(m_P y) \qquad \text{(C-8)}$$

where the constants have to be determined using the boundary conditions. After resolution, the solution is :

$$V_P(x,y) = \frac{2\, k_1}{m_P\, h_P}\, \Delta P_{eff}(x,y)\ \ th(m_P y) \qquad \text{(C-9)}$$

In eq.(C-9), an expression for the effective pressure term has to be found. From our assumptions (i-e : assumption 5) the following equation is deduced:

$$\frac{d\Delta P_{eff}(x,y)}{dy} = - \frac{dP_P(x,y)}{dy} \qquad \text{(C-10)}$$

Using eq.(C-4) in eq (C-10) yields :

$$\frac{d\Delta P_{eff}(x,y)}{dy} = \mu\, E_P\, V_P(x,y) \qquad \text{(C-11)}$$

Taking the second derivative of a combination of eq.(C-11) with eq.(C-5) gives :

$$\frac{d^2\Delta P_{eff}(x,y)}{dy^2} - m_P^2\, \Delta P_{eff}(x,y) = 0 \qquad \text{(C-12)}$$

which has to be solved using the following boundary conditions :

$$\text{(i) at } y = W \;\; ; \Delta P_{eff}(x,y) = \Delta P_{eff}(x,W)$$

$$\text{(ii) at } y = 0, \; \frac{d\Delta P_{eff}(x,0)}{dy} = 0$$

The solution of eq.(C-12) is found as :

$$\Delta P_{eff}(x,y) = \Delta P_{eff}(x,W)\, \frac{ch(m_P y)}{ch(m_P W)} \qquad \text{(C-13)}$$

Using eq.(C-13), eq.(C-9) becomes :

$$V_P(x,y) = \frac{2\, k_1}{m_P h_P}\, \Delta P_{eff}(x,W)\, \frac{sh(m_P y)}{ch(m_P W)} \qquad \text{(C-14)}$$

In eq.(C-14), if $\Delta P_{eff}(x,W)$ can be expressed in terms of x only then the integration of the above equation over the membrane axial lenght would give the average permeate velocity along y, i-e :

$$V_P(y) \int_0^L dx = \frac{2\, k_1}{m_P h_P}\, \frac{sh(m_P y)}{ch(m_P W)} \int_0^L \Delta P_{eff}(x,W)\, dx \qquad \text{(C-15)}$$

Therefore, at this stage, an analysis of the brine channel flow is required in order to obtain such information.

Brine channel :

As for the permeate channel, we start with the different balances formulated in differential form.

- Darcy's equation :

$$\frac{dP_B(x,y)}{dx} = -\mu\, E_B\, V_B(x,y) \qquad \text{(C-16)}$$

- Mass balance :

$$\frac{dV_B(x,y)}{dx} = -\frac{2}{h_B} J_1(x,y) = \frac{2\, k_1}{h_B} \Delta P_{eff}(x,y) \qquad \text{(C-17)}$$

Combining eqs.(C-16) and (C-17), and taking the second derivative of the resulting equation yields:

$$\frac{d^2V_B(x,y)}{dy^2} - m_B^2\, V_B(x,y) = 0 \qquad \text{(C-18)}$$

where :

$$m_B^2 = \frac{2\,\mu\, k_1 E_B}{h_B} \qquad \text{(C-19)}$$

Eq.(C-18) is solved using the following boundary conditions:

(i)- at x=0 ; $V_B(0,y) = V_{Feed}$

(ii)- at x ; $\frac{dV_B(x,y)}{dx} = -\frac{2\,k_1}{h_B}\,\Delta P_{eff}(x,y)$

The solution of eq.(C-18) is then :

$$V_B(x,y) = \left[\frac{V_{Feed}}{sh(m_B x)} - \frac{2\,k_1\,\Delta P_{eff}(x,y)}{h_B m_B}\right] th(m_B x) \qquad \text{(C-20)}$$

Or, by using eq.(C-13) :

$$V_B(x,y) = \left[\frac{V_{Feed}}{sh(m_B x)} - \frac{2\,k_1}{m_B h_B}\,\Delta P_{eff}(x,W)\,\frac{ch(m_P y)}{ch(m_P W)}\right] th(m_B x) \qquad \text{(C-21)}$$

In order to find the average brine velocity at any point x along the brine path, eq.(C-21) must be integrated over the membrane spiral length. This integration yields to :

$$V_B(x) = \frac{V_{Feed}}{ch(m_B x)} - \frac{2\,k_1}{m_B h_B}\,\frac{th(m_P W)}{m_P W}\,\Delta P_{eff}(x,W)\;\; th(m_B x) \qquad \text{(C-22)}$$

From eq.(C-22), the permeate collected up to the x coordinate can be evaluated by the following equation :

$$Q_P(x) = N_{le}\,h_B\,W\;\;(V_{Feed} - V_B(x)) \qquad \text{(C-23)}$$

However, it should be noted that so far no explicit expression of $\Delta P_{eff}(x,W)$ in terms of x has been formulated. To this issue, let consider the solution of eq.(C-18) with the following boundary conditions :

(i)- at $x=0$; $V_B(o,y) = V_{Feed}$

(ii)- at $x=0$; $\dfrac{dV_B(o,y)}{dx} = \dfrac{2\,k_1}{h_B}\,\Delta P_{eff}(0,y)$

The solution of eq.(C-18) becomes :

$$V_B(x,y) = V_{Feed}\ ch(m_B x) - \frac{2\,k_1}{h_B m_B}\,\Delta P_{eff}(0,y)\ sh(m_B x) \qquad \text{(C-24)}$$

Eqs.(C-22) and (C-24) are both solution of eq.(C-18). Thus, if both equations are taken at $y = W$, the respective set of resulting equations would be as follows :

$$V_B(x,W) = \left[\frac{V_{Feed}}{sh(m_B x)} - \frac{2\,k_1}{m_B h_B}\,\Delta P_{eff}(x,W)\right]\ th(m_B x) \qquad \text{(C-25)}$$

and,

$$V_B(x,W) = V_{Feed}\ ch(m_B x) - \frac{2\,k_1}{m_B h_B}\,\Delta P_{eff}(0,W)\ sh(m_B x) \qquad \text{(C-26)}$$

By using eqs (C-25) and (C-26) an expression for $\Delta P_{eff}(x,W)$ is found as :

$$\Delta P_{eff}(x,W) = \Delta P_{eff}(0,W)\ ch(m_B x) - \left(\frac{m_B h_B}{2\,k_1}\right) V_{Feed}\ sh(m_B x) \qquad \text{(C-27)}$$

Thus, by integration of eq.(C-27) over the membrane lenght, an average effective pressure at $y=W$, $\Delta P_{eff}(W)$, can be found as :

$$\int_0^L \Delta P_{eff}(W)\,dx = \int_0^L \left(\Delta P_{eff}(0,W)\ ch(m_B x) - \frac{\mu\,E_B\,V_{Feed}}{m_B}\,sh(m_B x)\right)dx \qquad \text{(C-28)}$$

Thus,

$$\Delta P_{eff}(W) = \Delta P_{eff}(0,W)\ \frac{sh(m_B L)}{m_B L} - \frac{\mu\, E_B\, V_{Feed}}{m_B^2 L}\left(ch(m_B L) - 1\right) \qquad \text{(C-29)}$$

Recalling eq.(C-15), we have :

$$V_P(y)\int_0^L dx = \frac{2\,k_1}{m_P h_P}\,\frac{sh(m_P y)}{ch(m_P W)}\int_0^L \Delta P_{eff}(x,W)\,dx$$

Therefore,

$$V_P(y) = \frac{2\,k_1}{m_P h_P}\,\frac{sh(m_P y)}{ch(m_P W)}\,\Delta P_{eff}(W) \qquad \text{(C-30)}$$

At, y = W, eq (C-30) gives the averaged outlet permeate velocity , V_{PF}, as follows :

$$V_{PF} = V_P(W) = \frac{2\,k_1}{m_P h_P}\,th(m_P W)\ \Delta P_{eff}(W) \qquad \text{(C-31)}$$

or the avearged permeate flow, Q_{PF}, as :

$$Q_{PF} = \frac{2\,k_1 L}{m_P}\,\Delta P_{eff}(W)\ th(m_P W) \qquad \text{(C-32)}$$

Finally, an expression for the permeate friction parameter is deduced as :

$$m_P = \frac{2\,k_1 L\,\Delta P_{eff}(W)}{Q_{PF}}\,th(m_P W) \qquad \text{(C-33)}$$

Eq.(C-33) represents a non-linear equation in terms of m_P or in terms of EP via

eq.(C-7). Therefore, for a given set of experimental pure water data and geometrical data, the above non-linear equation can be solved using a numerical method. Further, it is clear at this stage that, in addition of pure water data, the water permeability coefficient and the brine friction parameter are required too.

APPENDIX D

Tabulated Results.

In this appendix the experimental data and the predictions of both the "Spiral" and the "Slit" programs are reported.

Table D-1 : Comparison between experimental and predicted results for the Roga module at T=25 [°C].

P_F (bar)	Q_F (cc/s)	C_F (ppm)	Q_P (cc/s)			C_P(ppm)		
			Exp	SP	SL	Exp	SP	SL
35.6	517	1940	46.50	47.14	46.50	55.2	52.7	53.4
34.9	390	1895	47.50	46.45	45.90	57.2	54.2	55.0
34.5	265	1953	47.00	46.02	45.52	57.7	59.9	60.6
33.9	134	1899	46.10	45.09	44.67	71.7	71.5	72.8
33.9	104	1887	45.70	44.77	44.43	84.0	82.2	84.1
29.0	528	1982	35.70	37.39	36.82	63.4	64.6	65.6
27.9	375	1924	37.60	36.23	35.74	66.7	66.6	67.5
27.8	250	1973	37.70	36.27	35.86	67.6	72.1	73.1
27.2	122	1895	36.90	35.47	35.13	82.4	82.5	83.9
27.2	90	1879	37.00	35.28	34.95	92.3	92.1	94.0
34.8	399	PW*	49.20	48.88	48.28	-	-	-
28.0	379	PW*	39.80	38.87	38.36	-	-	-

* Pure water experiments.

Table D-2 : Comparison between experimental and predicted results for the FT30 module at C_F=25000 (ppm) and Q_B= 155.88 (cc/s).

T (°C)	P_F (bar)	Q_F (cc/s)	Q_P(cc/s)			C_P(ppm)		
			Exp	SP	SL	Exp	SP	SL
20	50	172.67	16.78	16.24	16.05	95	113	117
20	55	175.00	19.12	18.62	18.38	89	103	106
20	60	177.05	21.17	20.93	20.67	89	95	98
25	50	175.82	19.93	18.31	18.07	103	130	134
25	55	178.18	22.30	21.00	20.71	95	118	122
25	60	180.77	24.88	23.62	23.31	89	109	113
25	70	185.92	30.03	28.72	28.33	83	97	101
25	80	190.17	34.80	33.58	33.13	79	89	93
30	50	178.80	22.92	20.63	20.35	121	150	155
30	55	181.70	25.82	23.68	23.35	111	136	141
30	60	184.85	28.97	26.67	26.29	103	126	131
30	70	190.60	34.72	32.44	31.98	95	112	117
35	50	182.23	26.35	23.20	22.85	138	173	179
35	55	185.60	29.72	28.09	27.53	125	142	150

Table D-3 : Comparison between experimental and predicted results for the FT30 module at C_F=35000 (ppm) and Q_B= 155.88 (cc/s).

T (°C)	P_F (bar)	Q_F (cc/s)	Q_P(cc/s)			C_P(ppm)		
			Exp	SP	SL	Exp	SP	SL
20	50	167.77	11.88	11.56	11.41	220	207	212
20	55	169.97	14.08	13.77	13.59	187	180	185
20	60	172.07	16.18	15.94	15.73	166	162	167
20	70	175.72	19.83	20.13	19.86	141	137	142
25	50	168.67	12.78	12.85	12.67	270	240	246
25	55	171.67	15.78	15.36	15.15	216	209	215
25	60	173.68	17.75	17.80	17.55	182	187	193
25	70	177.87	21.98	22.52	22.20	146	159	165
30	50	170.57	14.68	14.30	14.09	285	278	286
30	55	173.18	17.30	17.12	16.86	248	243	250
30	60	175.72	19.83	19.87	19.57	228	217	224
30	70	180.77	24.88	25.19	24.81	187	185	192
30	80	184.85	28.97	30.25	29.78	162	165	173
35	50	172.17	16.28	15.86	15.61	332	324	333
35	55	175.00	19.12	19.02	18.71	279	282	291
35	60	178.82	22.93	22.13	21.78	245	253	261
35	70	183.48	27.60	28.08	27.61	218	216	224
35	80	188.68	32.80	33.75	33.19	200	194	202

Table D-4 : Comparison between experimental and predicted results for the FT30 module at C_F=40000 (ppm) and Q_B= 155.88 (cc/s).

T (°C)	P_F (bar)	Q_F (cc/s)	Q_P(cc/s)			C_P(ppm)		
			Exp	SP	SL	Exp	SP	SL
20	50	164.75	8.87	9.40	9.27	288	281	287
20	55	167.18	11.30	11.54	11.39	237	237	243
20	60	169.27	13.38	13.64	13.46	216	208	214
20	70	172.88	17.00	17.70	17.46	162	172	177
20	80	176.33	20.45	21.59	21.28	145	150	156
25	50	166.28	10.40	10.38	10.24	342	327	334
25	55	168.57	12.68	12.80	12.61	296	276	283
25	60	171.07	15.18	15.16	14.95	242	241	248
25	70	174.90	19.02	19.73	19.44	200	199	207
25	80	179.22	23.33	24.10	23.74	162	175	181
30	50	167.18	11.30	11.46	11.28	401	381	391
30	55	170.47	14.58	14.18	13.97	358	321	330
30	60	172.47	16.58	16.83	16.57	289	281	290
30	70	177.47	21.58	21.97	21.62	235	232	240
30	80	181.92	26.03	26.87	26.44	207	204	212
35	50	169.07	13.18	12.61	12.41	484	446	458

Table D-5 : Comparison between experimental and predicted results for the FT30 module at C_F=25000 (ppm) and Q_B= 200.5 (cc/s).

T (°C)	P_F (bar)	Q_F (cc/s)	Q_P(cc/s)			C_P(ppm)		
			Exp	SP	SL	Exp	SP	SL
20	50	217.72	17.10	16.70	16.67	92	107	109
20	55	219.83	19.33	19.15	19.11	89	97	99
20	60	222.08	21.58	21.55	21.51	86	89	91
20	70	226.32	25.82	26.21	26.16	79	78	80
20	80	230.53	30.03	30.69	30.63	72	71	73
25	50	220.75	20.25	18.86	18.82	98	123	125
25	55	223.32	22.82	21.64	21.59	95	111	113
25	60	225.80	25.30	24.66	24.32	89	96	105
25	70	231.05	30.75	29.67	29.61	82	90	92
25	80	235.43	34.95	34.75	34.67	72	82	86
30	50	224.03	23.53	21.31	21.26	118	140	144
30	55	226.73	26.23	24.48	24.41	108	127	130
30	60	230.10	29.60	27.58	27.52	100	117	120
35	50	227.17	26.67	24.01	23.95	129	162	165
35	55	230.73	30.23	27.61	27.53	121	147	150

Table D-6 : Comparison between experimental and predicted results for the FT30 module at C_F=35000 (ppm)and Q_B= 200.5 (cc/s).

T (°C)	P_F (bar)	Q_F (cc/s)	Q_P(cc/s)			C_P(ppm)		
			Exp	SP	SL	Exp	SP	SL
20	50	212.48	11.99	11.97	11.94	211	196	199
20	55	214.98	14.48	14.28	14.25	178	170	173
20	60	217.08	16.58	16.54	16.51	158	151	154
20	70	220.95	20.45	20.93	20.89	137	128	130
20	80	223.73	23.23	25.13	25.07	129	113	116
25	50	213.88	13.38	13.35	13.32	248	226	230
25	55	216.68	16.19	15.97	15.93	207	196	199
25	60	218.82	18.32	18.53	18.48	179	175	178
25	70	223.32	22.82	23.49	23.43	141	147	151
25	80	227.27	26.77	28.24	28.16	129	131	134
30	50	215.48	14.98	14.90	14.86	279	261	266
30	55	219.02	18.52	17.87	17.81	238	226	230
30	60	221.05	20.55	20.75	20.69	220	202	206
30	70	226.22	25.72	26.36	26.28	178	170	175
30	80	230.85	30.35	31.73	31.63	158	151	155
35	50	216.98	16.48	16.57	16.52	322	304	308
35	55	219.93	19.43	19.91	19.84	277	262	268
35	60	223.42	22.92	23.18	23.10	243	234	239

Table D-7 : Comparison between experimental and predictedresults for the FT30 module at C_F=40000 (ppm) and Q_B= 200.5 (cc/s).

T (°C)	P_F (bar)	Q_F (cc/s)	Q_P(cc/s)			C_P(ppm)		
			Exp	SP	SL	Exp	SP	SL
20	50	210.02	9.52	9.77	9.74	275	265	269
20	55	212.10	11.60	12.01	11.98	228	223	227
20	70	218.10	17.60	18.48	18.44	158	160	163
20	80	221.97	21.47	22.58	22.52	135	139	142
25	50	211.10	10.60	10.82	10.79	332	308	313
25	55	213.68	13.12	13.35	13.32	277	259	263
25	60	216.08	15.58	15.84	15.80	232	226	230
25	70	220.23	19.73	20.66	20.60	182	185	189
25	80	223.70	23.20	25.26	25.18	150	160	165
30	50	212.00	11.50	11.98	11.94	372	358	364
30	55	215.38	14.88	14.84	14.80	330	300	305
30	60	217.50	17.00	17.64	17.59	276	261	266
30	70	222.70	22.20	23.08	23.00	220	214	219
30	80	227.90	27.40	28.30	28.20	189	186	191
35	50	213.98	13.48	13.23	13.18	382	417	424
35	55	216.78	16.28	16.44	16.38	378	349	355
35	60	219.83	19.33	19.60	19.52	356	304	310
35	70	225.38	24.88	25.71	25.60	273	249	255
35	80	231.05	30.55	31.56	31.43	222	217	223

Table D-8 : Comparison between experimental and predicted results for the FT30 module at C_F=25000 (ppm) and Q_B= 246.22 (cc/s).

T (°C)	P_F (bar)	Q_F (cc/s)	Q_P(cc/s)			C_P(ppm)		
			Exp	SP	SL	Exp	SP	SL
20	50	263.42	17.20	17.02	16.99	89	103	105
20	55	265.55	19.33	19.52	19.49	89	93	94
20	60	267.88	21.68	21.99	21.95	83	85	87
20	70	272.25	26.03	26.77	26.73	75	74	76
20	80	276.55	30.35	31.38	31.33	69	67	69
25	50	266.57	20.35	19.25	19.21	98	117	120
25	55	269.23	23.02	22.10	22.06	89	106	108
25	60	271.73	25.52	24.91	24.86	83	97	99
25	70	276.88	30.67	30.36	30.30	75	85	87
30	50	269.75	23.53	21.79	21.74	111	134	137
30	55	272.88	26.67	25.05	24.99	104	121	124
30	60	275.93	29.72	28.24	28.18	93	111	114
35	50	273.08	26.87	24.61	24.55	125	154	157
35	55	276.98	30.77	28.32	28.25	115	139	142
35	60	280.52	34.30	31.95	31.87	106	128	131

Table D-9 : Comparison between experimental and predicted results for the FT30 module at C_F=35000 (ppm) and Q_B= 246.22 (cc/s).

T (°C)	P_F (bar)	Q_F (cc/s)	Q_P(cc/s)			C_P(ppm)		
			Exp	SP	SL	Exp	SP	SL
20	50	258.50	12.28	12.27	12.24	198	188	191
20	55	260.90	14.68	14.65	14.62	169	162	165
20	60	262.90	16.68	16.98	16.95	149	144	147
20	70	267.18	20.97	21.52	21.48	133	121	123
20	80	269.85	23.63	25.87	25.82	129	106	109
25	50	259.90	13.68	13.72	13.69	242	216	220
25	55	262.60	16.38	16.42	16.38	196	187	190
25	60	267.18	18.62	19.10	19.05	168	166	169
25	70	269.55	23.33	24.21	24.15	135	139	142
25	80	273.72	27.50	29.14	29.08	122	122	125
30	50	261.70	15.48	15.34	15.31	271	249	253
30	55	264.22	18.00	17.40	18.35	220	215	219
30	60	266.97	20.75	21.41	21.35	207	191	195
30	70	272.25	25.43	27.23	27.16	166	160	164
30	80	276.88	30.67	32.82	32.73	141	141	145
35	50	263.10	16.88	17.11	17.06	311	288	293
35	55	266.15	19.93	20.57	20.51	269	249	253
35	60	269.55	23.33	23.97	23.89	223	221	226
35	70	275.72	29.50	30.56	30.46	198	185	190
35	80	281.05	34.83	36.86	36.74	162	164	168

Table D-10 : Comparison between experimental and predicted results for the FT30 module at C_F=40000 (ppm) and Q_B= 246.22 (cc/s).

T (°C)	P_F (bar)	Q_F (cc/s)	Q_p(cc/s)			C_p(ppm)		
			Exp	SP	SL	Exp	SP	SL
20	50	255.93	9.72	10.04	10.01	275	255	258
20	55	258.10	11.88	12.35	12.33	224	214	217
20	60	260.30	14.08	14.63	14.60	200	186	189
20	70	264.22	18.00	19.06	19.02	147	151	154
25	50	257.05	10.75	11.14	11.11	322	295	299
25	55	259.60	13.38	13.77	13.73	273	247	251
25	60	262.10	15.88	16.35	16.31	225	215	218
25	70	266.15	19.93	21.35	21.29	169	174	178
25	80	270.58	24.37	26.15	26.09	141	151	154
30	50	257.90	11.68	12.36	12.33	369	342	347
30	55	261.30	15.08	15.34	15.30	317	285	290
30	60	263.72	17.50	18.25	18.20	271	248	252
30	70	269.03	22.82	23.92	23.85	216	201	206
30	80	273.92	27.00	29.35	29.27	182	174	178
35	50	259.90	13.68	13.69	13.64	448	398	404

APPENDIX E

Instrumentation Calibration.

This appendix is concerned with the calibration of the different instruments used for the test cell experiments presented in chapter IV.

1- Calibration of the Paddle Wheel flow meter :

The Paddle Wheel flow meter used for the measurement of the feed flow rate was a "Flowget of type F15". The principle of operation of this rotameter is quite simple : a jet of liquid is directed at a free running turbine in a specially shaped chamber. The turbine blade cuts a beam of infra-red light and converts it to a pulse output. The frequency of these pulses is proportional to the flow rate.

The calibration procedure for this rotameter consisted in measuring the volume of water passing through it at a given time and recording the corresponding output value in volts from the digital multimiter. After several runs over the flow range of interest, the following calibration plot was obtained.

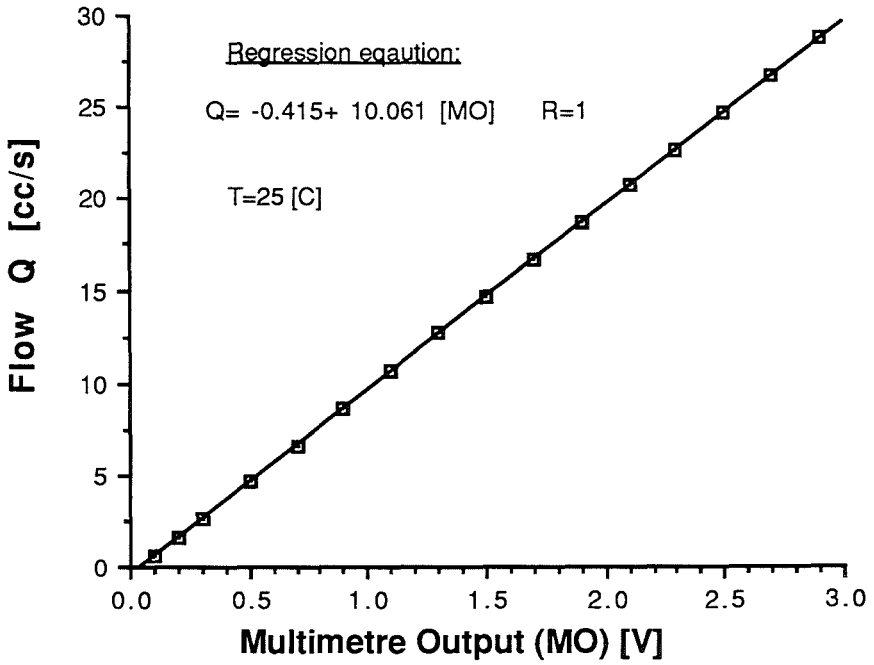

FIG.1-E: Calibration curve for the rotameter.

2- Calibration of the Conductivity meter :

The conductivity meter used for the measurement of the concentrations of the feed and permeate solutions was a PTI-18 digital type.

The calibration procedure consisted in measuring, for each temperature, the conductivity of samples of known concentrations. This procedure was performed for both high and low "instant sea water" concentrations. The resulting plots together with the regression equations are shown in Figs.2-E and 3-E.

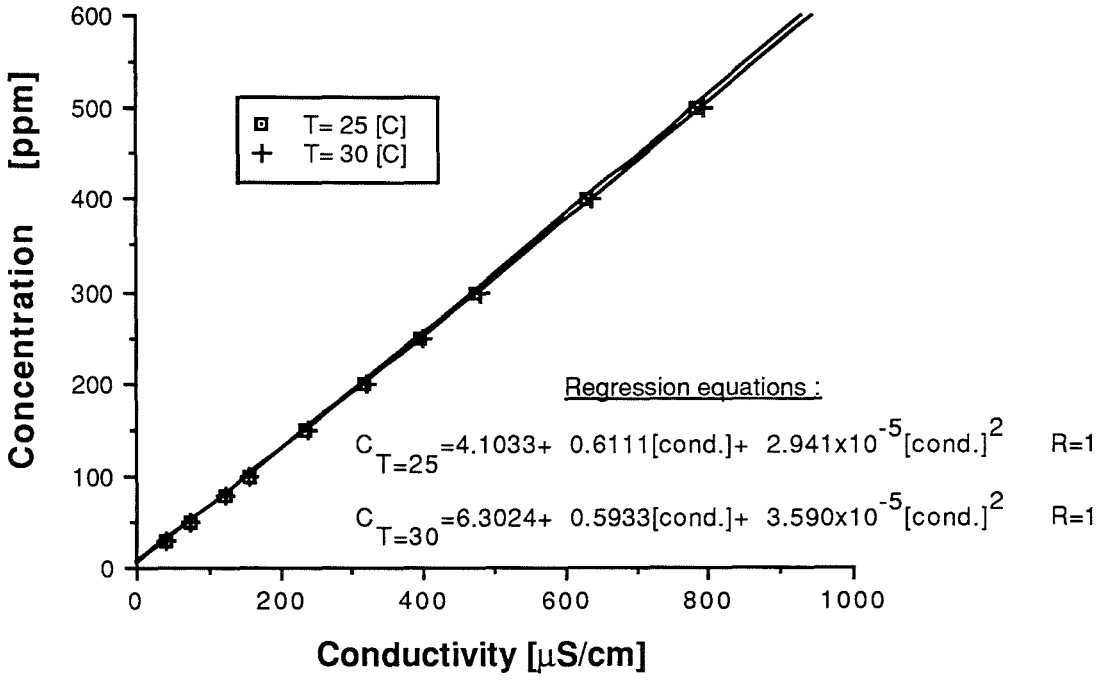

FIG.2-E: Conductivity meter calibration curves for low sea water concentrations.

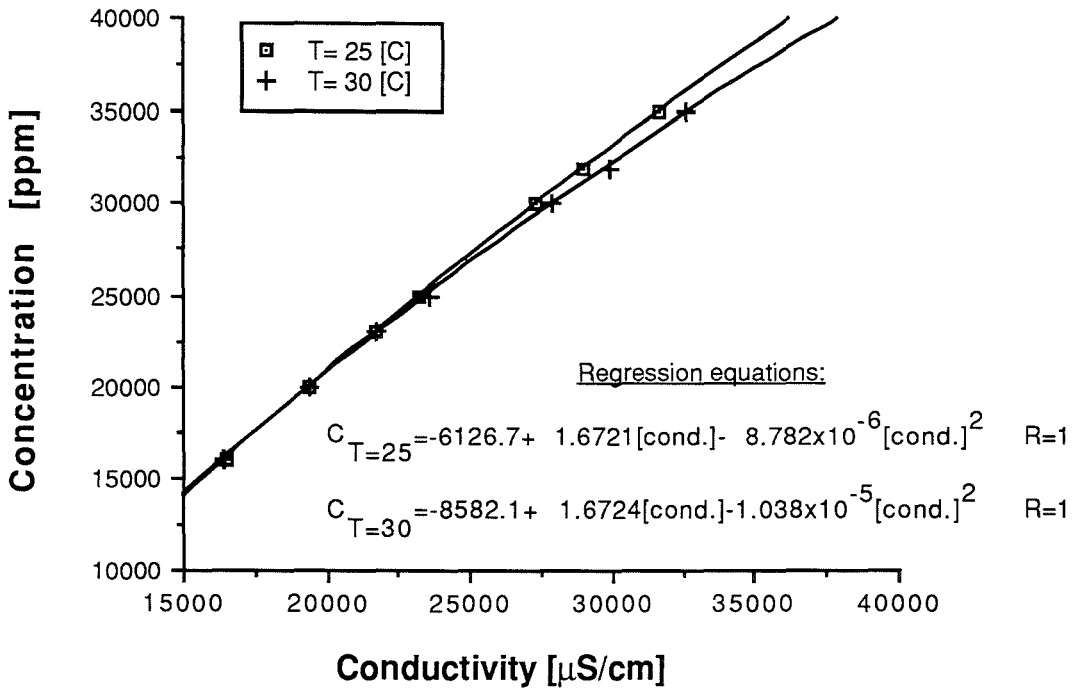

FIG.3-E: Conductivity meter calibration curves for high sea water concentrations.

3- Pressure transducer calibration :

The pressure transducer used was manufactured by " Transamerica Instruments" and was of BHL-4250 type and was connected to a digital pressure indicator (type SC-1100) of the same make. The system is suitable for pressures of up to 100 [bar]. Despite the fact that this pressure transducer was calibrated by the supplier, a checking test was made by using a dead-weight pressure gauge tester and the system was found to perform very accurately.

REFERENCES

1- Reid, C.E. and Breton, E.J.,"Water and Ion Flow Across Cellulosic Membranes", J. Appl. Poly. Sci., 1, 133 (1959).

2- Loeb, S. and Sourirajan, S.,"Sea Water Demineralization by Means of Semipermeable Membrane", UCLA Engineering Report No 60-60 (1960).

3- Richter, D.W. and Moehn, M.M., U.S. Patent No. 3 507 032.

4- Cadotte, O.E, U.S. Patent No. 4 277 344.

5- Cadotte., J.E., Petersen, R.J., Larson, R.E. and Erickson, E.E.," A New Thin-Film Composite Seawater Reverse Osmosis Membrane", Desalination, 32, 25 (1980).

6- Bates, W.T. and Maravich, R.,"Crossflow Ceramic Microfiltration for Water Purification", 26th annual Liberty Bell Corrosion Water Course, Sept.26-28, (1988).

7- Merten, U., OSW 165 (1966).

8- Skiens, W.E. and Mahon, H.I.,"Permeation Rate Constants for Water and Salt Flux through Synthetic Membranes", J. Appl. Poly. Sci., 7, 1549 (1963).

9- Caracciolo, V.P., Rosenblatt, N.W. and Tomsic, V.J.,"Dupont's Hollow Fiber Membranes", in Reverse Osmosis and Synthetic Membranes; Theory, Technology, Engineering, S.Sourirajan (ed.), National Research Council of Canada Publication No. NRCC 15627, 343, (1977).

10- Kedem, O. and Katchalsky, A.,"Thermodynamic Analysis of the Permeability of Biological Membranes to Non-Electrolytes", Biochemica et Biophysica Acta, 27, 229 (1958).

11- Spiegler, K.S. and Kedem, O.,"Thermodynamics of Hyperfiltration (Reverse Osmosis) : Criteria for Efficient Membranes", Desalination, 1, 311 (1966).

12- Soltanieh, M. and Gill, W.N.,"Review of Reverse Osmosis Membranes and Transport Models", Chem. Eng. Commun., 12, 279 (1981).

13- Lonsdale, H.K., Merten, U. and Riley, R.L.,"Transport Properties of Cellulose Acetate Osmotic Membranes", J. Appl. Pol. Sci., 9, 1341 (1965).

14- Banks, W. and Sharples, A.,"Studies on Desalination by Reverse Osmosis : III-Mechanism of Solute Rejection", J. Appl. Chem., 16, 153 (1966).

15- Sherwood, T.K., Brian, P.L.T. and Fisher, R.E.," Desalination by Reverse Osmosis", I.& E.C. Fund., 6, 2 (1967).

16- Sourirajan, S.,"Reverse Osmosis", Chapt.3, Academic Press, NY (1970).

17- Matsuura, T., Taketani, Y. and Sourirajan, S.," Synthetic Membranes II", ACS Symposium Series, Turbak ed., 315 (1981).

18- Sirkar, K.K., Dang, P.T. and Rao, G.H.,"Approximate Design Equations for Reverse Osmosis Desalination by Spiral-Wound Modules", Ind. Eng. Chem. Process Des. Dev., 21, 517 (1982).

19- Prasad, R. and Sirkar, K.K.," Analytical Design Equations for Multicomponent Reverse Osmosis Processes by Spiral-Wound Modules", Ind. Eng. Chem. Process Des. Dev., 24, 350 (1985).

20- Evangelista, F.,"Improved Analytical Method for the Design of Spiral Wound Modules ", The Chemical Engng. J., 38, 33 (1988).

21- Evangelista, F., "Explicit Expressions for Permeate Flux and Concentration in Hyperfiltration", Chem. Eng. Sci., 41, 1913 (1986).

22- Evangelista, F. and Jonsson, G., "Optimal Design and Performance of Spiral Wound Modules, II : Analytical Method ", Chem. Eng. Comm., 72, 83 (1988).

23- Chiolle, A.; Gianotti, G.; Gramondo, M.; and Parrini, G.,"Mathematical Model of Reverse Osmosis in Parallel-Wall Channels with Turbulence Promoting Nets ", Desalination, 26, 3 (1978).

24- Winograd, Y., Solan, A. and Torren, M.,"Mass Transfer in Narrow Channels in the Presence of Turbulence Promoters", Desalination, 13, 171 (1973).

25- Rautenbach, R. and Dahm, W., "Design and Optimisation of Spiral Wound and Hollow Fiber RO Modules ", Desalination, 65, 259 (1987).

26- Evangelista, F. and Jonsson, G., " Optimal Design and Performance of Spiral Wound Modules, I : Numerical Method ", Chem. Eng. Comm., 72, 69 (1988).

27- Shock, G. and Miquel, A., "Mass Transfer and Pressure Loss in Spiral-Wound Modules", Desalination, 64, 339 (1987).

28- Avlonitis, S., "Spiral Wound Modules Performance. An Analytical Solution", Ph.D Thesis, Glasgow University, 1991.

29- Taniguchi, Y., "An Analysis of Reverse Osmosis Characteristics of Roga Spiral Wound Modules ", Desalination, 25, 71 (1978).

30- Gekas, V. and Hallstrom, B., "Mass transfer in the membrane concentration polarization layer under turbulent cross flow.I. Critical review and adaption of existing Sherwood correlations to membrane operations", J. Membrane Sci., 30, 153 (1987).

31- Davis, J.L., "Finite Difference Methods in Continuous Media", McMillan Publishing Company, NY (1986).

32- Ben Boudinar, M., Hanbury, W.T. and Avlonitis, S., "Numerical Simulation and Optimisation of Spiral Wound Modules", submitted for publication in Desalination, 1991.

33- U.S. Dept. of the Interior, Office of Saline Water Research and Development Progress Report No 363 (Sept. 1968).
34- U.S. Agency for International Development (U.S.A.I.D.), Desalination Manual, Washington D.C.,1980.

GLASGOW UNIVERSITY LIBRARY